arXiv:1910.00131v3 [stat.ME] 30 May 2022

Fast and Fair Simultaneous Confidence Bands for Functional Parameters

Dominik Liebl*† Matthew Reimherr‡

Abstract

Quantifying uncertainty using confidence regions is a central goal of statistical inference. Despite this, methodologies for confidence bands in Functional Data Analysis are still underdeveloped compared to estimation and hypothesis testing. In this work, we present a new methodology for constructing simultaneous confidence bands for functional parameter estimates. Our bands possess a number of striking qualities: (1) they have a nearly closed-form expression and thus are fast to compute, (2) they can be constructed adaptively according to a desired criterion, where we focus on the fairness constraint of *false positive rate balance* across partitions of the bands' domain which facilitates both global and local interpretations, and (3) they do not require an estimate of the full covariance function and thus can be used in the case of fragmentary functional data. Simulations show the excellent finite-sample behavior of our bands in comparison to existing alternatives. The practical use of our bands is demonstrated in two case studies on sports biomechanics and fragmentary growth curves.

Keywords: functional data analysis; simultaneous inference; hypothesis testing; fairness constraints; false positive rate balance; Kac-Rice formula

1 Introduction

As part of the big data revolution, statistical tools have made astonishing strides towards handling increasingly complex and structured data. Data gathering technologies have allowed scientists, businesses, and government agencies to collect data on increasingly sophisticated phenomena, including high-dimensional measurements, functions, surfaces, and images. A major tool set that has emerged for handling such highly complex and smooth structures is Functional Data Analysis, FDA (Ramsay and Silverman, 2005; Ferraty and

*Dominik Liebl (dliebl@uni-bonn.de), Institute of Finance and Statistics, University of Bonn, Adenauerallee 24-42, 53113 Bonn, Germany

†Hausdorff Center for Mathematics, Endenicher Allee 62, 53115 Bonn, Germany

‡Department of Statistics, Penn State University, 411 Thomas Building, University Park, PA 16802

Vieu, 2006; Hsing and Eubank, 2015; Kokoszka and Reimherr, 2017). There, one has access to rich, dynamic, and smooth structures, while also having some degree of repetition, allowing researchers to fit complex and flexible nonparametric statistical models.

Despite the success and maturity of FDA, some foundational questions remain unanswered or underdeveloped. This work is concerned with a fundamental goal of statistical inference: quantifying estimation uncertainty with simultaneous confidence bands. Simultaneous confidence bands have received increasing attention in recent years, however, current solutions usually suffer from one of several major drawbacks: they are computationally expensive, they result in bands that are very conservative, they cannot be used in the case of fragmentary functional data, or they can only be interpreted globally—not locally. In this work we present a broad framework based on random process theory that solves the aforementioned issues. Our bands possess a number of desirable qualities, but two are especially striking.

First, they can be chosen adaptively according to a desired criterion, where in this work we focus on the fairness constraint of false positive rate balance. Simultaneous confidence bands for functional parameters (mean functions, regression functions, etc.) are used to detect the *locations* of effects within the band's domain. These detected locations often inform high-stakes decisions in medicine (Donoghue et al., 2008; Boschi et al., 2021), economics (Liebl, 2019; Bamisile et al., 2021), and forensics (Sulovská et al., 2017; Kelly, 2020), and thus it is sensible to require that no segment in the band's domain disproportionately favours the occurrence of false positives. To achieve false positive rate balance, we use an adaptive critical value function that assigns to any given partition of the domain a balanced false positive rate that is proportional to the Lebesgue measure of each partition. This approach allows global as well as local interpretations of our bands. As far as we know, we are the first to propose fair simultaneous confidence bands, but the importance of fairness constraints, such as false positive rate balance, is well acknowledged in the machine learning literature on classification problems (Hardt et al., 2016; Morgenstern and Roth, 2022).

Second, our bands do not require estimation of the full covariance function of the estimator. Instead, only a narrow band along the diagonal is needed and then only to ascertain the pointwise uncertainty of the estimate and its derivative. No other FDA method in the literature, that we are aware of, for quantifying uncertainty globally posses such a property. This has broad implications in FDA as many tools are being actively developed for data consisting of functional fragments, where estimation of the full covariance is generally impossible (Delaigle and Hall, 2016; Descary and Panaretos, 2019; Delaigle et al., 2020; Liebl and Rameseder, 2019; Kneip and Liebl, 2020).

The central idea behind our methodology is a simple connection between the supremum of a stochastic process and the expected Euler characteristic of an excursion set. Consider a real valued random function over a closed interval, $X = \{X(t) : t \in [0, 1]\}$, where restricting the domain to $[0, 1]$ is without loss of generality (for any closed finite interval) and common in FDA to ease notation. Instead of finding the probability that X ever crosses a critical value function, $u = \{u(t) : t \in [0, 1]\}$, i.e., $P(\exists t \in [0, 1] : X(t) \geq u(t))$, the expected Euler characteristic inequality suggests to consider the task of counting the events when X crosses u in an upward trajectory. While a seemingly small change, the latter ends up being

far more tractable. Thus far, the literature on random process/field theory has focused on constant critical values $u(t) \equiv u \in \mathbb{R}$ X; see, for instance, Adler and Taylor, 2007, and Azaïs and Wschebor, 2009. In this paper, we demonstrate how to handle the more general case of non-constant critical value functions, which, as we will see, opens up the exciting opportunity to produce tight and fair bands. The number of up-crossings of X about u on the interval $[0, 1]$ is defined as

$$N_{u,X}([0,1]) := \#\{0 \leq t \leq 1 : X(t) = u(t), X'(t) > u'(t)\}.$$

If this quantity is zero, then the only way that $X(t)$ could have exceeded $u(t)$ was if X started above of u at $t = 0$, since both functions, X and u, are continuous. This logic leads to the expected Euler characteristic inequality by applying Boole's and Markov's inequality

$$\begin{aligned} P\big(\exists t \in [0,1] : X(t) \geq u(t)\big) &= P\big(\{X(0) \geq u(0)\} \text{ or } \{N_{u,X}([0,1]) \geq 1\}\big) \\ &\leq P\big(X(0) \geq u(0)\big) + P\big(N_{u,X}([0,1]) \geq 1\big) \\ &\leq P\big(X(0) \geq u(0)\big) + \mathbb{E}\left[N_{u,X}([0,1])\right] = \mathbb{E}\left[\varphi_{u,X}(0)\right], \end{aligned} \tag{1}$$

where $\varphi_{u,X}(0) := \mathbb{1}_{X(0) \geq u(0)} + N_{u,X}([0,1])$ denotes the Euler (or Euler-Poincaré) characteristic of the excursion set $\{t \in [0,1] : X(t) \geq u(t)\}$. Intuitively, this quantity counts exceedance events by starting at $t = 0$, checking if $X(0) > u(0)$ and then moving through the domain to check for additional up-crossings.

Sharpness of the expected Euler characteristic inequality. The accuracy of the inequality in (1) is not a main focus of our paper, but was studied under different assumptions on the stochastic process X. For instance, Piterbarg (1982) and Azaïs et al. (2002) considered the case of smooth Gaussian processes with stationary covariance functions and without global singularities (i.e. $\mathrm{Cor}(X(t), X(s)) = 1 \Leftrightarrow t = s$). These authors showed, under some further technical assumptions, that the approximation error for large $u \to \infty$ is $|P\big(\exists t \in [0,1] : X(t) \geq u(t)\big) - \mathbb{E}[\varphi_{u,X}(0)]| \leq c_1 \exp\left(-c_2 u^2/2\right)$ for some positive constants c_1 and c_2. Taylor et al. (2005) showed that similar results hold for non-stationary covariance functions, without global singularities. These results generalize to our case of non-constant critical value functions $u(t)$ by considering $u \equiv \min_{0 \leq t \leq 1} u(t)$ for large $u \to \infty$. Note that global singularities are allowed in (1), but make the approximation less sharp.

To construct non-constant critical value functions $u(t)$ that are both tight and fair, it is necessary to generalize the expected Euler characteristic inequality (1) and to allow starting the counting at some mid point, $t_0 \in [0, 1]$ and then count crossings moving away from t_0 in both directions. When moving from t_0 down to 0, up-crossings as t decreases are equivalent to down-crossings as t increases (see Figure 8 of the supplementary paper Liebl and Reimherr (2022b)). We therefore work with the following generalized expected Euler characteristic

$$P\big(X(t_0) \geq u(t_0)\big) + \mathbb{E}[N^-_{u,X}([0,t_0])] + \mathbb{E}[N_{u,X}([t_0,1])] = \mathbb{E}[\varphi_{u,X}(t_0)], \tag{2}$$

where $N^-_{u,X}[0,t_0] := \#\{0 \leq t \leq t_0 : X(t) = u(t), X'(t) < u'(t)\}$ denotes the number of down-crossings over $[0, t_0]$.

In this work, we derive new expressions for $\mathbb{E}[\varphi_{u,X}(t_0)]$ allowing for varying critical value functions $u(t)$. Given such an expression and a significance level $\alpha \in (0,1)$, solving $\mathbb{E}[\varphi_{u,X}(t_0)] = \alpha/2$ allows one to derive powerful (two-sided) simultaneous confidence bands, where $t_0 \in [0,1]$ will be determined by the imposed fairness constraint. For instance, in many applications in FDA, one is interested in estimating a functional parameter, $\theta = \{\theta(t) : t \in [0,1]\}$, for a particular FDA model. Suppose that $\hat{\theta}(t)$ is an estimator of $\theta(t)$, such that $\big(\hat{\theta}(t) - \theta(t)\big)$ is, possibly asymptotically, a mean zero Gaussian process. Then we can take the standardized Gaussian process $X(t) = \big(\hat{\theta}(t) - \theta(t)\big)/(\mathrm{Var}(\hat{\theta}(t)))^{1/2} \sim \mathcal{N}(0,1)$ for each $t \in [0,1]$, and compute the critical value function $u_{\alpha/2}(t)$ that solves $\mathbb{E}[\varphi_{u,X}(t_0)] = \alpha/2$. Our Theorem 3.1 ensures that

$$[\hat{\theta}_l(t), \hat{\theta}_u(t)] = \hat{\theta}(t) \pm u_{\alpha/2}(t)\sqrt{\mathrm{Var}\left(\hat{\theta}(t)\right)}, \quad t \in [0,1], \tag{3}$$

is a valid $(1-\alpha) \times 100\%$ simultaneous (two-sided) confidence band for the parameter $\theta(t)$ over $[0,1]$. Our Theorem 3.2 ensures that the simultaneous confidence band in (3) also holds asymptotically when the underlying covariance parameters (and therefore u) are estimated. Moreover, our Corollary 3.3 can be used for finite sample corrections using t-processes to take into account estimation errors in the covariance estimates.

The main hurdle in finding a $u_{\alpha/2}(t)$ that solves $\mathbb{E}[\varphi_{u,X}(t_0)] = \alpha/2$ is to find general expressions for $\mathbb{E}[N^-_{u,X}([0,t_0])]$ and $\mathbb{E}[N_{u,X}([0,t_0])]$, since a formula for the correction term, $P(X(t_0) \geq u(t_0))$, follows directly from the (possibly asymptotic) distribution of X. Focusing on symmetric distributions, a formula for the up-crossings can be translated into one for the down-crossings since $\mathbb{E}[N^-_{u,X}([0,t])] = \mathbb{E}[N_{-u,X}([0,t])]$. Explicit formulas for $\mathbb{E}[N_{u,X}([0,1])]$ are grouped together under "Kac-Rice formulas" acknowledging the works of Kac (1943) and Rice (1945). In this paper we generalize the existing Kac-Rice formulas by allowing for adaptive critical value functions $u(t)$. Another apparent challenge is that $\mathbb{E}[\varphi_{u,X}(t_0)] = \alpha/2$ will not, in general, have a unique solution when we allow for more general $u(t)$. However, far from being a liability, we show how this allows one to select bands adaptively, for instance, according to a given fairness constraint. While other criteria such as minimum width bands are possible too (see our discussion in Section 6), we focus on fairness, which has been a recent focus in machine learning, but so far wasn't discussed in the context of confidence bands.

The recent literature in FDA provides different approaches and methods to simultaneous inference for functional data, and simulation based methods belong to the most successful approaches. Degras (2011), Cao et al. (2012), and Wang et al. (2020) propose bands based on the parametric bootstrap. A further simulation based approach is the interval-wise testing (IWT) procedure proposed by Pini and Vantini (2016) and Pini and Vantini (2017b) which uses permutations. Simulation based approaches are computationally intensive and, as shown in our simulation study can perform weakly in small samples. An exception are the multiplier bootstrap bands proposed by Dette et al. (2020), Dette and Kokot (2022) and Telschow and Schwartzman (2022), which perform well also in small samples. Another typical approach is to apply a dimension reduction based on function principal component analysis and to build multivariate confidence ellipses; see, for instance, Yao et al. (2005) and Goldsmith et al. (2013). As shown by Choi and Reimherr (2018), however, these procedures lead to ellipses with zero-coverage. As a solution to this problem, Choi and

Reimherr (2018) proposed an approach that transforms confidence hyper-ellipsoids into valid confidence bands. Also related is the work of Olsen et al. (2021) who adapt the Benjamini-Hochberg procedure to the case of functional data. Early theoretical results on Kac-Rice formulas were developed by Ito (1963), Cramér and Leadbetter (1965), and Belyaev (1966), among others. Fundamental introductions to random process/field theory, including different versions of the Kac-Rice formula, are given in the textbooks of Adler and Taylor (2007), Azaïs and Wschebor (2009), and Cramér and Leadbetter (2013). The random process/field theory based methods have seen a tremendous success in the applied neuroimaging and biomechanics literature (Friston et al., 2007; Wager et al., 2009; Pataky et al., 2016; Wen et al., 2018), where these methods are subsumed under the term Statistical Parametric Mapping. Recently, Telschow and Schwartzman (2022) published random process/field theory based simultaneous confidence bands. The authors consider the case of t-processes and contribute new inference results, but for the well-known existing Gaussian kinematic formulas; i.e. higher dimensional Kac-Rice formulas. By contrast, we consider the more the more general cases of elliptical processes, non-constant adaptive critical value functions, and fragmentary functional data.

The paper and its contributions are structured as follows. Section 2 motivates and introduces Definition 2.1 of false positive rate balance for stochastic processes. In Section 3, we collect our core methodological and theoretical contributions: Theorem 3.1 contains our generalized Kac-Rice formula for variable critical value functions and general elliptical processes, Theorem 3.2 contains our asymptotic results, Algorithm 1 shows how to select fair critical value functions, and Proposition 3.2 together with Lemma 3.2 shows that our fair bands fulfill the Definition 2.1 of false positive rate balance. Simulations in Section 4 show the excellent finite-sample behavior of our fair confidence bands for fully observed and fragmentary functional data. Section 5 contains applications to data from sports biomechanics and to fragmentary growth curves. Lastly, Section 6 contains our discussion.

2 False Positive Rate Balance

To explain and motivate the definition of false positive rate balance, let us consider, for a moment, the trivial special case of a moment estimator $\hat{\theta}_n(t) = n^{-1}\sum_{i=1}^n S_i(t)$, $t \in [0,1]$, that estimates the mean function $\theta(t) = \mathbb{E}(S_i(t))$ from an iid Gaussian random process sample $S_i \overset{\text{iid}}{\sim} \mathcal{N}(\theta, C)$, $i = 1, \dots, n$, with independent, piecewise constant sample paths[1]: two equidistant constant sections over $[0, 1/3]$, eight over $[1/3, 2/3]$, and 32 over $[2/3, 1]$; see Figure 1. Under the null hypothesis H_0: $\theta(t) = \theta_0(t)$, the z-test statistic is a Gaussian process $X(t) = \sqrt{n}\big(\hat{\theta}_n(t) - \theta_0(t)\big)/\sqrt{C(t,t)} \overset{\mathrm{H}_0}{\sim} \mathcal{N}(0,1)$.

Testing simultaneous hypothesis about the mean function θ requires a critical value $u_{\alpha/2} > 0$ that controls the false positive rate simultaneously for all $t \in [0,1]$ at a given significance level $\alpha \in (0,1)$. For the here considered trivial case of a Gaussian process X

[1]The corresponding covariance function $C(s,t) = \mathrm{Cov}(S_i(t), S_i(s)$ is non-stationary, bloc-diagonal with 42 blocs $C(t,s) = \kappa_j > 0$ for $s, t \in [a_{j-1}, a_j)$, $1 \le j \le 42$, formed by two equidistant intervals $[a_{j-1}, a_j)$, $1 \le j \le 2$, in $[1, 1/3]$, eight equidistant intervals $[a_{j-1}, a_j)$, $2 \le j \le 10$, in $[1/3, 2/3]$, and 32 equidistant intervals $[a_{j-1}, a_j)$, $10 \le j \le 42$, in $[2/3, 1]$.

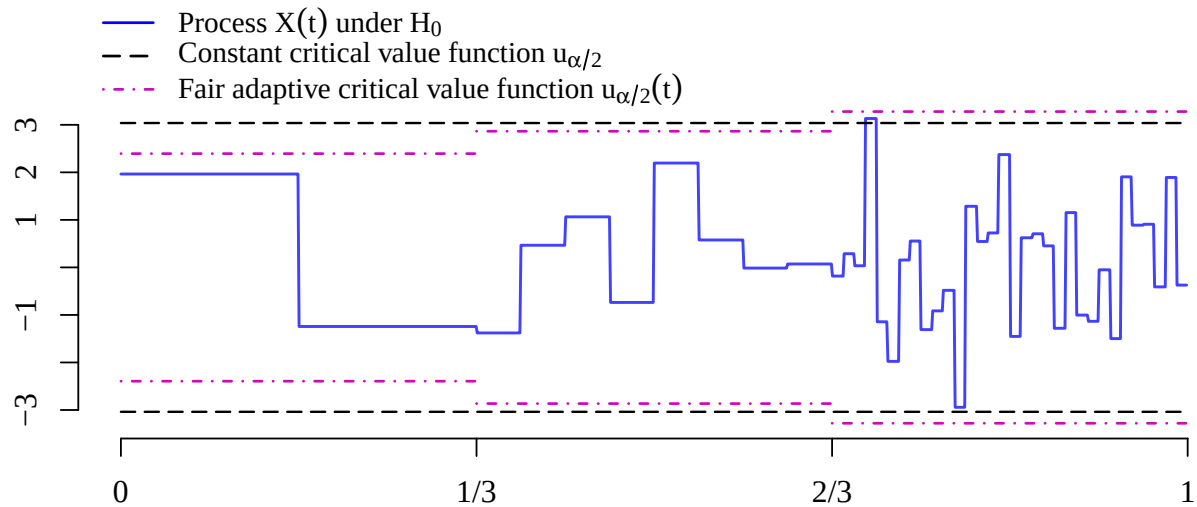

Figure 1: A realization of the piecewise constant z-test statistic process $X(t)$ as defined at the beginning of Section 2, the unfair constant critical value $u_\alpha = |z_{\alpha/24}|$ and the fair adaptive critical value function.

with 42 independent piecewise constant sections, the correct critical value is given by a Bonferroni correction $u_{\alpha/2} = |z_{(\alpha/2)/42}|$ with $z_{(\alpha/2)/42}$ denoting the $(\alpha/2)/42$-quantile of the standard normal distribution, since

$$P_{\mathrm{H}_0}(\exists t \in [0,1] : |X(t)| \geq u_{\alpha/2}) = 42P(|Z| \geq |z_{(\alpha/2)/42}|) = 42(\alpha/42) = \alpha,$$

where $Z \sim \mathcal{N}(0,1)$. However, since $C(s,t)$ is non-stationary, the constant critical value $u_{\alpha/2} = |z_{(\alpha/2)/42}|$ leads to unbalanced false positive rates. Only $(2/42) \approx 5\%$ of all false positive events occur over $[0,1/3]$, $(8/42) \approx 19\%$ over $[1/3,2/3]$, but $(32/42) \approx 76\%$ over $[2/3,1]$,

$$\begin{array}{rclcl} P_{\mathrm{H}_0}(\exists t \in [0,1/3] : |X(t)| \geq u_{\alpha/2}) & = & 2P(|Z| \geq |z_{(\alpha/2)/42}|) & = & (2/42)\,\alpha \\ P_{\mathrm{H}_0}(\exists t \in [1/3,2/3] : |X(t)| \geq u_{\alpha/2}) & = & 8P(|Z| \geq |z_{(\alpha/2)/42}|) & = & (8/42)\,\alpha \\ P_{\mathrm{H}_0}(\exists t \in [2/3,1] : |X(t)| \geq u_{\alpha/2}) & = & 32P(|Z| \geq |z_{(\alpha/2)/42}|) & = & (32/42)\,\alpha. \end{array}$$

To balance the false positive rates over the partition $0 < 1/3 < 2/3 < 1$ one needs an adaptive critical value function $u_{\alpha/2}(t)$ that allocates the significance level α according to the Lebesgue measure (interval length) of each partition, i.e. $\lambda([0,1/3])\alpha = (1/3)\alpha$, $\lambda([1/3,2/3]) = (1/3)\alpha$, and $\lambda([2/3,1]) = (1/3)\alpha$. In the trivial case of a Gaussian process with independent, piecewise constant sample path sections, such a fair critical value function is simply derived using local partition wise Bonferroni correction $u_{\alpha/2}(t) = |z_{(\alpha/2)/6}|$ for $t \in [0,1/3)$, $u_{\alpha/2}(t) = |z_{\alpha/24}|$ for $t \in [1/3,2/3)$, and $u_{\alpha/2}(t) = |z_{\alpha/96}|$ for $t \in [2/3,1)$, which yields balanced false positive rates

$$\begin{array}{rclcl} P_{\mathrm{H}_0}(\exists t \in [0,1/3] : X(t) \geq u_{\alpha/2}(t)) & = & 2P(|Z| \geq |z_{(\alpha/2)/6}|) & = & (1/3)\,\alpha \\ P_{\mathrm{H}_0}(\exists t \in [1/3,2/3] : X(t) \geq u_{\alpha/2}(t)) & = & 8P(|Z| \geq |z_{(\alpha/2)/24}|) & = & (1/3)\,\alpha \\ P_{\mathrm{H}_0}(\exists t \in [2/3,1] : X(t) \geq u_{\alpha/2}(t)) & = & 32P(|Z| \geq |z_{(\alpha/2)/96}|) & = & (1/3)\,\alpha \end{array}$$

while at the same time the fair critical value function $u_{\alpha/2}(t)$ correctly bounds the false positive rate over $[0,1]$, i.e. $P_{\mathrm{H}_0}(\exists t \in [0,1] : X(t) \geq u_{\alpha/2}(t)) = \alpha$.

This trivial example motivates Definition 2.1 of false positive rate balance for stochastic processes which adapts the fairness constraint of false positive rate balance from the machine learning literature (Hardt et al., 2016; Morgenstern and Roth, 2022). Unlike the above trivial case, however, we consider the non trivial case of stochastic processes, X_i, with smooth sample paths, $X_i \in C^1[0,1]$, and *unknown covariance function*, $\mathrm{Cov}(X_i(t), X_i(s))$ that is allowed to be *non-stationary* and *non-zero* for all $t, s \in [0,1]$.

Definition 2.1. (False Positive Rate Balance) *Let $0 = a_0 < a_1 < \cdots < a_p = 1$, $p \geq 2$, be a given partition of $[0,1]$, let $\alpha \in (0,1)$ denote the significance level and let H_0 denote the null hypothesis. A simultaneous statistical hypothesis test satisfies false positive rate balance if for each $j = 1, \ldots, p$*

$$P(\textit{Reject } H_0 \textit{ over } [a_{j-1}, a_j] | H_0 \textit{ is true over } [a_{j-1}, a_j]) \leq \lambda([a_{j-1}, a_j])\, \alpha,$$
$$\textit{and} \quad P(\textit{Reject } H_0 \textit{ over } [0,1] | H_0 \textit{ is true over } [0,1]) \leq \lambda([0,1])\, \alpha,$$

where $\lambda([a,b]) = (b-a)$ denotes the Lebesgue measure of $[a,b]$.

Simultaneous confidence bands that fulfill Definition 2.1 are interpretable globally, over $[0,1]$, as well as locally over subintervals $[a_{j-1}, a_j]$, $j = 1, 2, \ldots, p$ or combinations thereof.

3 Theory and Methods

Our first main result is Theorem 3.1, which establishes the Kac-Rice formula for variable critical value functions, $u = \{u(t) : t \in [0,1]\}$, and general elliptical processes, $X = \{X(t) : t \in [0,1]\}$. The results are established under the very mild assumption that the considered process, X, is in $C^1[0,1]$ and that the critical value function, $u(t)$, is in $C[0,1]$ and continuously differentiable almost everywhere. In our second main result, Theorem 3.2, we consider the problem of estimating the confidence band for a process that is only asymptotically normal/elliptical. A key point is that we only need consistent estimates of the covariance parameters about the diagonal. This interesting property makes our method applicable even for fragmentary functional data where an estimation of the full covariance function is impossible. Throughout this paper we will make the following assumption.

Assumption 3.1. *We assume that $X = \{X(t) : 0 \leq t \leq 1\}$ is a centered elliptical process with $X \in C^1[0,1]$ almost surely.*

The assumption that $X \in C^1[0,1]$ almost surely means that the realized paths of X will, with probability one, be one time continuously differentiable, which excludes, for instance, Brownian motion. As our methodology is based on counting up-crossings, some smoothness is required, otherwise the number of up-crossings may be infinite. Of course, not every stochastic process is elliptical, but allowing X to be elliptically distributed provides at least two major benefits. First, it allows one to include a finite sample correction into confidence bands by using t-processes, and second it allows for better uncertainty quantification when forecasting heavy tailed processes.

One key aspect of elliptical processes is that they can be expressed as scalar mixtures of Gaussians; see, for instance, Boente et al. (2014) for the case of functional data and Fang et al. (2018) for a general overview in the case of multivariate data.

Lemma 3.1. *If $X = \{X(t) : 0 \leq t \leq 1\}$ is a centered elliptical process with a covariance operator that does not have finite rank, then there exists a strictly positive random variable $V > 0$ and a mean zero Gaussian process, $Z = \{Z(t) : 0 \leq t \leq 1\}$, such that V and Z are independent and satisfy $\{X(t) : 0 \leq t \leq 1\} \overset{D}{=} \{VZ(t) : 0 \leq t \leq 1\}$.*

If V is heavy tailed, then $X(t)$ need not even have a finite mean. We will thus refer to the covariance of $Z(t)$, $c(t,s) = \mathrm{Cov}(Z(t), Z(s))$, as the *dispersion function* of $X(t)$. If V has a finite and non-zero variance, then the covariance function of X is given by $\mathrm{Cov}(X(t), X(s)) = \mathrm{Var}(V)c(t,s)$ for all $t, s \in [0,1]$. In the Gaussian case, where $V \equiv \sigma$, the covariance function of X is given by $\mathrm{Cov}(X(t), X(s)) = \sigma^2 c(t,s)$ for all $t, s \in [0,1]$. Since we are working with an arbitrary critical value function $u(t)$, we can always assume that it has been scaled by the standard deviation of $Z(t)$, $\sqrt{c(t,t)}$, so that, without loss of generality, we can assume $c(t,t) = 1$.

3.1 Main Theoretical Results

In this section we present our key theoretical results. We begin with our first theorem, which establishes a generalized Kac-Rice formula for varying critical value functions $u(t)$ and elliptical processes $X(t)$. We employ notation such as $\partial_{12}c(t,t)$ to denote partial derivatives of $c(t,s)$ in the first and second coordinates, but then evaluated at $t = s$. Moreover, we write $C^1_{a.e.}[0,1]$ to denote the space of all continuous functions that are continuously differentiable almost everywhere on $[0,1]$. Note that $C^1[0,1] \subset C^1_{a.e.}[0,1]$, since $C^1_{a.e.}[0,1]$ also contains, for instance, piece-wise linear functions.

Theorem 3.1. *Let Assumption 3.1 hold and assume that $u \in C^1_{a.e}[0,1]$. Let $V > 0$ be the mixing coefficient of X, such that $X(t) \overset{D}{=} VZ(t)$, and define $\mathcal{V} = V^{-2}$ along with its moment generating function, $M_{\mathcal{V}}(\cdot)$. Let $\tau(t)^2 = \partial_{12}c(t,t) = \mathrm{Var}(Z'(t))$, where $c(t,s)$ is the dispersion function of $X(t)$, equivalently the covariance function of $Z(t)$. Assume $X(t)$ has a constant pointwise unit dispersion, $c(t,t) = \mathrm{Var}(Z(t)) = 1$, and $\tau(t) > 0$ for all $t \in [0,1]$. Then we have for any fixed $t_0 \in [0,1]$*

$$\begin{aligned}\mathbb{E}[\varphi_{u,X}(t_0)] =& P\big(X(t_0) \geq u(t_0)\big) + \int_0^1 \frac{\tau(t)}{2\pi} M_{\mathcal{V}}\left(-\frac{1}{2}\left[u(t)^2 + \frac{u'(t)^2}{\tau(t)^2}\right]\right)\, dt \\ &+ \int_0^{t_0}\int_0^{\infty} \frac{u'(t)}{2\pi\tau(t)} M'_{\mathcal{V}}\left(-\frac{1}{2}\left[u(t)^2 + \frac{(y-u'(t))^2}{\tau(t)^2}\right]\right)\, dy\, dt \\ &- \int_{t_0}^1\int_0^{\infty} \frac{u'(t)}{2\pi\tau(t)} M'_{\mathcal{V}}\left(-\frac{1}{2}\left[u(t)^2 + \frac{(y+u'(t))^2}{\tau(t)^2}\right]\right)\, dy\, dt.\end{aligned} \tag{4}$$

Note that since $\mathcal{V}$ is strictly positive the above integrals are finite regardless of the mixture distribution, meaning $X(t)$ can be heavy tailed and the expression still holds. Thus $X(t)$ need not even have a finite mean or variance which allows us to model even

extreme value processes. The roughness parameter function τ allows to quantify the extent of the local multiple testing problem across the domain $[0,1]$.

The proof of Theorem 3.1 proceeds in several steps. First, we condition on the mixing parameter $\mathbb{E}[\varphi_{u,X}(t_0)] = \mathbb{E}[\mathbb{E}[\varphi_{u,VZ}(t_0)|V]] = \mathbb{E}[\mathbb{E}[\varphi_{u/V,Z}(t_0)|V]]$ so that we can exploit the connection to Gaussian processes. Conditioned on V, we build up two key approximations, which are common in random process theory, though much more complicated here since u is not restricted to a constant function. One is based on approximating the number of up-crossings by integrating a particular continuous kernel, and the second is based on a linear interpolation along dyadics. Both approximations make the expectation easier to calculate and then we justify taking appropriate limits.

The following three corollaries consider important special cases that simplify the interpretation of our general formula (4) in Theorem 3.1.

Corollary 3.1. (Constant band for elliptical processes) *Let the conditions of Theorem 3.1 hold. If $u(t) \equiv u$ for all $t \in [0,1]$, then one obtains the elliptical version of the classic Kac-Rice formula $\mathbb{E}[\varphi_{u,X}(0)] = P\big(X(0) \geq u\big) + \frac{\|\tau\|_1}{2\pi} M_{\mathcal{V}}\left(-\frac{u^2}{2}\right)$, where $\|f\|_1 = \int_0^1 |f(t)|dt$ denotes the L^1-norm.*

Corollary 3.1 directly follows from Theorem 3.1 since $u' \equiv 0$ for constant critical values, $\tau(t) \geq 0$ for all $t \in [0,1]$ such that $\int_0^1 \tau(t)dt = ||\tau||_1$, and $X(t_0) \overset{D}{=} X(0)$ for all $t_0 \in [0,1]$.

Corollary 3.2. (Gaussian processes) *Let the conditions of Theorem 3.1 hold.*
a) Variable band: When $X(t)$ is a Gaussian process, we set $V \equiv \sigma$ such that $\mathrm{Var}(X(t)) = \sigma^2 \mathrm{Var}(Z(t)) = \sigma^2$ for all $t \in [0,1]$. Formula (4) in Theorem 3.1 then leads to

$$\begin{aligned}\mathbb{E}[\varphi_{u,X}(t_0)] = \Phi\left(\frac{-u(t_0)}{\sigma}\right) &+ \int_0^1 \frac{\tau(t)}{2\pi} \exp\left\{-\frac{1}{2\sigma^2}\left[u(t)^2 + \frac{u'(t)^2}{\tau(t)^2}\right]\right\} dt \\ &+ \int_0^{t_0} \frac{u'(t)}{\sqrt{2\pi\sigma^2}} \exp\left\{-\frac{u(t)^2}{2\sigma^2}\right\} \Phi\left(\frac{u'(t)}{\sigma\tau(t)}\right) dt \\ &- \int_{t_0}^1 \frac{u'(t)}{\sqrt{2\pi\sigma^2}} \exp\left\{-\frac{u(t)^2}{2\sigma^2}\right\} \Phi\left(\frac{-u'(t)}{\sigma\tau(t)}\right) dt.\end{aligned} \tag{5}$$

b) Constant band: If additionally $u(t) \equiv u$, one obtains the classic Kac-Rice formula

$$\mathbb{E}[\varphi_{u,X}(0)] = \Phi\left(\frac{-u}{\sigma}\right) + \frac{\|\tau\|_1}{2\pi} \exp\left\{-\frac{u^2}{2\sigma^2}\right\}. \tag{6}$$

Corollary 3.3. (t-processes) *Let the conditions of Theorem 3.1 hold.*
a) Variable band: When $X(t)$ is a t-process with ν degrees of freedom, meaning $\mathcal{V} \sim \chi^2_\nu/\nu$, formula (4) in Theorem 3.1 leads to

$$\begin{aligned}\mathbb{E}[\varphi_{u,X}(t_0)] &= F_t(-u(t_0);\nu) + \int_0^1 \frac{\tau(t)}{2\pi}\left(1 + \frac{u(t)^2}{\nu} + \frac{u'(t)^2}{\nu\tau(t)^2}\right)^{-\nu/2} dt \\ &+ \int_0^{t_0} \frac{u'(t)}{2\pi\tau(t)}\left(1 + \frac{u(t)^2}{\nu}\right)^{-\nu/2-1} \frac{\Gamma((\nu+1)/2)\sqrt{(\nu+1)\pi}a(t)}{\Gamma((\nu+2)/2)} F_t\left(\frac{u'(t)}{a(t)};\nu+1\right) dt \\ &- \int_{t_0}^1 \frac{u'(t)}{2\pi\tau(t)}\left(1 + \frac{u(t)^2}{\nu}\right)^{-\nu/2-1} \frac{\Gamma((\nu+1)/2)\sqrt{(\nu+1)\pi}a(t)}{\Gamma((\nu+2)/2)} F_t\left(\frac{-u'(t)}{a(t)};\nu+1\right) dt,\end{aligned} \tag{7}$$

where $a(t)^2 := \nu\tau(t)^2(1 + u(t)^2/\nu)/(\nu + 1)$, Γ *denotes the gamma function, and* $F_t(.;\nu)$ *denotes the cumulative distribution function of a t-distribution with* ν *degrees of freedom.*

b) Constant band: If additionally $u(t) \equiv u$*, one obtains the t-version of the classic Kac-Rice formula*

$$\mathbb{E}[\varphi_{u,X}(0)] = F_t(-u;\nu) + \frac{||\tau||_1}{2\pi}\left(1 + \frac{u^2}{\nu}\right)^{-\nu/2}. \tag{8}$$

As with the Gaussian distribution, the t-expression does not have a closed form in general. However, in terms of numerically finding $u(t)$, the above formulations can be readily employed. Equivalently for more general elliptical distributions the critical value u can be found numerically, as long as one has a convenient form for $M_{\mathcal{V}}$.

Our second main result concerns statistical estimation of the bands in practice. Let $X_n = \hat{\theta}_n - \theta$ be the correctly (under the null hypothesis) centered estimator $\hat{\theta}_n$ of some functional parameter θ. Here, we assume that X_n is only asymptotically (large n) Gaussian/elliptical in $C^1[0,1]$. In practice, we usually do not know the dispersion function $c(t,s)$ and thus cannot immediately normalize to assume $\mathrm{Cov}(Z(t), Z(t)) = c(t,t) = 1$ as assumed in Theorem 3.1 which is without loss of generality due to the variable critical value functions. Instead, we assume that we have a sequence of uniformly consistent estimates $\hat{c}_n(t,t)$ of the dispersion $c(t,t)$ and its partial derivatives, where $c(t,t) > 0$.

Assumption 3.2. *Let* $c(t,s) = \mathrm{Cov}(Z(t), Z(s))$ *be the dispersion function of* X *and assume the limiting distribution (for large* n*) of* V *in* $X = VZ$ *is known. Assume that we have a sequence of estimators,* $\hat{c}_n(t,s)$*, for* $n = 1, 2, \ldots$ *satisfying,* $\sup_{0\le t\le 1} |\hat{c}_n(t,t) - c(t,t)| = o_P(1)$*,* $\sup_{0\le t\le 1} |\partial_1\hat{c}_n(t,t) - \partial_1 c(t,t)| = o_P(1)$*, and* $\sup_{0\le t\le 1} |\partial_{12}\hat{c}_n(t,t) - \partial_{12} c(t,t)| = o_P(1)$ *and that* $c(t,t) > 0$ *for all* $0 \le t \le 1$*.*

In cases where c can be estimated by averaging a random sample of stochastic processes, Theorem 1 in Dette and Kokot (2022) can be used to establish these convergence results.

Remark 1. If V has a finite and non-zero variance, then $c(t,s)$ can be estimated by $\hat{c}_n(t,s) = \mathrm{Var}(V)^{-1}\widehat{\mathrm{Cov}}_n(X(t), X(s))$. Since $c(t,s)$ is symmetric, $\partial_1\hat{c}_n(t,t) = \partial_2\hat{c}_n(t,t)$ and $\partial_1 c(t,t) = \partial_2 c(t,t)$. Moreover, note that we do not require estimation of the full dispersion, $c(t,s)$, only its diagonal, which is needed to normalize the process, and the derivatives along the diagonal, which are needed to estimate $\tau(t)$. Practically, this would usually require that $\hat{c}_n$ converges to c in say C^2. However, notice that $\partial_1 c(t,t) = \mathrm{Cov}(Z(t), Z'(t))$ and that $\partial_{12} c(t,t) = \mathrm{Var}(Z'(t)) = \tau(t)^2$. Therefore, in many settings, it is possible to estimate these covariance quantities more directly, as for instance in the arguably most relevant case, where $X(t)$ is formed by averaging a random sample of stochastic processes. Equation (17) in Example 2 gives an example of such a more direct estimation of τ by using that $\tau(t)^2 = \mathrm{Var}(Z'(t))$.

Remark 2. Given an estimator $\hat{c}_n$ we can normalize X_n such that, by Slutsky's lemma, it follows that $\tilde{X}_n(t) := c_n^{-1/2}(t,t)X_n(t) \xrightarrow{D} c^{-1/2}(t,t)X(t) = \tilde{X}(t)$ as $n \to \infty$. The process $\tilde{X}(t)$ fulfills then the assumptions of Theorem 3.1, so we need only plug in its corresponding $\tilde{\tau}(t)$ into Theorem 3.1 to find corresponding bands. By Assumption 3.2,

we can construct a sequence of uniformly consistent estimators $\tilde{\tau}_n(t) \to \tilde{\tau}(t)$. While this presents a minor notational annoyance, practically, it simply amounts to constructing the band from standardized data or using $\hat{c}_n(t,s)/\sqrt{\hat{c}_n(t,t), \hat{c}_n(s,s)}$ to find $u(t)$; see Examples 1 and 2 below.

Our other key assumption is that the space of potential bands, $\mathcal{U} \subseteq C^1_{a.e}[0,1]$, is convex, compact, and contains the constant functions (up to an appropriate bound). Compactness is commonly needed in estimation theory to ensure that the estimators are well behaved. The convexity combines with the constant functions to eliminate some pathological limiting problems. In particular, it ensures that if $u \in \mathcal{U}$ isn't on the boundary, then $u(t) + c$ will also be in $\mathcal{U}$ for c small. This helps ensure that no asymptotic band is "isolated", in the sense that one cannot construct a corresponding sequence of estimators for which it is the corresponding limit.

Theorem 3.2. *Let Assumptions 3.1 and 3.2 hold and fix $\alpha \in (0,1)$ and $t_0 \in [0,1]$. Define $\tilde{\tau}_n(t) = \partial_{12}\tilde{c}_n(t,s)$ where $\tilde{c}_n(t,s) := c_n(t,s)/\sqrt{c_n(t,t)c_n(s,s)}$ and define $\tilde{\tau}(t)$ analogously. Assume that $\{u \in \mathcal{U}\} \subseteq C^1_{a.e.}[0,1]$, where $\mathcal{U}$ is convex, compact, and contains the constant functions (up to an appropriate threshold to maintain compactness). For $\mathbb{E}[\varphi_{u,X}(t_0)]$ as in (4), for a general $\eta \in C[0,1]$ with $\eta(t) \geq 0$ for all $t \in [0,1]$, and for a non-negative real-valued slackness function $\varsigma : u \in \mathcal{U} \mapsto \varsigma(u) \in \mathbb{R}_{\geq 0}$ that is continuous for all $u \in \mathcal{U}$, define the function*

$$f(u,\eta) := \mathbb{E}[\varphi_{u,X}(t_0)] + \varsigma(u)$$

$$\text{and the sets} \quad S_n := f^{-1}_{\tilde{\tau}_n}(\alpha) = \{u \in \mathcal{U} : f(u,\tilde{\tau}_n) = \alpha/2\}$$

$$\text{and} \quad S := f^{-1}_{\tilde{\tau}}(\alpha) = \{u \in \mathcal{U} : f(u,\tilde{\tau}) = \alpha/2\}.$$

Then we have the following:

1. *The sets $\{S_n\}$ and S are nonempty and closed with probability 1.*
2. *If $\{u_n : n = 1, \dots\}$ is any sequence with $u_n \in S_n$, then $f(u_n, \tilde{\tau}) \xrightarrow{P} \alpha/2$ as $n \to \infty$.*
3. *$S_n \to S$ in Hausdorff distance[2] with probability one.*

The slackness function, $0 \leq \varsigma(u) < \infty$, facilitates the consideration of additional constraints like fairness constraints. Theorem 3.2 provides several important asymptotic results that tie consistency of the band to consistency of the functional parameter estimates. The overall message is that if one finds a $\hat{u}$ such that $f(\hat{u}, \tilde{\tau}_n) = \alpha/2$, then, with probability tending to one, $\hat{u}$ will be close to a u that satisfies $f(u, \tilde{\tau}) = \alpha/2$, which would be the target, but $\tilde{\tau}$ must be estimated. However, there is a certain awkwardness in stating and establishing these results since each $\alpha \in (0,1)$ leads to entire set of critical value functions one could use. The first result simply says, with probability one, there exists a non-empty set of candidate critical value functions using either the true, $\tilde{\tau}$, or estimate, $\tilde{\tau}_n$. The second result states that any sequence of critical value functions selected using the estimate, $\tilde{\tau}_n$ will asymptotically give the correct coverage. The third result states that, as sets, the set of critical value functions using the estimate, $\tilde{\tau}_n$, converges to the set one would obtain using the true $\tilde{\tau}$.

The set $\mathcal{U}$ is used to define the class of bands that one wants to consider. In the case of the classic Kac-Rice formula, one would take $\mathcal{U}$ to be the set of constant functions (up

[2] The Hausdorff distance is given by $d(S_n, S) = \max\left\{\sup_{u_n \in S_n} \inf_{u \in S} \|u_n - u\|, \sup_{u \in S} \inf_{u_n \in S_n} \|u_n - u\|\right\}$.

to some bound to ensure compactness). However, our theory allows for much more general compact sets containing non-constant, possibly infinite dimensional critical value functions. For example, if $\{e_i : i = 1, \ldots, m\} \subset C^1[0,1]$ is a finite collection of linearly independent functions, then we can take $\mathcal{U} = \text{span}\{e_1, \ldots, e_m\} \cap B_c(\delta)$, with m not necessarily finite and $B_c(\delta)$ being the closed ball of radius $\delta < \infty$ around constant critical value functions c.

3.2 Fair Critical Value Function $u^\star_{\alpha/2}$

Any critical value function $u_{\alpha/2} \in \mathcal{U}_{\alpha/2}(t_0)$ with $\mathcal{U}_{\alpha/2}(t_0) = \{u \in \mathcal{U} : \mathbb{E}[\varphi_{u,X}(t_0)] + \varsigma(u) = \alpha/2\}$, for given $\alpha \in (0,1)$ and $t_0 \in [0,1]$, leads to a valid $(1-\alpha) \times 100\%$ simultaneous confidence band $[\hat{\theta}_l, \hat{\theta}_u]$ as in (3). This generates a whole family of valid simultaneous confidence bands $\mathcal{F}_{\alpha,t_0} = \{[\hat{\theta}_l, \hat{\theta}_u] : u_{\alpha/2} \in \mathcal{U}_{\alpha/2}(t_0)\}$ and one can develop procedures for selecting specific simultaneous confidence bands $[\hat{\theta}^\star_l, \hat{\theta}^\star_u] \in \mathcal{F}_{\alpha,t_0}$ according to some constraint like minimal squared or absolute average band width or, as consided in the following, according to a fairness constraint.

Algorithm 1 below selects a fair critical value function $u^\star_{\alpha/2}$ that enables inference under the fairness constraint of false positive rate balance (Definition 2.1) over any given partition $0 = a_0 < a_1 < a_2 < \cdots < a_p = 1$. The following theorem states that the fair critical value function $u^\star_{\alpha/2}$, selected by Algorithm 1, allocates the fair proportional shares $(\alpha/2)\lambda([a_{j-1}, a_j]) = (\alpha/2)(a_j - a_{j-1})$ of the nominal (two-sided) significance level $\alpha/2$ to each sub-interval $[a_{j-1}, a_j]$, $j = 1, 2, \ldots, p$, and combinations thereof.

Lemma 3.2. (Fairness of $u^\star_{\alpha/2}$) *Let the conditions of Theorem 3.1 hold. Choose a significance level $\alpha \in (0,1)$ and consider a partition $0 = a_0 < a_1 < a_2 < \cdots < a_p = 1$ with $1 \le p < \infty$. The critical value function, $u^\star_{\alpha/2}$, selected by Algorithm 1, allocates the fair proportional shares $(\alpha/2)(a_j - a_{j-1})$ of the nominal (one-sided) significance level $\alpha/2$ to each local sub-process $\{X(t) : t \in [a_{j-1}, a_j]\}$, $j = 1, 2, \ldots, p$, such that for any $\mathcal{J} \subseteq \{1, 2, \ldots, p\}$*

$$P\left(\exists t \in \bigcup_{j \in \mathcal{J}} [a_{j-1}, a_j] : X(t) \ge u^\star_{\alpha/2}(t)\right) \le \sum_{j \in \mathcal{J}} \frac{\alpha}{2}(a_j - a_{j-1}). \tag{9}$$

Inverting Lemma 3.2 to the case of simultaneous confidence bands allows us to show that our simultaneous confidence bands fulfill the fairness constraint of false positive rate balance (Definition 2.1); see Proposition 3.2 below.

Algorithm 1. (Selecting the fair critical value function $u^\star_{\alpha/2}$)

Initialization: Choose a significance level $\alpha \in (0,1)$ and a partition $0 = a_0 < a_1 < a_2 < \cdots < a_p = 1$ with $1 \le p < \infty$. Let $u_p(t)$ denote the following initially constant (over $[a_0, a_1]$) piecewise linear function:

$$u_p(t) := c_1 + c_2(t - a_1)_+ + \cdots + c_p(t - a_{p-1})_+, \quad \text{where} \quad (x)_+ = \max\{x, 0\}.$$

Comment: We use $u_p(t)$ and $u'_p(t)$ for modelling $u(t)$ and $u'(t)$ in (4) of Theorem 3.1. By partitioning the integrals in (4) into separate integrals over subintervals $[a_{j-1}, a_j]$, $j = 1, \ldots, p$, we determine the coefficients c_j of u_p consecutively for each $j = 1, \ldots, q$.

For $j = 1$**:** Since $u_p(t) = c_1$ and $u_p'(t) = 0$ for all $t \in [a_0, a_1]$, the integrals in (4), restricted to $[a_0, a_1]$, simplify such that $c_1 > 0$ can be determined by solving

$$P\big(X(a_1) \geq u_p(a_1)\big) + \int_{a_0}^{a_1} \frac{\tau(t)}{2\pi} M_{\mathcal{V}}\left(-\frac{c_1^2}{2}\right)\, dt = \frac{\alpha}{2}\big(a_1 - a_0\big). \tag{10}$$

For $j = 2, 3, \ldots, p$ **do:**
Given $c_1, \ldots, c_{j-1}$, $u_p(t)$ and $u_p'(t)$ for $t \in [a_{j-1}, a_j]$ only depend on c_j such that

$$u_p(t) \equiv u_p(t; c_j) = c_1 + \sum_{\ell=2}^{j} c_\ell (t - a_\ell)_+ \quad \text{and} \quad u_p'(t) \equiv u_p'(t; c_j) = \sum_{\ell=2}^{j} c_\ell.$$

If j **is even,** determine the parameter $-\infty < c_j < \infty$ that solves

$$\begin{aligned} &P\big(X(a_{j-1}) \geq u_p(a_{j-1}; c_j)\big) + \int_{a_{j-1}}^{a_j} \frac{\tau(t)}{2\pi} M_{\mathcal{V}}\left(-\frac{1}{2}\left[u_p(t; c_j)^2 + \frac{u_p'(t; c_j)^2}{\tau(t)^2}\right]\right)\, dt \\ &- \int_{a_{j-1}}^{a_j} \int_0^\infty \frac{u_p'(t; c_j)}{2\pi\tau(t)} M_{\mathcal{V}}'\left(-\frac{1}{2}\left[u_p(t; c_j)^2 + \frac{(y + u_p'(t; c_j))^2}{\tau(t)^2}\right]\right)\, dy\, dt = \frac{\alpha}{2}\big(a_j - a_{j-1}\big). \end{aligned} \tag{11}$$

If j **is odd,** determine the parameter $-\infty < c_j < \infty$ that solves

$$\begin{aligned} &P\big(X(a_j) \geq u_p(a_j; c_j)\big) + \int_{a_{j-1}}^{a_j} \frac{\tau(t)}{2\pi} M_{\mathcal{V}}\left(-\frac{1}{2}\left[u_p(t; c_j)^2 + \frac{u_p'(t; c_j)^2}{\tau(t)^2}\right]\right)\, dt \\ &+ \int_{a_{j-1}}^{a_j} \int_0^\infty \frac{u_p'(t; c_j)}{2\pi\tau(t)} M_{\mathcal{V}}'\left(-\frac{1}{2}\left[u_p(t; c_j)^2 + \frac{(y - u_p'(t; c_j))^2}{\tau(t)^2}\right]\right)\, dy\, dt = \frac{\alpha}{2}\big(a_j - a_{j-1}\big). \end{aligned} \tag{12}$$

End do
Return: $u_{\alpha/2}^\star := u_p$

Imposing fairness constraints can make inference conservative: in tendency, the larger the number of fairness partitions, p, the more conservative the inference procedure becomes. Such costs of imposing fairness constraints are well known in the literature (Corbett-Davies et al., 2017). The expensive part in the construction of the fair critical value function $u_{\alpha/2}^\star$ are the additional correction terms, $P(X(a_j) \geq u(a_j))$, needed for odd $j = 3, 5, \ldots$ with $j \leq p$. While the expected Euler characteristic inequality in (1) with at most two, $1 \leq p \leq 2$, partitioning intervals $[0, a_1]$ and $[a_1, 1]$, with $a_1 \in [0, 1]$, requires only one correction term, $P(X(a_1) \geq u(a_1))$, larger numbers of fairness partitions, $p \geq 3$, require additional correction terms. Algorithm 1 is designed to minimize the fairness costs by using as few as possible corrections terms; namely, only one for each pair of partitioning intervals $[0, a_j]$ and $[a_j, 1]$, for odd $j = 1, 3, \ldots$ with $j \leq p$. This feature of Algorithm 1 allows us to quantify the price of fairness.

Proposition 3.1. (The price of fairness) *The expected Euler characteristic inequality when using the fair critical value function $u^\star_{\alpha/2}$ determined by Algorithm 1 is*

$$P\big(\exists t \in [0,1] : X(t) \geq u(t)\big) \leq \mathbb{E}[\varphi_{u^\star_{\alpha/2},X}(a_1)] + \varsigma_p(u^\star_{\alpha/2}) = \frac{\alpha}{2}, \tag{13}$$

$$\textit{where} \quad \varsigma_p(u^\star_{\alpha/2}) = \begin{cases} 0 & \textit{if } 1 \leq p \leq 2 \\ \sum_{\substack{3 \leq j \leq p \\ j\,:\,odd}} P\big(X(a_j) \geq u^\star_{\alpha/2}(a_j)\big) > 0 & \textit{if } p \geq 3. \end{cases}$$

That is, for $1 \leq p \leq 2$ partitioning intervals, the expected Euler characteristic inequality (13) based on the fair critical value function, $u^\star_{\alpha/2}$, does not require more slackness than the basic expected Euler characteristic inequality (1) based on a non-fair critical value function with $a_1 = t_0$. For $p \geq 3$ partitioning intervals, the fair critical value function, $u^\star_{\alpha/2}$, becomes costly as we need to consider $\#\{3 \leq j \leq p : j \text{ odd}\}$ additional correction terms.

3.3 Constructing Fair Confidence Bands

In this section we first consider two prototypical examples for constructing simultaneous confidence bands using the above described results and methods. Example 1 is a generic example which applies to any asymptotically Gaussian functional parameter estimator $\hat{\theta}$. Example 2 considers the practically relevant special case of t-distributed estimators, $\hat{\theta}$, of the mean function θ. Second, we introduce the formal fairness property of our simultaneous confidence bands.

Example 1. (Asymptotically Gaussian Estimators) Let $\{\hat{\theta}(t), 0 \leq t \leq 1\}$ be an asymptotically Gaussian (parametric or nonparametric) estimator of a functional parameter $\{\theta(t), 0 \leq t \leq 1\}$ such that

$$\sqrt{r_n}\left(\hat{\theta}(t) - \text{Bias}\left(\hat{\theta}(t)\right) - \theta(t)\right) \xrightarrow{D} \mathcal{N}(0, C_\theta(t,t)) \quad \text{for all} \quad t \in [0,1], \tag{14}$$

as $n \to \infty$, where $\sqrt{r_n}$ denotes the parametric, $\sqrt{r_n} = \sqrt{n}$, or nonparametric, $\sqrt{r_n} = o(\sqrt{n})$, convergence rate of $\hat{\theta}(t)$, Bias$(\hat{\theta}(t))$ denotes the known (or consistently estimable) possibly non-zero bias, and $C_\theta(t,t)$ denotes the known (or consistently estimable) covariance function. This situation is fairly general and arises, for instance, when estimating the mean or covariance function from sparse or dense functional data (Li and Hsing, 2010; Degras, 2011; Zhang and Wang, 2016), in eigenfunction/value estimation (Kokoszka and Reimherr, 2013; Kraus, 2019), in function-on-scalar regressions (Chen et al., 2016), in concurrent function-on-function regressions (Manrique et al., 2018), etc. Generally, as discussed in Choi and Reimherr (2018), the asymptotic normality in (14) requires *tightness* of the estimate to ensure that the convergence in distribution occurs in the strong topology. Typically, this rules out estimates from ill-posed inverse problems such as, for instance, the classic scalar-on-function regression estimators (cf. Cardot et al., 2007).

From (14) we have that

$$X_n(t) = \frac{\left(\hat{\theta}(t) - \text{Bias}\left(\hat{\theta}(t)\right) - \theta(t)\right)}{\sqrt{C_\theta(t,t)/r_n}} \xrightarrow{D} \mathcal{N}(0,1) \quad \text{for all} \quad t \in [0,1],$$

such that $X_n \xrightarrow{D} X$, where $X(t) \stackrel{D}{=} VZ(t)$ with $V \equiv \sigma = 1$ for all $t \in [0,1]$. That is, the covariance function of X equals its dispersion function $\mathrm{Cov}(X(t), X(s)) = c(t,s)$ with $c(t,t) = 1$ for all $t, s \in [0,1]$ and the only missing parameter required to compute the formula in Corollary 3.2 is the roughness parameter function $\tau(t) = (\partial_{12} c(t,t))^{1/2}$ which quantifies the multiple testing problem locally for each $t \in [0,1]$. Since $c(t,s) = \mathrm{Cov}(X(t), X(s))$ and $\mathrm{Cov}(X(t), X(s)) = \tilde{C}_\theta(t,s)$ with $\tilde{C}_\theta(t,s) = C_\theta(t,s)/\sqrt{C_\theta(t,t)C_\theta(s,s)}$ is follows that $\tau(t) = (\partial_{12}\tilde{C}_\theta(t,t))^{1/2}$ which is directly computable from the covariance function C_θ.

Plugging in the parameters $\sigma = 1$ and $\tau(t) = (\partial_{12}\tilde{C}_\theta(t,t))^{-1/2}$ into the Gaussian formula of Corollary 3.2 allows us to compute the fair critical value function, $u^\star_{\alpha/2}$, as described in Algorithm 1. The fair simultaneous confidence band for θ is then given by

$$\mathrm{FF}_z(t) = [\hat{\theta}^\star_l(t), \hat{\theta}^\star_u(t)] := \hat{\theta}(t) \pm u^\star_{\alpha/2}(t)\sqrt{C_\theta(t,t)/r_n} \quad \text{for all} \quad t \in [0,1]. \tag{15}$$

We denote this simultaneous confidence bands as Fast and Fair (FF) simultaneous confidence bands as it is considerably faster to compute than the alternative simulation based procedures. One-sided confidence bands, $[\hat{\theta}^\star_l, \infty]$ or $[-\infty, \hat{\theta}^\star_u]$, can be constructed from the one-sided version of $u^\star_\alpha$ which can be computed using Algorithm 1, but with substituting $\alpha/2$ by α. Usually, we do not know the covariance function C_θ or roughness parameter function τ and the have to plug in consistent estimators $\hat{C}_\theta$ and $\hat{\tau}$. The next example shows such estimators for the case where θ is the mean function.

Example 2. (Estimators of the Mean Function (Unknown Covariance)) Let us consider an iid sample $\{S_i\}_{i=1}^n$ from a Gaussian process $\mathcal{N}(\theta, C_\theta)$ with unknown mean function $\theta(t) = \mathbb{E}[S_i(t)]$ and unknown covariance function $C_\theta(t,s) = \mathrm{Cov}(S_i(t), S_i(s))$. We estimate the mean and covariance functions using the sample estimators $\hat{\theta}(t) = n^{-1}\sum_{i=1}^n S_i(t)$ and $\hat{C}_{\theta,n}(t,s) = (n-1)^{-1}\sum_{i=1}^n (S_i(t) - \hat{\theta}(t))(S_i(s) - \hat{\theta}(s))$, for $t, s \in [0,1]$. This setup yields that

$$X_n(t) = \frac{\hat{\theta}(t) - \theta(t)}{\sqrt{\hat{C}_\theta(t,t)/n}} \sim t_\nu \quad \text{with} \quad \nu = n-1 \quad \text{for all} \quad t \in [0,1],$$

such that $X_n(t) \stackrel{D}{=} V_n Z(t)$ with $V_n = \sqrt{\nu/\chi^2_\nu}$ and $Z(t) \sim \mathcal{N}(0,1)$ for all $t \in [0,1]$, where $\mathrm{Cov}(X_n(t), X_n(s)) = \mathrm{Var}(V_n)\,\mathrm{Cov}(Z(t), Z(s)) = (\nu/(\nu-2))c(t,s)$ for all $\nu > 2$ with $c(t,t) = 1$ for all $t, s \in [0,1]$. Moreover, straight forward derivations show that $\mathrm{Cov}(X_n(t), X_n(s)) = C_\theta(t,s)(C_\theta(t,t)C_\theta(s,s))^{-1/2}$. Thus, $c(t,s) = ((\nu-2)/\nu)\,\mathrm{Cov}(X_n(t), X_n(s))$ can be estimated consistently by $\hat{c}_n(t,s) = \big((\nu-2)/\nu\big)\hat{C}_{\theta,n}(t,s)\big(\hat{C}_{\theta,n}(t,t)\hat{C}_{\theta,n}(s,s)\big)^{-1/2}$ for $t, s \in [0,1]$, and the roughness parameter function $\tau(t)$ can be estimated consistently by

$$\hat{\tau}_1(t) = \big(\partial_{12}\hat{c}_n(t,t)\big)^{1/2}. \tag{16}$$

Alternatively, as explained in Remark 1, we can use the following equivalent estimator:

$$\hat{\tau}_2(t) = \Big(\widehat{\mathrm{Var}}\big(\tilde{S}'_1(t), \ldots, \tilde{S}'_n(t)\big)\Big)^{1/2} \quad \text{for} \quad t \in [0,1], \tag{17}$$

where $\widehat{\mathrm{Var}}\big(\tilde{S}_1'(t),\ldots,\tilde{S}_n'(t)\big) = (n-1)^{-1}\sum_{i=1}^n(\tilde{S}'(t) - n^{-1}\sum_{i=1}^n \tilde{S}'(t))^2$ denotes the empirical variance of the standardized and differentiated sample functions $\tilde{S}_i(t) = (S_i(t) - \hat{\theta}(t))/(\hat{C}_\theta(t,t))^{1/2}$. Plugging in the degrees of freedom $\nu = n-1$ and an estimate, $\hat{\tau}_1(t)$ or $\hat{\tau}_2(t)$, of $\tau(t)$ into the generalized Kac-Rice formula (7) in Corollary 3.3 allows us to compute the fair critical value function, $u^\star_{\alpha/2}$, as described in Algorithm 1. This then leads to the fair simultaneous confidence band

$$\mathrm{FF}_t(t) = [\hat{\theta}^\star_l(t), \hat{\theta}^\star_u(t)] := \hat{\theta}(t) \pm \hat{u}^\star_{\alpha/2}(t)\sqrt{\hat{C}_\theta(t,t)/n}, \tag{18}$$

where the hat in $\hat{u}^\star_{\alpha/2}(t)$ indicates that the critical value function is based on an estimate, $\hat{\tau}_1$ or $\hat{\tau}_2$, of the roughness parameter function τ.

Remark 3. In the case where the random sample functions $\{S_i\}_{i=1}^n$ are fully observed, the estimators $\hat{\tau}_1$ and $\hat{\tau}_2$ in (16) and (17) are equivalent. However, if the sample functions are only sparsely observed $\hat{\tau}_2$ becomes infeasible since S_i' cannot be computed from sparse functional data. In this case, an estimator similar to $\hat{\tau}_1$ can be used, where the sample estimator $\hat{C}_\theta$ has to be substituted by a nonparametric covariance estimator.

The following proposition formally describes the fairness property of the fair simultaneous confidence bands FF_z and FF_t in (15) and (18).

Proposition 3.2. (Fair confidence bands) *Let the conditions of Theorems 3.1 and 3.2 hold and let $u^\star_{\alpha/2}$ be selected by Algorithm 1 with respect to a given partition $0 = a_0 < a_1 < a_2 < \cdots < a_p = 1$ and a given $\alpha \in (0,1)$. Let $[\hat{\theta}^\star_l, \hat{\theta}^\star_u]$ denote the simultaneous confidence band FF_z in (15) or FF_t in (18). Then we have that*

$$P\left(\theta(t) \in [\hat{\theta}^\star_l(t), \hat{\theta}^\star_u(t)],\ \forall t \in \bigcup_{j\in\mathcal{J}}[a_{j-1}, a_j]\right) \geq 1 - \sum_{j\in\mathcal{J}} \alpha(a_j - a_{j-1}) \geq 1-\alpha \tag{19}$$

for any subset $\mathcal{J} \subseteq \{1,2,\ldots,p\}$. Thus, under H_0: $\theta = \theta_0$, the band $[\hat{\theta}^\star_l, \hat{\theta}^\star_u]$ fulfills the false positive rate balance Definition 2.1.

Proposition 3.2 simply inverts Lemma 3.2 to the case of simultaneous confidence bands. It states that the bands $[\hat{\theta}^\star_l, \hat{\theta}^\star_u]$ can be used as fair screening tools that allow to detect deviations from a null hypotheses under a balanced false positive rate across given subintervals $[a_{j-1}, a_j]$, $j = 1,2,\ldots,p$, and combinations thereof. This facilitates local interpretations over "regions of interest" $\mathrm{ROI} = \cup_{j\in\mathcal{J}}[a_{j-1}, a_j]$, $\mathcal{J} \subseteq \{1,2,\ldots,p\}$. While $[\hat{\theta}^\star_l, \hat{\theta}^\star_u]$ is a valid $\big(1-\alpha\big)\times 100\%$ simultaneous confidence band over $[0,1]$, it is also a valid $\big(1 - \sum_{j\in\mathcal{J}}\alpha(a_j - a_{j-1})\big)\times 100\%$ simultaneous confidence band over $\mathrm{ROI} = \cup_{j\in\mathcal{J}}[a_{j-1}, a_j]$. ROI analyses are common in the applied neuroimaging and biomechanics literature (Poldrack, 2007; Wager et al., 2008; Pataky et al., 2016; Wen et al., 2018); see also our application in Section 5.1.

4 Simulations

This section contains our simulation study to assess and illustrate the proposed fair simultaneous confidence bands. We focus on the special case of simultaneous inference for the mean function since this allows us to compare our bands with many alternative bands form the literature. Section 4.1 considers the case of fully observed random functions and Section 4.2 considers the case of fragmentary functions for which it is impossible to estimate the total covariance operator. We focus on the practically relevant case of *unknown* covariances, C_θ. All bands are computed based on the usual sample estimators $\hat{C}_\theta$ and $\hat{\theta}$ as defined in Example 2.

4.1 Fully Observed Functions

We generate samples of random functions $\{S_i\}_{i=1}^n \overset{\text{iid}}{\sim} \mathcal{N}(\theta, C_\theta)$ with mean function $\theta(t)$, $t \in [0,1]$, and covariance function $C_\theta(t,s)$, $t,s \in [0,1]$. The sample functions, S_i, are evaluated at 101 equidistant grid points $t = j/100$, $j = 0, \ldots, 100$, to emulate continuous functional data. We consider the following mean function scenarios based on shifting and scaling the polynomial mean function $\theta_0(t) = 10t^3 - 15t^4 + 6t^6$ by some $\Delta \geq 0$:

Mean1 $\theta(t) = \theta_0(t) + \Delta$ ('shift')
Mean2 $\theta(t) = \theta_0(t)(1+\Delta)$ ('scale')
Mean3 $\theta(t) = \theta_0(t) + \Delta \mathbb{1}\{(0 \leq t \leq 1/8)\}$ ('local')

The three mean function scenarios, Mean1-3, are shown in the upper row of Figure 3.

For the covariance operator, we take the Matérn covariance $C_\theta(t,s) = 0.25^2\big(2^{1-\upsilon}/\Gamma(\upsilon)\big)\big(\sqrt{2\upsilon}|t-s|\big)^{\upsilon} K_\upsilon\big(\sqrt{2\upsilon}|t-s|\big)$, where Γ is the gamma function, K_υ is the modified Bessel function of the second kind, and where $\upsilon \geq 0$ controls the roughness of the sample paths $\{S_i(t), 0 \leq t \leq 1\}$. We consider three different covariance scenarios:

Cov1 Stationary Matérn covariance C_θ with $\upsilon = 3/2$ ('smooth').
Cov2 Stationary Matérn covariance C_θ with $\upsilon = 1/2$ ('rough').
Cov3 Non-stationary Matérn-type covariance $C_\theta(t,s) = 0.25^2\big(2^{1-\upsilon_{ts}}/\Gamma(\upsilon_{ts})\big)\big(\sqrt{2\upsilon_{ts}}|t-s|\big)^{\upsilon_{ts}} K_{\upsilon_{ts}}\big(\sqrt{2\upsilon_{ts}}|t-s|\big)$, where $\upsilon_{ts} = 2 + \sqrt{\max(t,s)}(1/4 - 2)$ ('smooth to rough').

Cov1 results in smooth continuously differentiable sample functions as typical, for instance, for functional chemometric/spectrometric data (see Ferraty and Vieu, 2006, Ch. 2). Cov2 leads to rough non-differentiable sample functions as considered, for instance, in the literature on functional impact points (McKeague and Sen, 2010; Poß et al., 2020) and represents a violation of our smoothness Assumption 3.1. The non-stationary covariance Cov3 leads to sample functions with inhomogeneous roughness ('smooth to rough'). Sample paths, S_i, for each of the covariance scenario, Cov1-3, are shown in the upper row of Figure 2. Each of the covariance scenarios contains both local ($t \approx s$) and global ($t \ll s$ or $t \gg s$) dependencies. The lower dependency bounds are $\text{corr}(X(t), X(s)) \geq \text{corr}(X(0), X(1)) = 0.48$ for all $t,s \in [0,1]$ in case of Cov1, $\text{corr}(X(t), X(s)) \geq \text{corr}(X(0), X(1)) = 0.37$ for all $t,s \in [0,1]$ in case of Cov2, and $\text{corr}(X(t), X(s)) \geq \text{corr}(X(0), X(1)) = 0.29$ for all $t,s \in [0,1]$ in case of Cov3.

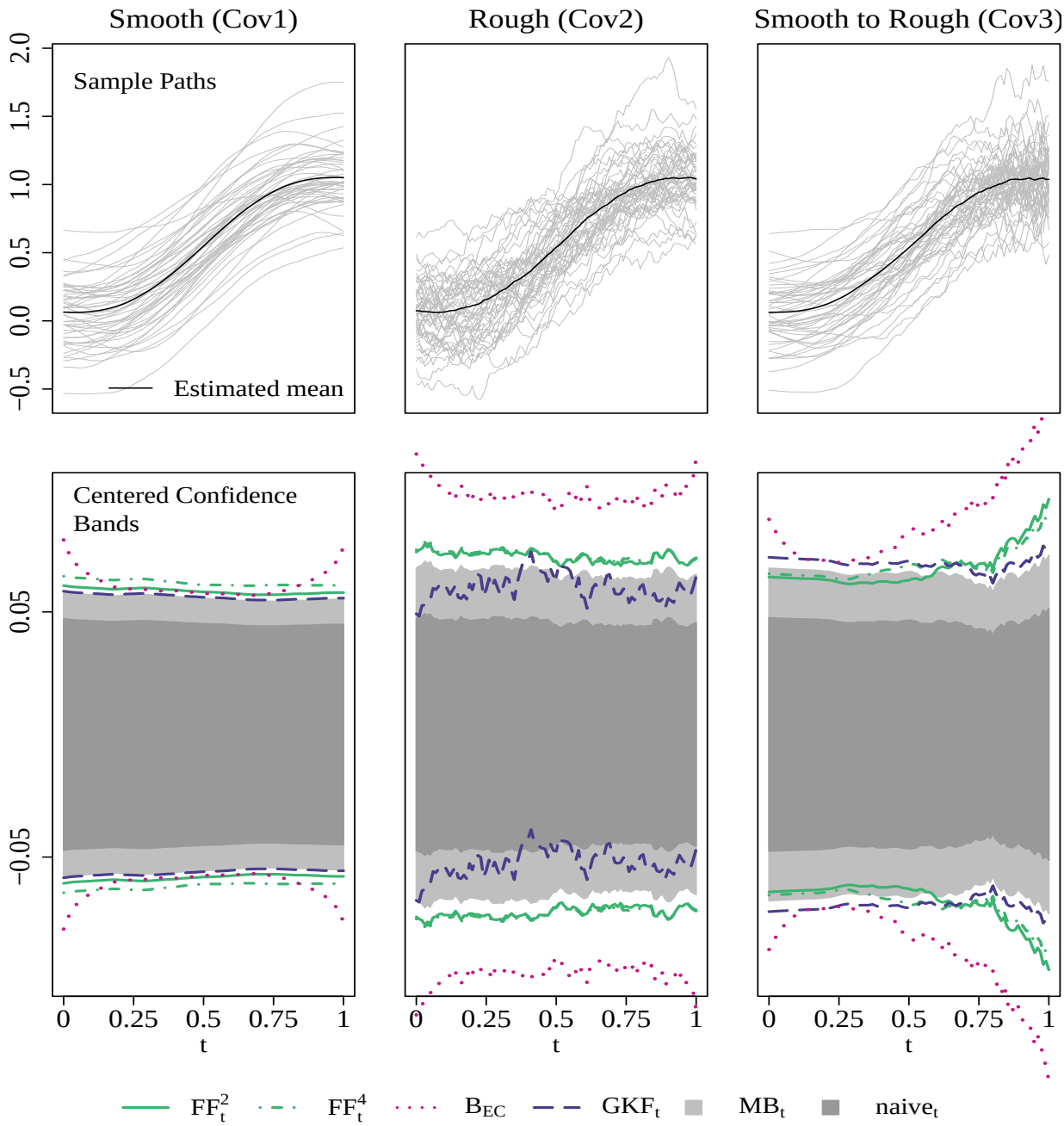

Figure 2: Upper Row: Sample paths and mean estimates. Lower Row: Centered 95% confidence bands, where centering by $\hat{\theta}$ is applied to improve the visual exposition.

Fair confidence bands and benchmark bands. The following list describes the specifications of our fair confidence bands and introduces the considered benchmark bands.

FF$_z^p$ and FF$_t^p$ Our Fast and Fair (FF) simultaneous confidence bands

$$\mathrm{FF}^p_{\mathrm{distr}}(t) = [\hat{\theta}^\star_l(t), \hat{\theta}^\star_u(t)] = \hat{\theta}(t) \pm \hat{u}^\star_{\alpha/2}(t)\big(\hat{C}_\theta(t,t)/n\big)^{1/2}, \quad t \in [0,1],$$

with distr $\in \{z, t\}$ denoting the distribution and $p \in \{1, 2, 4\}$ the number of equidistant domain partitions such as $a_0 = 0$, $a_1 = 1/4$, $a_2 = 2/4$, $a_3 = 3/4$, and $a_4 = 4/4$ in case of $p = 4$. The critical value function, $\hat{u}^{\star}_{\alpha/2}(t)$, is computed as described in Algorithm 1. For estimating the roughness parameter function, τ, we use $\hat{\tau}_2$ in (17). When $\hat{u}^{\star}_{\alpha/2}$ is based on the Gaussian formula (5) we write FF^p_z, and when $\hat{u}^{\star}_{\alpha/2}$ is based on the t-distribution formula (7) we write FF^p_t. The bands FF^1_z and FF^1_t use constant critical values, $u^{\star}_1(t) \equiv u^{\star}_1$, found by solving the equations (6) and (8), respectively.

$\mathbf{B_S}$ The simulation based bootstrap band proposed by Degras (2011) uses a constant critical value determined by a parametric bootstrap, where we use 10,000 bootstrap replications.

$\mathbf{B_{EC}}$ A modification of Scheffé's method to transform ellipsoid confidence regions into confidence bands proposed by Choi and Reimherr (2018).

$\mathbf{GKF_t}$ The simultaneous confidence band using the Gaussian kinematic formula of t-processes by Telschow and Schwartzman (2022).

$\mathbf{MB_t}$ The simultaneous confidence band based on a Rademacher multiplier-t bootstrap as proposed in Telschow and Schwartzman (2022).

IWT The interval-wise testing procedure proposed by Pini and Vantini (2017b) and further extended in Abramowicz et al. (2018).

$\mathbf{naive_t}$ The naive pointwise confidence interval based on the t-distribution without adjusting for multiple testing. (Only used as a visual reference.)

The IWT procedure is implemented in the R-package `fdatest` (Pini and Vantini, 2017a). The GKF_t band and the MB_t band are implemented in the R-package `SIRF` (Telschow, 2022). Our FF^p_t and FF^P_t bands and all remaining bands are implemented in our R-package `ffscb` (Liebl and Reimherr, 2022a). In the following, we report the results for the t-distribution based bands FF^p_t which take into account the estimation errors in $\hat{C}_\theta$. The results of the Gaussian versions, FF^p_z are summarized in the tables of Appendix B of the supplementary paper Liebl and Reimherr (2022b). In the case of small samples, the FF^p_z bands are typically too narrow; however, for large samples, the FF^p_z bands perform similarly to, and partially better than the FF^p_t bands.

Band shapes. The lower row of Figure 2 shows exemplary results of the (centered) confidence bands FF^2_t, FF^4_t, B_{EC}, GKF_t, MB_t, and naive_t for each of the covariance scenarios Cov1-3. The bands FF^1_t and $\mathrm{B_S}$ are omitted to improve the visual exposition: the omitted $\mathrm{B_S}$ band performs worse (too tight) than the alternative bootstrap based band MB_t, and the omitted FF^1_t band performs similar to, but more stable than the GKF_t band. As expected, the adaptive FF^2_t and FF^4_t bands do not show any adaptive shapes in the stationary covariance scenarios, Cov1 and Cov2, but they show adaptive shapes in the non-stationary covariance scenario, Cov3, where they are tight over the initial area with high positive correlations and wide over the final area with low correlations. The $\mathrm{B_{EC}}$ band shows a seemingly adaptive behavior, but (a) its shape cannot be interpreted, and (b) the band becomes very wide (conservative) in the case of rough processes. The rough covariance scenario Cov2 violates the smoothness Assumptions of FF^2_t, FF^4_t, and GKF_t, but while our fair bands remain stable, the GKF_t band gets unstable in this scenario. The FF^4_t band is wider (more conservative) than the FF^2_t band as expected due to the price of fairness property (Proposition 3.1).

Computational costs. Table 4 in the Appendix B of the supplementary paper Liebl and Reimherr (2022b) shows summary statistics of the computations times for all bands. While the computational costs of the non-simulation based bands, FF_z^p, FF_t^p, GKF_t, and B_{EC}, are all of the same order of magnitude[3], those of the simulation based bands, B_{S}, IWT, and MB_t, are ca. 5, 15, and 33 times larger.

Verifying Type-I Error Rate

To evaluate our fair confidence bands and to compare them with the above introduced alternative approaches, we use the duality of confidence bands with simultaneous hypothesis tests and test the hypothesis

$$\mathrm{H}_0\colon\ \theta(t) = \theta_0(t)\ \forall\ t \in [0,1] \quad \text{vs.} \quad \mathrm{H}_1\colon\ \exists t \in [0,1] \text{ s.t. } \theta(t) \neq \theta_0(t).$$

We reject H_0 if θ_0 is not covered by a band for at least one of grid points t. For the IWT procedure we reject H_0 if $p_{\mathrm{IWT}}(t) < \alpha$ for at least one of the grid points. As the significance level we choose $\alpha = 0.05$ which means that we consider 95% simultaneous confidence bands.

To verify the type-I error rates, we draw 50,000 Monte Carlo samples $\{S_i\}_{i=1}^n \overset{\text{iid}}{\sim} \mathcal{N}(\theta_0, C_\theta)$ for each covariance function scenario Cov1-3. We examine a challenging small sample size of $n = 15$ and a large sample size $n = 100$. Since the IWT procedure is computationally very expensive we had to reduce the number of Monte Carlo replications for this method to 5,000.[4] Table 1 contains the empirical type-I error rates and we can summarize the results as following:

(a) All bands are able to keep the nominal α-level in all scenarios and sample sizes, except for the B_{S} band which is too tight leading to over-rejections in all scenarios.
(b) Among the methods that are able to keep the α-level, the type-I error rates of the FF_t^1 and MB_t bands are closest to $\alpha = 0.05$.
(c) The B_{EC} band is very conservative for large sample sizes and rough processes (Cov2-3).
(d) The larger p the more conservative the FF_t^p bands become due to the price of fairness property (Proposition 3.1).

Verifying False Positive Rate Balance

In this section, we assess the interpretable fairness property (Proposition 3.2) of our FF_t^p bands. To evaluate the fairness constraints of our bands, we use again the duality of confidence bands with hypothesis tests ($\alpha = 0.05$), but this time we consider interval specific hypotheses:

$$\mathrm{H}_0^j\colon\ \theta(t) = \theta_0(t)\ \forall\ t \in [a_{j-1}, a_j] \quad \text{vs.} \quad \mathrm{H}_1^j\colon\ \exists t \in [a_{j-1}, a_j] \text{ s.t. } \theta(t) \neq \theta_0(t), \quad j = 1, \ldots, p$$

where we reject H_0^j if θ_0 is not covered by a band for at least one grid point t in $[a_{j-1}, a_j]$. The following interval scenarios are considered:

[3] Between 0.025 sec and 0.05 sec on a standard laptop computer.
[4] Abramowicz et al. (2018) use only 1,000 Monte Carlo replications.

Table 1: Type-I error rates.

	$n = 15$			$n = 100$		
Band	Cov1	Cov2	Cov3	Cov1	Cov2	Cov3
FF_t^1	0.051	0.038	0.044	0.048	0.033	0.038
FF_t^2	0.037	0.036	0.038	0.036	0.029	0.034
FF_t^4	0.025	0.032	0.031	0.025	0.025	0.029
B_{EC}	0.051	0.036	0.035	0.027	0.001	0.006
B_{S}	0.088	0.122	0.120	0.055	0.061	0.059
MB_t	0.039	0.036	0.036	0.048	0.050	0.048
GKF_t	0.037	0.018	0.023	0.046	0.024	0.029
IWT	0.036	0.028	0.027	0.036	0.029	0.028

Nominal type-I error rate: $\alpha = 0.05$

4 Intervals: $[0, 1/4]$, $[1/4, 2/4]$, $[2/4, 3/4]$, and $[3/4, 1]$ with fair nominal significance level for each interval: $\alpha(a_j - a_{j-1}) = \alpha/4$, $j \in \{1, 2, 3, 4\}$.
2 Intervals: $[0, 1/2]$ and $[1/2, 1]$ with fair nominal significance level for each interval: $\alpha(a_j - a_{j-1}) = \alpha/2$, $j \in \{1, 2\}$.

Table 2 shows the empirical type-I error rates of our FF_t^p bands for $p \in \{1, 2, 4\}$ for the case of for $n = 100$ and the challenging non-stationary covariance scenario Cov3, where adaptivity matters. The results for all other bands and all other covariance scenarios, Cov1 and Cov2, and sample sizes are reported in the tables of Appendix B of the supplementary paper Liebl and Reimherr (2022b); however, the results for all scenarios can be summarized as following:

(a) The FF_t^2 and the FF_t^4 band keep the nominal interval specific type-I error rates in the 2 interval and the 4 interval scenario, respectively.
(b) The FF_t^4 band is able to keep the nominal interval specific type-I error rates in *both* interval scenarios. This is in accordance with Proposition 3.2 since the scenarios are nested.
(c) The non-adaptive FF_t^1 band is only able to keep the nominal type-I error rates over $[0, 1]$ since Cov3 is a non-stationary covariance scenario. (The same applies to all benchmark bands as shown in Appendix B of the supplementary paper Liebl and Reimherr (2022b).)

Comparing Power

For comparing the power of the hypothesis tests, we generate data using the mean function scenarios Mean1-3 with increasingly large perturbations $\Delta > 0$. The hypothetical mean function, θ_0, and the different true mean functions, θ, are shown in the upper row of Figure 3. For the small sample szenario, $n = 15$, we consider the perturbations $\Delta \in \{0.05, 0.15, 0.25, 0.35, 0.45\}$ and for the large sample szenario, $n = 100$, we consider the smaller perturbations $\Delta \in \{0.02, 0.04, 0.06, 0.08, 0.1\}$. Each of these mean function perturbations is considered for each of the covariance scenarios Cov1-3. We reduce the

Table 2: Checking false positive rate balance for $n = 100$ and covariance scenario Cov3.

	4 Intervals $\alpha/4 = 0.0125$					2 Intervals $\alpha/2 = 0.025$			1 Interval $\alpha = 0.05$	
Band	$[0, \frac{1}{4}]$	$[\frac{1}{4}, \frac{2}{4}]$	$[\frac{2}{4}, \frac{3}{4}]$	$[\frac{3}{4}, 1]$	Check	$[0, \frac{1}{2}]$	$[\frac{1}{2}, 1]$	Check	$[0, 1]$	Check
FF_t^1	0.007	0.009	0.013	0.025	✗	0.012	0.031	✗	0.038	✓
FF_t^2	0.015	0.018	0.016	0.009	✗	0.024	0.021	✓	0.034	✓
FF_t^4	0.012	0.013	0.011	0.011	✓	0.017	0.018	✓	0.029	✓

number of Monte Carlo repetitions from 50,000 to 10,000, except for the computationally costly IWT procedure where we keep the 5,000 repetitions as used above.

The lower row of Figure 3 shows the power plots for the large sample, $n = 100$, and the challenging non-stationary covariance scenario Cov3. The legends are ranked according to the methods' average powers over $\Delta > 0$. The results of the $\mathrm{B_S}$ band and the FF_t^4 band are omitted to improve the visual exposition, but all results for all scenarios can be found in Appendix B of the supplementary paper Liebl and Reimherr (2022b). The common conclusion is as following:

(a) In scenario Mean1, all bands show similar power curves, except for the $\mathrm{B_{EC}}$ band which has a relatively low power.
(b) In scenario Mean2, the bands MB_t, FF_t^1, GKF_t, and FF_t^2 show similar power curves, except for the IWT procedure and the $\mathrm{B_{EC}}$ band which have relatively low powers.
(c) In scenario Mean3, the band FF_t^2 has highest power since the fairness adaptation facilitates the detecting the local violation of the null hypothesis which is located in the initial area with high correlations. The IWT method of Pini and Vantini (2017b) is essentially not able to detect the considered local violation of the null hypothesis (Mean3).
(d) In all scenarios, the power of the bootstrap band, $\mathrm{B_S}$, (not shown in Figure 3) is inflated as this band cannot keep the nominal α-level (see Table 1).

4.2 Fragmentary Functions

In this section, we consider fragmentary functional data generated from the mean and covariance scenarios, Mean1-3 and Cov1-3. In a first step, we draw random sample functions $\{S_i\}_{i=1}^n \overset{\text{iid}}{\sim} \mathcal{N}(\theta, C_\theta)$ and evaluate them at 101 equidistant grid points in $[0, 1]$ as in Section 4.1. In a second step, we fragment the curves by declaring all grid points $t \notin [A_i, B_i] \subset [0, 1]$ as missing, where $B_i = A_i + 0.4$ and $A_i = \tilde{A}_i/100$ with $\{\tilde{A}_i\}_{i=1}^n \overset{\text{iid}}{\sim} \mathrm{BeB}(N = 60, \alpha = 0.3, \beta = 0.3)$ and with $\mathrm{BeB}(N, \alpha, \beta)$ denoting the discrete Beta-Binomial distribution. This leads to a challenging case of fragmentary functions, S_i, since no function covers the total domain $[0, 1]$. Consequently, the covariance function, C_θ, can only be estimated over a band along the diagonal, namely, over $\{(t, s) \in [0, 1]^2 : |t - s| \leq 0.4\} \subset [0, 1]^2$. We consider a relatively large sample size of $n = 500$ since fragmenting the functions reduces the local sample size, $n_t \leq n$, considerably. In our simulation study, the local sample size varied between $n_t = 44$

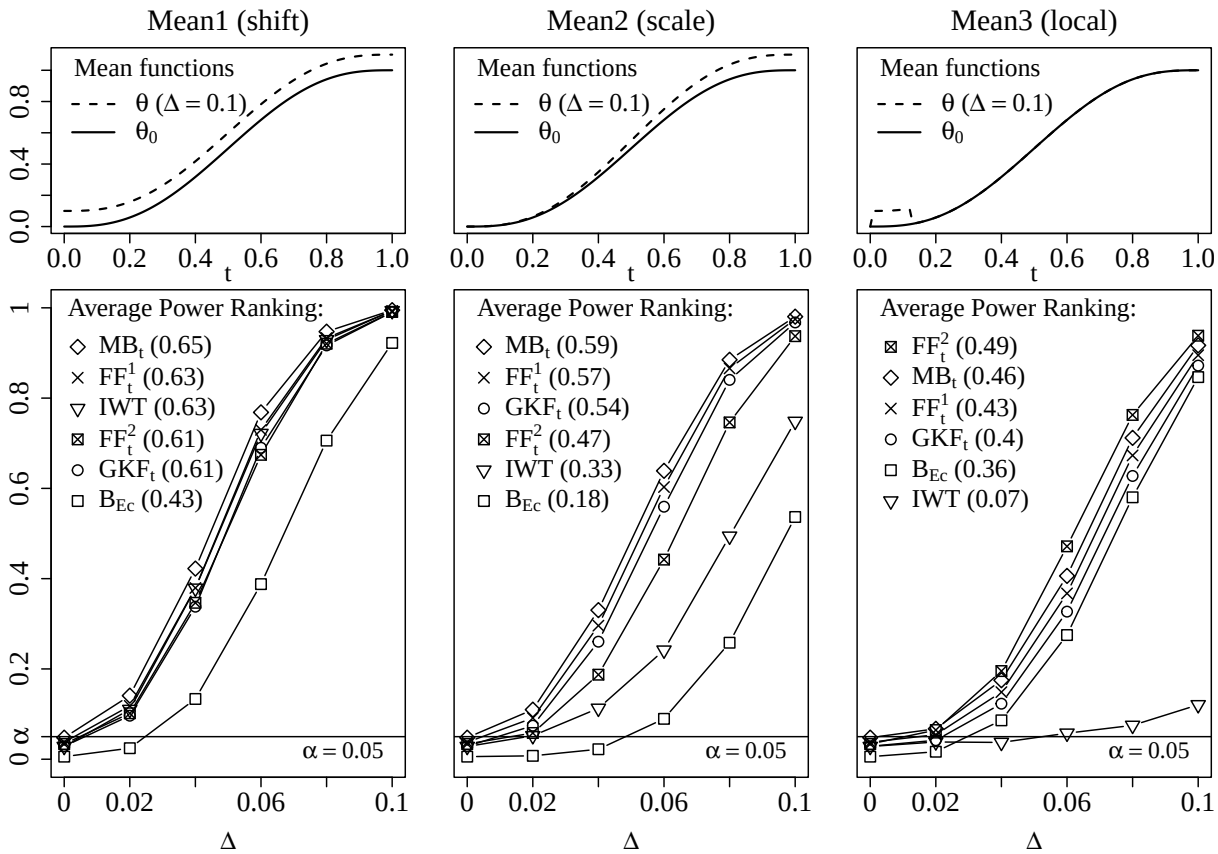

Figure 3: Upper Row: Different mean function scenarios Mean 1-3. Lower Row: Power comparisons for the 'smooth to rough' covariance scenario Cov3 and sample size $n = 100$. The average power values are averages over all mean perturbations $\Delta > 0$.

and $n_t = 332$. The upper row in Figure 4 shows exemplary fragmented sample paths for each of the covariance scenarios Cov1-3.

For estimating the mean, θ, and covariance, C_θ, we use the following estimators for fragmentary functional data:

$$\hat{\theta}_{\text{frag}}(t) = \frac{I_1(t)}{n_t} \sum_{i=1}^{n} O_i(t)\, S_i(t),$$

$$\hat{C}_{\text{frag}}(t,s) = \frac{I_2(t,s)}{n_{ts}} \sum_{i=1}^{n} O_i(t) O_i(s) \left(S_i(t) - \hat{\theta}_{\text{frag}}(t)\right)\left(S_i(s) - \hat{\theta}_{\text{frag}}(s)\right),$$

with $n_t = \sum_{i=1}^{n} O_i(t)$ and $n_{ts} = \sum_{i=1}^{n} O_i(t)O_i(s)$, where $O_i(t) = \mathbb{1}\{S_i(t) \text{ is not missing}\}$. The operators $I_1(t) = \mathbb{1}\{\sum_{i=1}^{n} O_i(t) > 0\}$ and $I_2(t,s) = \mathbb{1}\{\sum_{i=1}^{n} O_i(t)O_i(s) > 0\}$ prevent divisions by zero through defining $0/0 :=$ `Missing`. Recent works using these estimators are, for instance, Delaigle and Hall (2013), Kraus (2015), and Liebl and Rameseder (2019).

To the best of our knowledge, the following fragment versions, $\text{FF}^p_{\text{frag}}$, or our FF bands are the only simultaneous confidence bands that can be used in the challenging case of

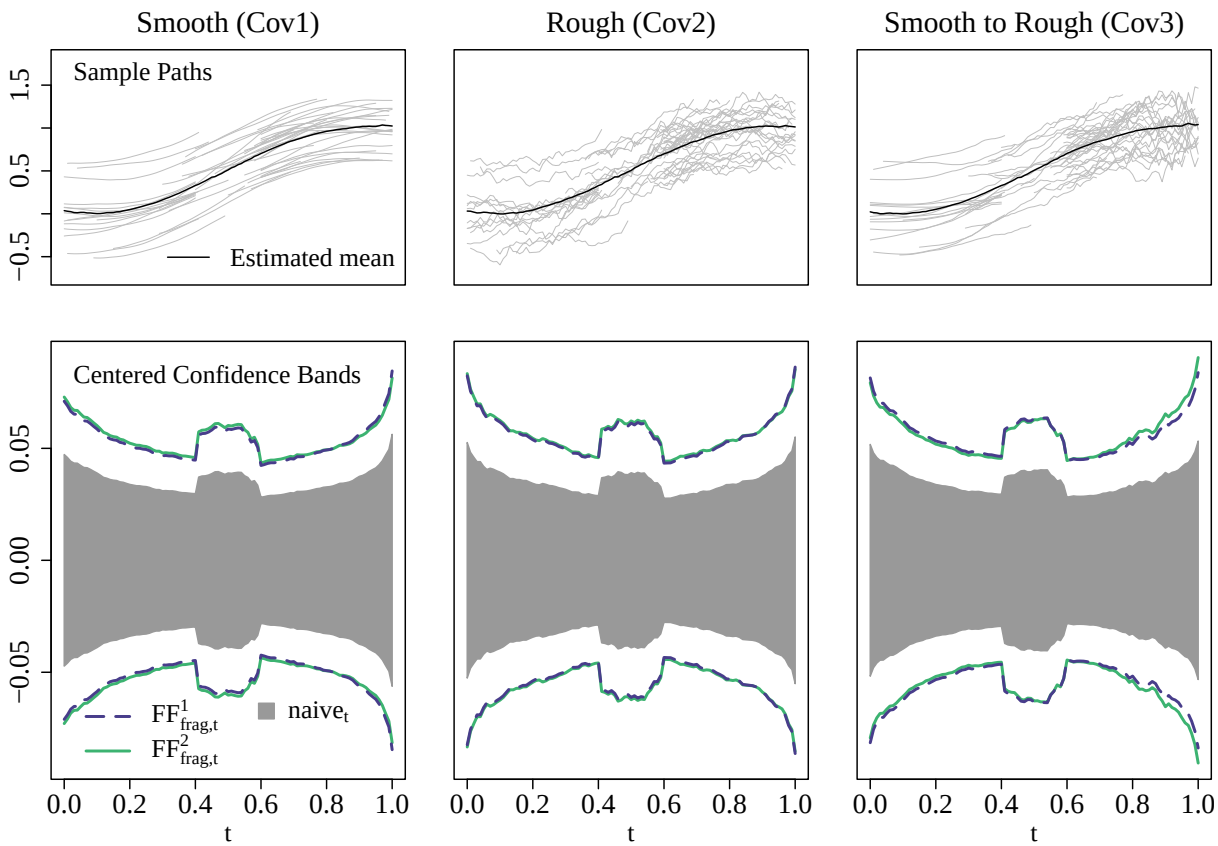

Figure 4: Upper Row: Sample paths and mean estimates, $\hat{\theta}_{\text{frag}}$. Lower Row: Centered 95% confidence bands, where centering by $\hat{\theta}_{\text{frag}}$ is applied to improve the visual exposition.

fragmentary functional data which prevents estimating the full covariance:

$$\text{FF}^p_{\text{frag,distr}}(t) = [\hat{\theta}^\star_{\text{frag},l}(t), \hat{\theta}^\star_{\text{frag},u}(t)] = \hat{\theta}_{\text{frag}}(t) \pm \hat{u}^\star_{\text{frag},\alpha/2}(t)\big(\hat{C}_{\text{frag}}(t,t)/n_t\big)^{1/2}, \quad t \in [0,1],$$

with distr $\in \{z, t\}$, and where we focus here on $p \in \{1, 2\}$. As an estimator of the roughness parameter function, τ, we use the following fragment version of $\hat{\tau}_1$ in (16):

$$\hat{\tau}_{\text{frag}}(t) = \big(\partial_{12}\hat{c}_{\text{frag}}(t,t)\big)^{1/2} \quad \text{with} \quad \hat{c}_{\text{frag}}(t,s) = \hat{C}_{\text{frag}}(t,s)\big(\hat{C}_{\text{frag}}(t,t)\hat{C}_{\text{frag}}(s,s)\big)^{-1/2}$$

for $t, s \in [0, 1]$. This estimator is feasible even when the covariance estimate $\hat{C}_{\text{frag}}(t, s)$ can only be computed at the diagonal and a narrow band along the diagonal. For a given $\hat{\tau}_{\text{frag}}$ estimate, $\hat{u}^\star_{\text{frag},\alpha/2}$ can be computed using Algorithm 1 as in the case of fully observed functional data. As degrees of freedom of the t-process we use $\nu = \min_t(n_t) - 1$. We test the hypothesis H_0: $\theta(t) = \theta_0(t)\ \forall\, t \in [0, 1]$ vs. H_1: $\exists t \in [0, 1]$ s.t. $\theta(t) \neq \theta_0(t)$ at the nominal significance level $\alpha = 0.05$.

The lower row of Figure 4 shows examples of the 95% simultaneous confidence bands $\text{FF}^1_{\text{frag},t}$ and $\text{FF}^2_{\text{frag},t}$. It is striking that the shapes of the bands are essentially equivalent to each other—even in the case of the non-stationary covariance scenario Cov3. The reason

for this is that the missingness process, O_i, introduces an additional source of roughness into the covariance structure of the estimator $\hat{\theta}_{\text{frag}}$. This additional roughness component becomes here the dominating roughness component leading to equivalent band shapes since we consider the same missingness process for all covariance scenarios Cov1-3. The unusual shape of the bands is due to the varying local sample sizes: n_t is relatively small at the boundaries and over $[0.4, 0.6]$ which makes the bands wide at the boundaries of $[0, 1]$ and causes the bump shape over $[0.4, 0.6]$.

Table 3: The type-I error rates and power values of the fragment bands $\text{FF}^1_{\text{frag},t}$ and $\text{FF}^2_{\text{frag},t}$ in the non-stationary covariance scenario Cov3.

		H_0	H_1					Avg.
Mean	Band	$\Delta = 0$	$\Delta = 0.02$	$\Delta = 0.04$	$\Delta = 0.06$	$\Delta = 0.08$	$\Delta = 0.1$	Power
Mean1	$\text{FF}^1_{\text{frag},t}$	0.042	0.243	0.798	0.992	1.000	1.000	0.81
Mean1	$\text{FF}^2_{\text{frag},t}$	0.041	0.244	0.803	0.992	1.000	1.000	0.81
Mean2	$\text{FF}^1_{\text{frag},t}$	0.042	0.130	0.486	0.855	0.987	0.999	0.69
Mean2	$\text{FF}^2_{\text{frag},t}$	0.042	0.119	0.455	0.835	0.984	0.999	0.68
Mean3	$\text{FF}^1_{\text{frag},t}$	0.043	0.074	0.254	0.620	0.908	0.992	0.57
Mean3	$\text{FF}^2_{\text{frag},t}$	0.041	0.078	0.273	0.645	0.919	0.994	0.58

Table 3 summarizes the empirical type-I error rates and power values of the fragment bands $\text{FF}^1_{\text{frag},t}$ and $\text{FF}^2_{\text{frag},t}$ in the challenging non-stationary covariance scenario Cov3; the results for all other scenarios are summarized in the tables of Appendix B of the supplementary paper Liebl and Reimherr (2022b). They all lead to the same conclusions; namely, that the $\text{FF}^1_{\text{frag},t}$ and $\text{FF}^2_{\text{frag},t}$ bands perform very similar. Both are able to keep the nominal α-level at comparable type-I error rates and both show similar power values.

5 Applications

In this section we demonstrate the use of our fair confidence bands in two case studies. Section 5.1 considers an example from sports biomechanics where scientists often collect and analyze fully observed functional data. Section 5.2 considers the case of fragmentary growth curves where the estimation of the total covariance function is impossible.

5.1 Fully Observed Functions

Empirical research in biomechanics uses functional data for describing human (or animal) movements over time (Vanrenterghem et al., 2012; Hamacher et al., 2016; Warmenhoven et al., 2019). The data shown in Figure 5 comes from a sports biomechanics experiment designed to assess the differences between extra cushioned vs. normal cushioned running shoes. The experiment was conducted at the biomechanics lab of the German Sport University, Cologne. A sample of $n = 18$ recreational runners with a habitual heel strike running

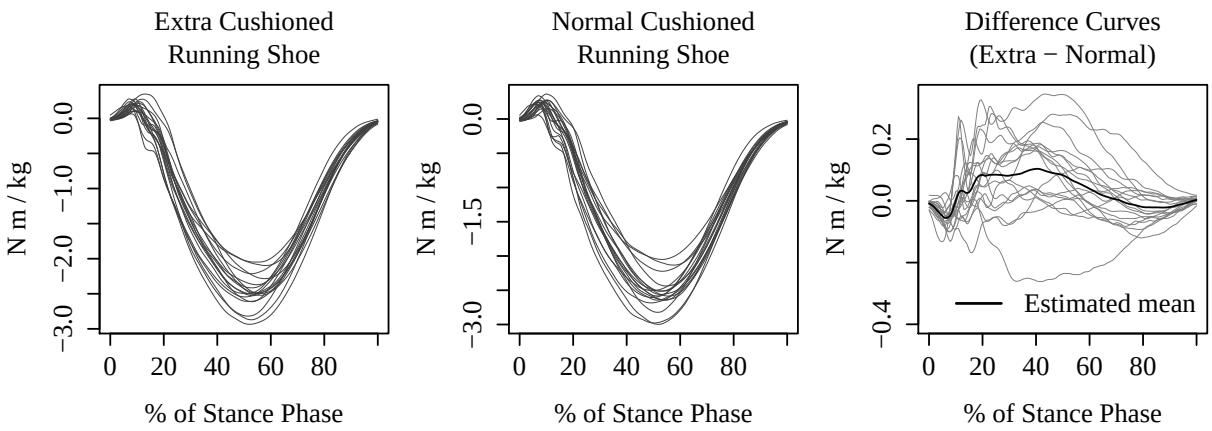

Figure 5: Left and Middle Plot: Paired sample of $n = 18$ torque curves measured at the ankle joint in sagittal pane. Right Plot: Sample of $n = 18$ difference-curves computed from the paired sample.

pattern were included into the experiment. The outcome of interest are torque curves describing the temporal torques acting at the right ankle joint in sagittal pane during the stance phase of one running stride.[5] The torques are measured in Newton metres (N m) standardized by the bodyweights (kg) of the participants. At $t = 0\%$ the heel strikes the ground and at $t = 100\%$ the forefoot leaves the ground. Further details on the data can be found in Liebl et al. (2014).

For each participant there are two torque curves—one when running with a certain extra cushioned running shoe and another when running with a certain normal cushioned running shoe (left and middle plot of Figure 5). In order to test for differences in the mean torque curves, we consider the pairwise difference-curves (extra minus normal cushioned) shown in the right plot of Figure 5 and test the hypotheses H_0: $\theta(t) = 0\ \forall t \in [0\%, 100\%]$ vs. H_1: $\exists t \in [0\%, 100\%]$ s.t. $\theta(t) \neq 0$. To conduct this test, we use the fair 95% simultaneous confidence band FF_t^5 with $p = 5$ equidistant domain partitions $a_0 = 0$, $a_1 = 20\%$, $a_2 = 40\%$, $a_3 = 60\%$, $a_4 = 80\%$, and $a_5 = 100\%$ as indicated by the tick marks in Figure 5. A particular interest lies on the initial ROI $= [0, 20\%]$ which corresponds to the heel strike phase where the extra cushioning is supposed to have a particular effect. We compare our adaptive fair FF_t^5 band with the non-fair, non-adaptive FF_t^1 band.

The upper-left plot in Figure 6 shows the estimate of the roughness parameter function, τ. The roughness is relatively large over the initial interval $[0\%, 20\%]$, relatively low over $[20\%, 80\%]$, and increases again over the final interval $[80\%, 100\%]$. The lower-left plot demonstrates how the adaptive fair critical value function takes into account this roughness pattern. In contrast, the non-fair, non-adaptive constant critical value of the FF_t^1 band remains constant over the whole domain.

[5]The stance phase is the phase of a running stride during which the foot has ground contact. The individual stance phases are standardized to a common unit interval $[0\%, 100\%]$ using simple linear affine time transformations. This simple 'warping' method leads to a good alignment of the data and is common in the biomechanics literature.

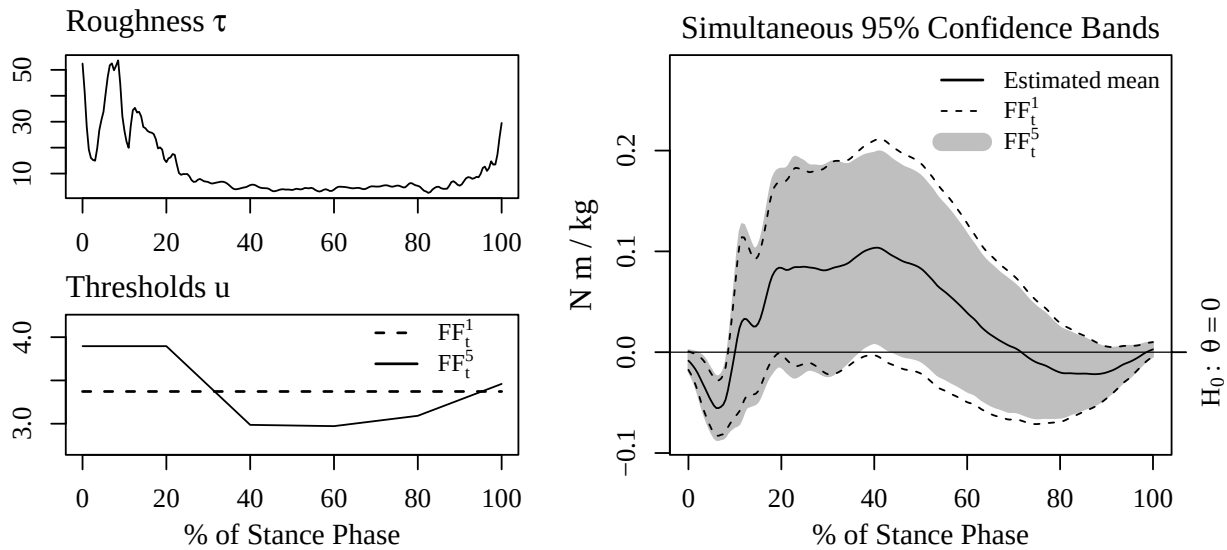

Figure 6: Upper-Left Plot: Estimate of the roughness parameter function, τ. Lower-Left Plot: Adaptive fair critical value function of the FF_t^5 band and non-adaptive constant critical value of the FF_t^1 band. Right Plot: Simultaneous 95% confidence bands.

The right plot of Figure 6 shows the simultaneous 95% confidence bands. The FF_t^5 band is initially wider than the FF_t^1 band, but tighter over the remaining parts. Both bands show significant differences over the initial stance phase from 2% to 8%. The FF_t^5 band shows an additional significant difference over the middle stance phase from 37% to 44%. The fair FF_t^5 band can also be interpreted locally (see Proposition 3.2): over the ROI $= [0\%, 20\%]$, the FF_t^5 band corresponds to a $1 - \big(\alpha(20\% - 0\%)\big) = 99\%$ simultaneous confidence band.

5.2 Fragmentary Functional Data

The bone mineral acquisition data were first described in Bachrach et al. (1999) and further analyzed by James and Hastie (2001), Delaigle and Hall (2013), and Delaigle and Hall (2016).[6] The spinal Bone Minearal Density (BMD) measurements (g/cm^2) were taken for each individual at two to four time points over short time intervals; therefore, linear interpolations of the measurements give good approximations of the underlying smooth mineral acquisition growth processes. The left plot in Figure 7 shows the fragmentary growth curves of $n_{\mathrm{f}} = 140$ female (f) and $n_{\mathrm{m}} = 113$ male (m) participants after restricting the data to a common domain (9.6 to 24.5 years of age) and at least two measurements.

We test the hypotheses of equal means H_0: $\theta_{\mathrm{f}}(t) - \theta_{\mathrm{m}}(t) = 0\ \forall t \in [9.6\,\mathrm{yr}, 24.5\,\mathrm{yr}]$ vs. H_1: $\exists t \in [9.6\,\mathrm{yr}, 24.5\,\mathrm{yr}]$ s.t. $\theta_{\mathrm{f}}(t) \neq \theta_{\mathrm{m}}(t)$ using the following two-sample (2S) version of our FF simultaneous confidence band,

$$\mathrm{FF}^{p,2\mathrm{S}}_{\mathrm{frag},t}(t) = \big(\hat\theta_{\mathrm{f}}(t) - \hat\theta_{\mathrm{m}}(t)\big) \pm \hat u^{\star\,2\mathrm{S}}_{\mathrm{frag}\,\alpha/2}(t)\big(\hat C^{2\mathrm{S}}_{\mathrm{frag}}(t,t)\big)^{1/2} \quad \text{with} \quad p = 2 \quad \text{and}$$
$$\hat C^{2\mathrm{S}}_{\mathrm{frag}}(t,s) = \big((n^{\mathrm{f}}_{ts} - 1)\hat C^{\mathrm{f}}_{\mathrm{frag}}(t,s) + (n^{\mathrm{m}}_{ts} - 1)\hat C^{\mathrm{m}}_{\mathrm{frag}}(t,s)\big)/(n^{\mathrm{f}}_{ts} + n^{\mathrm{m}}_{ts} - 2)$$

[6]The data is freely available at the companion website of the textbook of Friedman et al. (2001).

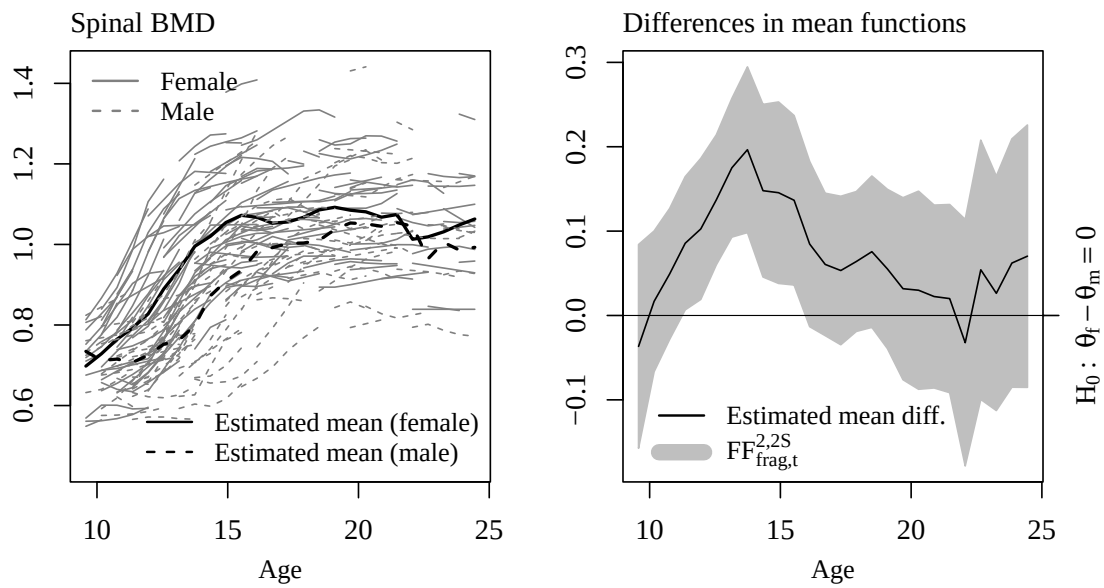

Figure 7: Left Plot: Fragmentary spinal bone mineral density aquisition curves. Right Plot: Simultaneous 95% confidence band, FF^2_t, for the difference mean function.

denoting the weighted average of the sample covariances, $\hat{C}^{\mathrm{f}}_{\mathrm{frag}}$ and $\hat{C}^{\mathrm{m}}_{\mathrm{frag}}$, with $n^{\mathrm{m}}_{ts} = \sum_{i=1} O^{\mathrm{m}}_i(t)O^{\mathrm{m}}_i(s)$, $n^{\mathrm{f}}_{ts} = \sum_{i=1} O^{\mathrm{f}}_i(t)O^{\mathrm{f}}_i(s)$, and $O^{\mathrm{f}}_i(t)$ and $O^{\mathrm{m}}_i(t)$ as defined in Section 4.2. The short fragments of the growth curves allow only an estimation of the covariances, $\hat{C}^{\mathrm{f}}_{\mathrm{frag}}$ and $\hat{C}^{\mathrm{m}}_{\mathrm{frag}}$, over narrow bands along the diagonal (see Figure 9 in Appendix B of Liebl and Reimherr (2022b)). The critical value function, $\hat{u}^{\star\,2\mathrm{S}}_{\mathrm{frag}\,\alpha/2}$, is computed using Algorithm 1 based on the significance level $\alpha = 0.05$, and empirical roughness parameter function, $\hat{\tau}^{2\mathrm{S}}$, computed from $\hat{C}^{2\mathrm{S}}_{\mathrm{frag}}$ using the estimator in (16). The right plot in Figure 7 shows a significant difference in the mean growth functions from 11.4 to 15.5 years of age and thus confirms the adolescent gender-differences described in Bachrach et al. (1999).

6 Discussion

In this paper, we propose a novel method for constructing simultaneous confidence bands for (fragmentary) functional data using adaptive critical value functions. While we focus on the construction of fair critical value functions, Theorem 3.1 can also be used to explore other selection criteria beyond fairness. For instance, a very simple approach would be to optimize the allocation of the total false positive rate over given domain partitions such that the minimum average width of the band is minimized. Another still unanswered question is the extension of our approach to the case of higher dimensional function domains or manifolds. Such extensions exist for the classic Kac-Rice formulas and thus, in principle, should be possible for our adaptive bands as well. Finally, another useful, but highly nontrivial extension would be to further relax the (asymptotic) distribution assumption. In particular, estimates for models such as scalar-on-function regression do not possess

any asymptotic distribution in the strong topology since they are not tight (Cardot et al., 2007). Instead, such estimates satisfy the CLT only in the weak topology. It is still unclear if confidence bands can be constructed for such estimates.

Supplementary materials. The supplementary paper Liebl and Reimherr (2022b) contains the mathematical proofs or our theoretical results, further simulation results, and additional plots. The R-package `ffscb` which implements the introduced methods is available at the first author's GitHub account.

Acknowledgments. We thank the mathematical research institute MATRIX in Creswick, Australia and the Simons Institute for the Theory of Computing at the UC Berkeley where parts of this research was performed. Many thanks go also to the four anonymous referees and the associate editor whose comments helped us to improve our manuscript.

References

Abramowicz, K., C. K. Häger, A. Pini, L. Schelin, S. Sjöstedt de Luna, and S. Vantini (2018). Nonparametric inference for functional-on-scalar linear models applied to knee kinematic hop data after injury of the anterior cruciate ligament. *Scandinavian Journal of Statistics 45*(4), 1036–1061.

Adler, R. J. and J. E. Taylor (2007). *Random Fields and Geometry*. Springer.

Azaïs, J.-M., J.-M. Bardet, and M. Wschebor (2002). On the tails of the distribution of the maximum of a smooth stationary gaussian process. *ESAIM: Probability and Statistics 6*, 177–184.

Azaïs, J.-M. and M. Wschebor (2009). *Level Sets and Extrema of Random Processes and Fields*. John Wiley & Sons.

Bachrach, L. K., T. Hastie, M.-C. Wang, B. Narasimhan, and R. Marcus (1999). Bone mineral acquisition in healthy asian, hispanic, black, and caucasian youth: A longitudinal study. *The Journal of Clinical Endocrinology & Metabolism 84*(12), 4702–4712.

Bamisile, O., O. Ojo, N. Yimen, H. Adun, J. Li, S. Obiora, and Q. Huang (2021). Comprehensive functional data analysis of china's dynamic energy security index. *Energy Reports 7*, 6246–6259.

Belyaev, Y. K. (1966). On the number of intersections of a level by a gaussian stochastic process. *Theory of Probability & Its Applications 11*(1), 106–113.

Boente, G., M. S. Barrera, and D. E. Tyler (2014). A characterization of elliptical distributions and some optimality properties of principal components for functional data. *Journal of Multivariate Analysis 131*, 254–264.

Boschi, T., J. Di Iorio, L. Testa, M. A. Cremona, and F. Chiaromonte (2021). Functional data analysis characterizes the shapes of the first covid-19 epidemic wave in italy. *Scientific reports 11*(1), 1–15.

Cao, G., L. Yang, and D. Todem (2012). Simultaneous inference for the mean function based on dense functional data. *Journal of Nonparametric Statistics 24*(2), 359–377.

Cardot, H., A. Mas, and P. Sarda (2007). Clt in functional linear regression models. *Probability Theory and Related Fields 138*(3-4), 325–361.

Chen, Y., J. Goldsmith, and R. T. Ogden (2016). Variable selection in function-on-scalar regression. *Stat 5*(1), 88–101.

Choi, H. and M. Reimherr (2018). A geometric approach to confidence regions and bands for functional parameters. *Journal of the Royal Statistical Society: Series B (Statistical Methodology) 80*(1), 239–260.

Corbett-Davies, S., E. Pierson, A. Feller, S. Goel, and A. Huq (2017). Algorithmic decision making and the cost of fairness. In *Proceedings of the 23rd ACM SIGKDD International Conference on Knowledge Discovery and Data Mining*, pp. 797–806.

Cramér, H. and M. R. Leadbetter (1965). The moments of the number of crossings of a level by a stationary normal process. *The Annals of Mathematical Statistics 36*(6), 1656–1663.

Cramér, H. and M. R. Leadbetter (2013). *Stationary and related stochastic processes: Sample function properties and their applications*. Courier Corporation.

Degras, D. A. (2011). Simultaneous confidence bands for nonparametric regression with functional data. *Statistica Sinica 21*(4), 1735–1765.

Delaigle, A. and P. Hall (2013). Classification using censored functional data. *Journal of the American Statistical Association 108*(504), 1269–1283.

Delaigle, A. and P. Hall (2016). Approximating fragmented functional data by segments of markov chains. *Biometrika 103*(4), 779–799.

Delaigle, A., P. Hall, W. Huang, and A. Kneip (2020). Estimating the covariance of fragmented and other related types of functional data. *Journal of the American Statistical Association 0*(0), 1–19.

Descary, M.-H. and V. M. Panaretos (2019). Recovering covariance from functional fragments. *Biometrika 106*(1), 145–160.

Dette, H. and K. Kokot (2022). Detecting relevant differences in the covariance operators of functional time series: a sup-norm approach. *Annals of the Institute of Statistical Mathematics 74*(2), 195–231.

Dette, H., K. Kokot, and A. Aue (2020). Functional data analysis in the banach space of continuous functions. *The Annals of Statistics 48*(2), 1168–1192.

Donoghue, O. A., A. J. Harrison, N. Coffey, and K. Hayes (2008). Functional data analysis of running kinematics in chronic achilles tendon injury. *Medicine and science in sports and exercise 40*(7), 1323–1335.

Fang, K.-T., S. Kotz, and K.-W. Ng (2018). *Symmetric Multivariate and Related Distributions* (1. ed.). Chapman and Hall/CRC.

Ferraty, F. and P. Vieu (2006). *Nonparametric Functional Data Analysis: Theory and Practice*. Springer.

Friedman, J., T. Hastie, and R. Tibshirani (2001). *The Elements of Statistical Learning*, Volume 1. Springer.

Friston, K., J. Ashburner, S. Kiebel, T. Nichols, and W. Penny (Eds.) (2007). *Statistical Parametric Mapping: The Analysis of Functional Brain Images*. Academic Press.

Goldsmith, J., S. Greven, and C. Crainiceanu (2013). Corrected confidence bands for functional data using principal components. *Biometrics 69*(1), 41–51.

Hamacher, D., K. Hollander, and A. Zech (2016). Effects of ankle instability on running gait ankle angles and its variability in young adults. *Clinical Biomechanics 33*, 73–78.

Hardt, M., E. Price, and N. Srebro (2016). Equality of opportunity in supervised learning. *Advances in Neural Information Processing Systems 29*, 3315–3323.

Hsing, T. and R. Eubank (2015). *Theoretical Foundations of Functional Data Analysis, with an Introduction to Linear Operators*. John Wiley & Sons.

Ito, K. (1963). The expected number of zeros of continuous stationary gaussian processes. *Journal of Mathematics of Kyoto University 3*(2), 207–216.

James, G. M. and T. J. Hastie (2001). Functional linear discriminant analysis for irregularly sampled curves. *Journal of the Royal Statistical Society: Series B (Statistical Methodology) 63*(3), 533–550.

Kac, M. (1943). On the average number of real roots of a random algebraic equation. *Bulletin of the American Mathematical Society 49*(4), 314–320.

Kelly, H. D. (2020). *Forensic Gait Analysis*. CRC Press.

Kneip, A. and D. Liebl (2020). On the optimal reconstruction of partially observed functional data. *The Annals of Statistics 48*(3), 1692 – 1717.

Kokoszka, P. and M. Reimherr (2013). Asymptotic normality of the principal components of functional time series. *Stochastic Processes and their Applications 123*(5), 1546–1562.

Kokoszka, P. and M. Reimherr (2017). *Introduction to Functional Data Analysis* (1. ed.). Chapman and Hall/CRC.

Kraus, D. (2015). Components and completion of partially observed functional data. *Journal of the Royal Statistical Society 77*(4), 777–801.

Kraus, D. (2019). Inferential procedures for partially observed functional data. *Journal of Multivariate Analysis 173*, 583–603.

Li, Y. and T. Hsing (2010). Uniform convergence rates for nonparametric regression and principal component analysis in functional/longitudinal data. *The Annals of Statistics 38*(6), 3321–3351.

Liebl, D. (2019). Nonparametric testing for differences in electricity prices: The case of the fukushima nuclear accident. *The Annals of Applied Statistics 13*(2), 1128–1146.

Liebl, D. and S. Rameseder (2019). Partially observed functional data: The case of systematically missing parts. *Computational Statistics & Data Analysis 131*, 104 – 115.

Liebl, D. and M. Reimherr (2022+a). *ffscb: Fast and fair simultanouse confidence for functional parameters*. R package version 0.0.10.

Liebl, D. and M. Reimherr (2022+b). Supplement to "fast and fair simultaneous confidence bands for functional parameters". *arXiv:1910.00131*.

Liebl, D., S. Willwacher, J. Hamill, and G.-P. Brüggemann (2014). Ankle plantarflexion strength in rearfoot and forefoot runners: A novel clusteranalytic approach. *Human Movement Science 35*, 104–120.

Manrique, T., C. Crambes, and N. Hilgert (2018). Ridge regression for the functional concurrent model. *Electronic Journal of Statistics 12*(1), 985–1018.

McKeague, I. W. and B. Sen (2010). Fractals with point impact in functional linear regression. *The Annals of Statistics 38*(4), 2559–2586.

Morgenstern, J. and A. Roth (2022). Fairness in prediction and allocation. In F. Echenique, N. Immorlica, and V. V. Vazirani (Eds.), *Online and Matching-Based Market Design*. Cambridge University Press (forthcoming).

Olsen, N. L., A. Pini, and S. Vantini (2021). False discovery rate for functional data. *Test 30*(3), 784–809.

Pataky, T. C., M. A. Robinson, and J. Vanrenterghem (2016). Region-of-interest analyses of one-dimensional biomechanical trajectories: Bridbridging 0d and 1d theory, augmenting statistical power. *PeerJ 4*, e2652.

Pini, A. and S. Vantini (2016). The interval testing procedure: A general framework for inference in functional data analysis. *Biometrics 72*(3), 835–845.

Pini, A. and S. Vantini (2017a). *fdatest: Interval wise testing for functional data.* R package version 2.1.0.

Pini, A. and S. Vantini (2017b). Interval-wise testing for functional data. *Journal of Nonparametric Statistics 29*(2), 407–424.

Piterbarg, V. I. (1982). Comparison of distribution functions of maxima of gaussian processes. *Theory of Probability & Its Applications 26*(4), 687–705.

Poldrack, R. A. (2007). Region of interest analysis for fmri. *Social Cognitive and Affective neuroscience 2*(1), 67–70.

Poß, D., D. Liebl, A. Kneip, H. Eisenbarth, T. D. Wager, and L. F. Barrett (2020). Superconsistent estimation of points of impact in non-parametric regression with functional predictors. *Journal of the Royal Statistical Society: Series B (Statistical Methodology) 82*(4), 1115–1140.

Ramsay, J. and B. Silverman (2005). *Functional Data Analysis* (2. ed.). Springer.

Rice, S. O. (1945). Mathematical analysis of random noise. *Bell System Technical Journal 24*, 46–156.

Sulovská, K., E. Fišerová, M. Chvosteková, and M. Adámek (2017). Appropriateness of gait analysis for biometrics: Initial study using fda method. *Measurement 105*, 1–10.

Taylor, J., A. Takemura, and R. J. Adler (2005). Validity of the expected euler characteristic heuristic. *The Annals of Probability 33*(4), 1362–1396.

Telschow, F. J. (2022). *SIRF: Statistical Inference for Random Fields.*

Telschow, F. J. and A. Schwartzman (2022). Simultaneous confidence bands for functional data using the gaussian kinematic formula. *Journal of Statistical Planning and Inference 216*, 70–94.

Vanrenterghem, J., E. Venables, T. Pataky, and M. A. Robinson (2012). The effect of running speed on knee mechanical loading in females during side cutting. *Journal of Biomechanics 45*(14), 2444–2449.

Wager, T. D., M. L. Davidson, B. L. Hughes, M. A. Lindquist, and K. N. Ochsner (2008). Prefrontal-subcortical pathways mediating successful emotion regulation. *Neuron 59*(6), 1037–1050.

Wager, T. D., M. A. Lindquist, T. E. Nichols, H. Kober, and J. X. Van Snellenberg (2009). Evaluating the consistency and specificity of neuroimaging data using meta-analysis. *Neuroimage 45*(1), S210–S221.

Wang, Y., G. Wang, L. Wang, and R. T. Ogden (2020). Simultaneous confidence corridors for mean functions in functional data analysis of imaging data. *Biometrics 76*(2), 427–437.

Warmenhoven, J., S. Cobley, C. Draper, A. Harrison, N. Bargary, and R. Smith (2019). Considerations for the use of functional principal components analysis in sports biomechanics: examples from on-water rowing. *Sports Biomechanics 18*(3), 317–341.

Wen, Y., H. Huang, Y. Yu, S. Zhang, J. Yang, Y. Ao, and S. Xia (2018). Effect of tibia marker placement on knee joint kinematic analysis. *Gait & Posture 60*, 99–103.

Yao, F., H.-G. Müller, and J.-L. Wang (2005). Functional data analysis for sparse longitudinal data. *Journal of the American Statistical Association 100*(470), 577–590.

Zhang, X. and J.-L. Wang (2016). From sparse to dense functional data and beyond. *The Annals of Statistics 44*(5), 2281–2321.

Supplement to

Fast and Fair Simultaneous Confidence Bands for Functional Parameters

Dominik Liebl
University of Bonn

Matthew Reimherr
Penn State University

A Proofs

The mathematical arguments are the same for any $t_0 \in [0,1]$ since the expected number of down-crossings about $u(t)$ is equal to the expected number of up-crossings about $-u(t)$. Thus we will fix $t_0 = 0$ in our arguments below. We first establish all of our results conditioned on the mixing coefficient, V, for the elliptical distribution, which can be thought of as computing $\mathbb{E}[\varphi_u(X)|V]$, which is then a Gaussian calculation. After establishing our results for the Gaussian case, we will then reintroduce V and compute the final expectation $\mathbb{E}[\mathbb{E}[\varphi_u(X)|V]]$.

The proof hinges on two approximations that simplify the calculations. The first step is to introduce a smooth approximation of the up-crossing count. This is accomplished using a kernel, $K(x)$. Since the kernel is merely a theoretical device, we will assume it is fairly simple in our lemmas. Intuitively, if $K((u(t) - X(t))/h)$ is large for some small bandwidth, h, then $X(t)$ is very close to crossing $u(t)$. Thus, by integrating this quantity (with appropriate normalizations) we can use it to approximate the up-crossing count.

Our second approximation consists of forming linear interpolations for both $X(t)$ and $u(t)$ on a dyadic grid. In particular, fix an integer k and an index $j = 1, \ldots, 2^k$. Then for any $t \in [0,1]$ such that $j - 1 < t2^k < j$ we form the quantities

$$\begin{aligned}
\widetilde{X}_k(t) &= X\left(\frac{j-1}{2^k}\right)\left(j - 2^k t\right) + X\left(\frac{j}{2^k}\right)\left(2^k t - j + 1\right), \\
\widetilde{u}_k(t) &= u\left(\frac{j-1}{2^k}\right)\left(j - 2^k t\right) + u\left(\frac{j}{2^k}\right)\left(2^k t - j + 1\right), \\
\widetilde{X}'_k(t) &= 2^k\left(X\left(\frac{j}{2^k}\right) - X\left(\frac{j-1}{2^k}\right)\right), \\
\widetilde{u}'_k(t) &= 2^k\left(u\left(\frac{j}{2^k}\right) - u\left(\frac{j-1}{2^k}\right)\right).
\end{aligned}$$

We continuously extend $\widetilde{X}_k$ and $\widetilde{u}_k$ at the dyadic points, $\widetilde{X}_k(j/2^k) = X(j/2^k)$ and $\widetilde{u}_k(j/2^k) = u_k(j/2^k)$ for $j = 0, 1, \ldots, 2^k$. Since the $\widetilde{X}'_k$ and $\widetilde{u}'_k$ are step functions, they cannot be continuously extended. For convenience, we take $\widetilde{X}'_k(j/2^k) = X'(j/2^k)$ and $\widetilde{u}'_k(j/2^k) = u'_k(j/2^k)$, though for the derivatives what happens on a set of measure zero will have no impact on our calculations. This choice also yields the convenient bounds

$$\sup_{0\le t\le 1} |\widetilde{X}_k(t)| \le \sup_{0\le t\le 1} |X(t)| \qquad \sup_{0\le t\le 1} |\widetilde{u}_k(t)| \le \sup_{0\le t\le 1} |u(t)|$$
$$\sup_{0\le t\le 1} |\widetilde{X}'_k(t)| \le \sup_{0\le t\le 1} |X'(t)| \qquad \sup_{0\le t\le 1} |\widetilde{u}'_k(t)| \le \sup_{0\le t\le 1} |u'(t)|.$$

A.1 Lemmas

In this section we state our technical lemmas which results in a proof of Corollary 3.2 on the Gaussian case (Lemma A.3).

Lemma A.1. *Let $f \in C[0,1]$ and suppose there only exits a finite number of zeros $\{t_1, \ldots, t_k\}$, that is, $f(t) = 0$ if and only if $t = t_i$ for some $i = 1, \ldots, k$. Then for any $\epsilon > 0$ there exists $h > 0$ such that*

$$f^{-1}(-h, h) \subseteq \bigcup_{i=1}^{k} (t_i - \epsilon, t_i + \epsilon). \tag{20}$$

Proof of Lemma A.1.
Consider a proof by contradiction. Suppose there exists $\epsilon > 0$ such that (20) does not hold for any h. Call the right hand side of (20) B_ϵ. Then consider the sets $A_l = f^{-1}(-2^{-l}, 2^{-l})$ for $l = 1, 2, \ldots$. By assumption, $A_l \cap B_\epsilon^c$ is nonempty for any l, so select an infinite sequence $\{x_l\}$ by taking $x_l \in A_l \cap B_\epsilon^c$. By construction, $|f(x_l)| \le 2^{-l}$, which implies that $f(x_l) \to 0$ as $l \to \infty$. However, since $[0,1]$ is compact, there exists a convergent subsequence $x_{l'}$ such that $x_{l'} \to x$, which implies $f(x) = 0$. However, $|x - t_i| \ge \epsilon$ for all $i = 1, \ldots, k$, which means x cannot be one of the zeros, which is a contradiction. □

Lemma A.2. *Counting Formula.*

(a) Let X be a Gaussian random function with $\mathrm{Var}(X(t)) > 0$ for every $t \in [0,1]$ and let u be a deterministic function. If $X \in C^1[0,1]$ almost surely, $u \in C[0,1]$ and u' is continuous almost everywhere, then the number of up-crossings is

$$\begin{aligned} N_u(X) &= \#\{t \in [0,1] \,:\, X(t) = u(t),\, X'(t) - u'(t) > 0\} \\ &= \lim_{h\to 0} \int_0^1 \frac{1}{h} K\left(\frac{u(t) - X(t)}{h}\right) \big(X'(t) - u'(t)\big) \mathbb{1}_{X'(t)-u'(t)>0}\, dt \;< \infty \quad a.s., \end{aligned}$$

where $\mathbb{1}$ denotes the indicator function and K is a symmetric kernel function with compact support, i.e., $K(t) = K(-t) \ge 0$, $K(t) = 0$ if $|t| > 1$, $K(t)$ is continuous on $[-1,1]$, and $\int K(t)\, dt = 1$.

(b) Let all requirements in (a) hold, then the dyadic linear interpolations satisfy

$$\begin{aligned} N_{\widetilde{u}_k}(\widetilde{X}_k) &= \#\{t \in [0,1] \,:\, \widetilde{X}_k(t) = \widetilde{u}_k(t),\, \widetilde{X}_k'(t) - \widetilde{u}_k'(t) > 0\} \\ &= \lim_{h\to 0} \int_0^1 \frac{1}{h} K\left(\frac{\widetilde{u}_k(t) - \widetilde{X}_k'(t)}{h}\right) \left(\widetilde{X}_k'(t) - \widetilde{u}_k'(t)\right) \mathbb{1}_{\widetilde{X}_k'(t) - \widetilde{u}_k'(t) > 0}\, dt \\ &\le \min\{2^k, N_u(X)\}, \end{aligned}$$

almost surely.

Proof of Lemma A.2 Part (a).
First consider the case of no up-crossings, $N_u(X) = 0$, which can happen in only one of two ways. The first possibility is that $X(t) < u(t)$ for all $t \in [0,1]$ or $X(t) > u(t)$ for all $t \in [0,1]$. Since $X(t) - u(t)$ is continuous and the domain is compact, there exists an $\epsilon > 0$ such that, $|X(t) - u(t)| \ge \epsilon$ for all $t \in [0,1]$. This implies that $K((u(t) - X(t))/h) = 0$ for all $t \in [0,1]$ with $h \le \epsilon$, thus trivially proving the claim. The second possibility is that we have exactly one down crossing, but no up-crossing. In this case, there is exactly one t_d such that $X(t_d) = u(t_d)$, but $X'(t_d) < u'(t_d)$. Note that t_d is random and equals a discontinuity point of u' with probability zero since u' is continuous almost everywhere. That is, we can take a small enough interval $(t_d - \delta, t_d + \delta)$ such that for all $t \in (t_d - \delta, t_d + \delta)$ we have $\mathbb{1}_{X'(t) > u'(t)} = 0$ with probability one. Then, $|X(t) - u(t)| \ge \epsilon > 0$ for all $t \in [0, t_d - \delta] \cup [t_d + \delta, 1]$ and we can again take h small enough that the integral is exactly zero almost surely.

For the case $N_u(X) = m$ with $m > 0$, define $X_u := X - u$ and let us consider the up-crossings of X_u above 0, which is equivalent to the up-crossings of X above u, that is,

$$\begin{aligned} N_u(X) &= \#\{t \in [0,1] \,:\, X(t) - u(t) = 0,\, X'(t) - u'(t) > 0\} \\ &= \#\{t \in [0,1] \,:\, X_u(t) = 0,\, X_u'(t) > 0\} \\ &= \lim_{h\to 0} \int_0^1 \frac{1}{h} K\left(\frac{X_u(t) - 0}{h}\right) X_u'(t) \mathbb{1}_{X_u'(t) > 0}\, dt. \end{aligned}$$

With probability one, no up-crossing location equals a discontinuity point of u', thus In addition, with probability one, no up-crossing location equals a discontinuity point of u', thus the $N_u(X)$ is a well defined quantity. $N_u(X)$ is a well defined quantity. Since $X(0) \ne u(0)$ and $X(1) \ne u(1)$ with probability 1, we can denote the (random) up-crossing locations as $0 < t_1 < \cdots < t_m < 1$. By Lemma A.1 for any sufficiently small h, the inverse image of $(-h, h)$ by the function X_u is contained in the union of m pairwise disjoint intervals $I_1, \ldots, I_m$ with $t_j \in I_j$, $j = 1, \ldots, m$. Observe that $X_u'(t_j) > 0$ for every up-crossing location t_j, $j = 1, \ldots, m$, and that X_u' is continuous; therefore, we can take the intervals small enough that the restriction of X_u to I_j is almost surely a diffeomorphism for each $j = 1, \ldots, m$.

Since $X_u'(t) = X'(t) + u'(t) > 0$ on I_j almost surely, we can perform a change of variables with $yh = X_u(t)$ and $hdy = X_u'(t)dt$ without changing the orientation of the integral. Since K is compactly supported, we can then take h small enough that

$$\int_{I_j} K\left(\frac{X_u(t)}{h}\right) \frac{X_u'(t)}{h}\, dt = \int_{-1}^1 K(y)\, dy = 1, \quad \text{for every} \quad j = 1, \ldots, m,$$

which implies that that

$$N_u(X) = \int_0^1 \frac{1}{h} K\left(\frac{u(t) - X(t)}{h}\right) \big(X'(t) - u'(t)\big) \mathbb{1}_{X'(t)-u'(t)>0}\, dt$$
$$= \sum_{j=1}^{m} \int_{I_j} \frac{1}{h} K\left(\frac{u(t) - X(t)}{h}\right) (X'(t) - u'(t)) \mathbb{1}_{X'(t)>u'(t)}\, dt = m$$

for all sufficiently small h.

Finally, the assumption that $X \in C^1([0,1])$ almost surely implies that the number of up-crossings is finite with probability 1, that is, $N_u(X) = m < \infty$ with probability 1. □

Proof of Lemma A.2 Part (b).
Since $X(t)$ is a Gaussian process it follows that $\widetilde{X}_k(j/2^k) \neq u(j/2^k)$ a.s. for each $j = 0, \ldots, 2^k$, meaning an up-crossing occurs only within one of the partitioned intervals $[(j-1)/2^k, j/2^k]$, $j = 1, \ldots, 2^k$. Observe that, restricted to an interval $((j-1)/2^k, j/2^k)$, $j = 1, \ldots, 2^k$, $\widetilde{X}_k$ is just a very simple Gaussian process and $\widetilde{u}_k$ is just a linear threshold – both fulfilling the requirements of Lemma A.2 part (a). Thus the result of Lemma A.2 part (a) holds also for each subinterval. So, almost surely, we can count the up-crossings for each partitioned interval and sum up the corresponding integrals

$$N_{\tilde{u}_k}(\widetilde{X}_k) = \lim_{h\to 0} \sum_{j=1}^{2^k} \int_{(j-1)/2^k}^{j/2^k} \frac{1}{h} K\left(\frac{\widetilde{u}_k(t) - \widetilde{X}_k(t)}{h}\right) \big(\widetilde{X}_k'(t) - \widetilde{u}_k'(t)\big) \mathbb{1}_{\widetilde{X}_k'(t)-\widetilde{u}_k'(t)>0}\, dt,$$

which shows the equality statement.

Since both $\widetilde{X}_k$ and $\widetilde{u}_k$ are piecewise linear, their difference is also linear. With probability one, this difference is not zero, thus by the fundamental theorem of algebra, there is at most one root/up-crossing. Therefore, the maximum number of up-crossings $N_{\tilde{u}_k}(\widetilde{X}_k)$ is bounded by the number of partitioned intervals, 2^k. However, within an interval $[(j-1)/2^k, j/2^k]$, $j = 1, \ldots, 2^k$, $\widetilde{X}_k$ crossing $\widetilde{u}_k$ implies X must cross u by the intermediate value theorem, but the reverse is not true since their can be a subsequent downcrossing. Namely, it is only possible to "miss" up-crossings with the linear interpolation, one cannot add additional crossings, which shows the inequality statement. □

The result of the following lemma is equivalent to the result in Corollary 3.2 a).

Lemma A.3. *Kac-Rice Formula for Non-Constant Critical Value Functions.*
Let $\{X(t) : t \in [0,1]\}$ be a continuously differentiable Gaussian process and $u(t)$ a continuously differentiable function. Let $\tau(t)^2 = \partial_x \partial_y C(x,y)|_{x=y=t}$, where $C(x,y)$ is the covariance function of $X(t)$. Assume $X(t)$ has a constant pointwise unit variance, $\mathrm{Var}(X(t)) = 1$ *for all $t \in [0,1]$. Then the expected value of $\varphi_{u,X}(t_0) = \mathbb{1}_{X(0)\geq u(0)} + N_u(X)$ is*

$$\mathbb{E}[\varphi_{u,X}(t_0)] = P(X(0) \geq u(0)) + \int_0^1 \frac{\tau(t)}{2\pi} \exp\left\{-\frac{1}{2}\left[u(t)^2 + \frac{u'(t)^2}{2\tau(t)^2}\right]\right\} dt - \int_0^1 \frac{u'(t)}{\sqrt{2\pi}} \exp\left\{-\frac{u(t)^2}{2}\right\} \Phi\left(\frac{-u'(t)}{\tau(t)}\right) dt,$$

where Φ is the standard normal cdf.

Proof of Lemma A.3.
From Lemma A.2 part (b) we have

$$\varphi_{\widetilde{u}_k}(\widetilde{X}_k) = \mathbb{1}_{X(0)\geq u(0)} + \lim_{h\to 0}\int_0^1 \frac{1}{h}K\left(\frac{\widetilde{u}_k(t)-\widetilde{X}_k(t)}{h}\right)\left(\widetilde{X}_k'(t)-\widetilde{u}_k'(t)\right)\mathbb{1}_{\widetilde{X}_k'(t)-\widetilde{u}_k'(t)>0}\,dt \quad a.s.,$$

where we use that $\widetilde{X}_k(0) = X(0)$ with probability 1. Let $g_{\widetilde{X}_k(t)\widetilde{X}_k'(t)}$ denote the joint density of $(\widetilde{X}_k(t), \widetilde{X}_k'(t))$ and note that by Lemma A.2 part (b) $\int_0^1 (1/h)K((\widetilde{u}_k(t)-\widetilde{X}_k'(t))/h)(\widetilde{X}_k'(t)-\widetilde{u}_k'(t))\mathbb{1}_{\widetilde{X}_k'(t)-\widetilde{u}_k'(t)>0}\,dt < 2^k$ (a.s.). Therefore, we can apply the dominated convergence theorem for an arbitrary but fix $k \geq 1$, such that

$$\begin{aligned}\mathbb{E}[\varphi_{\widetilde{u}_k}(\widetilde{X}_k)] =& P(X(0)\geq u(0)) + \\ &\lim_{h\to 0}\int_0^1 \frac{1}{h}\int_{-\infty}^{\infty}\int_{\widetilde{u}_k'(t)}^{\infty} K\left(\frac{\widetilde{u}_k(t)-x}{h}\right)\left(y-\widetilde{u}_k'(t)\right)g_{\widetilde{X}_k(t)\widetilde{X}_k'(t)}(x,y)\;dy\;dx\;dt.\end{aligned}$$

Applying a change of variables $x = zh + \widetilde{u}_k(t)$, the symmetry and compactness of K yields

$$\begin{aligned}\mathbb{E}[\varphi_u(\widetilde{X}_k)] =& P(X(0)\geq u(0)) + \\ &\lim_{h\to 0}\int_0^1 \int_{-1}^{1}\int_{\widetilde{u}_k'(t)}^{\infty} K(z)\left(y-\widetilde{u}_k'(t)\right)g_{\widetilde{X}_k(t)\widetilde{X}_k'(t)}(zh+\widetilde{u}_k(t),y)\;dy\;dz\;dt.\end{aligned}$$

As $g_{\widetilde{X}_k(t)\widetilde{X}_k'(t)}$ consists of a finite mixture of Gaussian densities for each $t \in [0,1]$, $g_{\widetilde{X}_k(t)\widetilde{X}_k'(t)}(x,y)$ it bounded uniformly for all x and y. Therefore, we can bring the limit inside the integral, which yields

$$\mathbb{E}[\varphi_u(\widetilde{X}_k)] = P(X(0)\geq u(0)) + \int_0^1\int_{\widetilde{u}_k'(t)}^{\infty}\left(y-\widetilde{u}_k'(t)\right)g_{\widetilde{X}_k(t)\widetilde{X}_k'(t)}(\widetilde{u}_k(t),y)\;dy\;dt. \tag{21}$$

We now finally want to take the limit as $k\to\infty$. For the left hand side of (21) we immediately have $\mathbb{E}[\varphi_{\widetilde{u}_k}(\widetilde{X}_k)] \to \mathbb{E}[\varphi_u(X)]$ as $k\to\infty$ by the monotone convergence theorem, since $N_u(\widetilde{X}_k) \nearrow N_u(X)$ as $k\to\infty$. For the right hand side of (21), we can rewrite the integral as

$$\int_0^1 \mathbb{E}[(\widetilde{X}_k'(t)-\widetilde{u}_k'(t))1_{\widetilde{X}_k'(t)\geq\widetilde{u}_k'(t)}|\widetilde{X}_k(t)=\widetilde{u}_k(t)]g_{\widetilde{X}_k(t)}(\widetilde{u}_k(t))\;dt.$$

To take pass the limit we need to be quite careful with our justification. In particular, we need to pass the limit twice: under the first integral and then under the expectation. We accomplish this in a series of steps.

1. For any $j-1\leq t2^k\leq j$ we can write

$$\widetilde{X}_k(t) = w_t X((j-1)/2^k) + (1-w_t)X(j/2^k),$$

for nonrandom weights $w_t = j-2^k t\in[0,1]$. Since the covariance of X is differentiable, it implies that X is mean squared continuous, thus there exists a k_0 such that for any $k\geq k_0$ we have $\mathrm{Cov}(X((j-1)/2^k, X(j/2^k))\geq 0$, which implies that $\mathrm{Var}(\tilde{X}_k(t))\geq 1$. Thus, for k large, the density $g_{\widetilde{X}_k}$ is uniformly bounded by $(2\pi)^{-1/2}$.

2. Next, since $(\widetilde{X}_k(t), \widetilde{X}'_k(t))$ are jointly mean zero Gaussian random variables (for each t), we have
$$\widetilde{X}'_k(t) = b_k(t)\widetilde{X}_k(t) + \epsilon_k(t),$$
where $b_k(t) = \mathbb{E}[\widetilde{X}_k(t)\widetilde{X}'_k(t)]/\,\mathbb{E}[\widetilde{X}_k(t)^2] = \mathrm{Cov}(\widetilde{X}_k(t), \widetilde{X}'_k(t))/\,\mathrm{Var}(\widetilde{X}_k(t))$, and $\epsilon_k(t)$ and $\widetilde{X}_k(t)$ are independent for each t.

   So then we have the bound
$$\begin{aligned}
&\mathbb{E}[(\widetilde{X}'_k(t) - \widetilde{u}'_k(t))1_{\widetilde{X}'_k(t)\geq \widetilde{u}'_k(t)}|\widetilde{X}_k(t) = \widetilde{u}_k(t)] \\
&\leq \mathbb{E}[|\widetilde{X}'_k(t) - \widetilde{u}'_k(t)|\ |\widetilde{X}_k(t) = \widetilde{u}_k(t)] \\
&= \mathbb{E}[|b_k(t)\widetilde{X}_k(t) + \epsilon_k(t) - \widetilde{u}'_k(t)|\ |\widetilde{X}_k(t) = \widetilde{u}_k(t)] \\
&\leq |b_k(t)\widetilde{u}_k(t) - \widetilde{u}'_k(t)| + \mathbb{E}[|\epsilon_k(t)|].
\end{aligned}$$

   By the independence of $\epsilon_k(t)$ and $\widetilde{X}_k(t)$,
$$\mathbb{E}[\widetilde{X}'_k(t)^2] = b_k(t)^2\,\mathbb{E}[\widetilde{X}_k(t)^2] + \mathbb{E}[\epsilon_k(t)^2] \quad \Rightarrow \quad \mathbb{E}[\epsilon_k(t)^2] \leq \mathbb{E}[\widetilde{X}'_k(t)^2].$$

   Jensen's inequality implies that
$$\mathbb{E}\,|\epsilon_k(t)| \leq \mathbb{E}[\widetilde{X}'_k(t)^2]^{1/2}.$$

   By definition we have that $\tilde{X}'(t) = 2^k[X(j/2^k) - X((j-1)/2^k)]$. By the Mean value theorem we have that $\widetilde{X}'_k(t) = X'(\xi)$ for some $\xi \in [(j-1)/2^k, j/2^k]$. Therefore $\widetilde{X}'(t)^2 \leq \left(\sup_{0\leq s\leq 1} X'(s)\right)^2$, which has a finite expectation by Theorem 2.9 of Azaïs and Wschebor (2009).

   By construction $\widetilde{u}_k$ and $\widetilde{u}'_k$ are uniformly bounded by sup norms of u and u' respectively. From arguments from step 1, for k large, $\mathrm{Var}(\widetilde{X}_k(t)) \geq 1$ and so
$$b_k(t)^2 \leq \mathbb{E}(\widetilde{X}'_k(t)^2) \leq \mathbb{E}\left(\left(\sup_{0\leq s\leq 1} X'(s)\right)^2\right) < \infty.$$

   Thus, we have a uniform bound over t for all k large and we can justify passing the limit as $k \to \infty$ under the integral.

3. Finally, with the limit under the integral we need only that the integrand converges for all or almost all t. Clearly the density term converges
$$g_{\widetilde{X}_k(t)}(\widetilde{u}_k(t)) \to \frac{1}{\sqrt{2\pi}}\exp\left\{-\frac{u(t)^2}{2}\right\},$$
   since $\mathrm{Var}(\widetilde{X}_k(t)) \to \mathrm{Var}(X(t)) = 1$ and $\widetilde{u}_k(t) \to u(t)$. For the conditional expected value term, using the same arguments as before, we have that
$$\begin{aligned}
&\mathbb{E}[(\widetilde{X}'_k(t) - \widetilde{u}'_k(t))1_{\widetilde{X}'_k(t)\geq \widetilde{u}'_k(t)}|\widetilde{X}_k(t) = \widetilde{u}_k(t)] \\
&= \mathbb{E}[(b_k(t)\widetilde{u}_k(t) + \epsilon_k(t) - \widetilde{u}'_k(t))1_{b_k(t)\widetilde{u}_k(t)+\epsilon_k(t)\geq \widetilde{u}'_k(t)}].
\end{aligned}$$

Clearly we have

$$(b_k(t)\widetilde{u}_k(t) + \epsilon_k(t) - \widetilde{u}_k'(t))1_{b_k(t)\widetilde{u}_k(t)+\epsilon_k(t)\geq \widetilde{u}_k'(t)} \leq |b_k(t)\widetilde{u}_k(t) + \epsilon_k(t) - \widetilde{u}_k'(t)|.$$

In the previous step we already showed that $b_k(t)$, $\widetilde{u}_k(t)$, $\widetilde{u}_k'(t)$, and $\mathbb{E}\,|\epsilon_k(t)|$ are uniformly bounded across k and t. Thus, by the DCT we can pass the limit as $k \to \infty$ to obtain

$$\begin{aligned}
&\mathbb{E}[(b_k(t)\widetilde{u}_k(t) + \epsilon_k(t) - \widetilde{u}_k'(t))1_{b_k(t)\widetilde{u}_k(t)+\epsilon_k(t)\geq \widetilde{u}_k'(t)}] \\
&\to \mathbb{E}[(b(t)u(t) + \epsilon(t) - u'(t))1_{b(t)u(t)+\epsilon(t)\geq u'(t)}] \\
&= \mathbb{E}[(X'(t) - u'(t))1_{X'(t)\geq u'(t)}|X(t) = u(t)],
\end{aligned}$$

as desired.

Unraveling the conditional expectation, we have shown that

$$\mathbb{E}[\varphi_u(X)] = P(X(0) \geq u(0)) + \int_0^1 \int_{u'(t)}^{\infty} \big(y - u'(t)\big) g_{X(t)X'(t)}(u(t), y)\, dydt.$$

Since we assume that $X(t)$ has constant variance, it follows that, for each t, $X(t)$ and $X'(t)$ are uncorrelated and thus independent. So we can express

$$\begin{aligned}
&\mathbb{E}[\varphi_u(X)] = P(X(0) \geq u(0)) + \\
&\qquad \int_0^1 \left[\frac{1}{\sqrt{2\pi}} \exp\left\{-\frac{u(t)^2}{2}\right\} \int_{u'(t)}^{\infty} \big(y - u'(t)\big) \frac{1}{\sqrt{2\pi\tau(t)^2}} \exp\left\{-\frac{y^2}{2\tau(t)^2}\right\} dy \right] dt.
\end{aligned}$$

Turning to the second component, basic calculus implies that

$$\int_{u'(t)}^{\infty} (y - u'(t)) \frac{1}{\sqrt{2\pi\tau(t)^2}} \exp\left\{-\frac{y^2}{2\tau(t)^2}\right\} dy = \frac{\tau(t)}{\sqrt{2\pi}} \exp\left\{-\frac{u'(t)^2}{2\tau(t)^2}\right\} - u'(t)\,\Phi\left(\frac{-u'(t)}{\tau(t)}\right),$$

where Φ is the standard normal cdf. This yields the final result

$$\begin{aligned}
&\mathbb{E}[\varphi_u(X)] = P(X(0) \geq u(0)) + \\
&\qquad \int_0^1 \frac{\tau(t)}{2\pi} \exp\left\{-\frac{u(t)^2}{2} - \frac{u'(t)^2}{2\tau(t)^2}\right\} dt - \int_0^1 \frac{u'(t)}{\sqrt{2\pi}} \exp\left\{-\frac{u(t)^2}{2}\right\} \Phi\left(\frac{-u'(t)}{\tau(t)}\right) dt. \quad \square
\end{aligned}$$

This result of Lemma A.3 equals the result in Corollary 3.2 a) for $t_0 = 0$. The general result for any $t_0 \in [0, 1]$ follows now directly from observing that (a), when moving from t_0 down to 0, up-crossings as t decreases are equivalent to down-crossings as t increases, and (b) that the expected number down-crossings about $u(t)$ is equal to the expected number of up-crossings about $-u(t)$. Corollary 3.2 b) follows directly from part a), since $u' \equiv 0$ for constant critical values $u(t) \equiv u$, $\tau(t) \geq 0$ for all $t \in [0, 1]$ and $X(t_0) \overset{D}{=} X(0)$ for all $t_0 \in [0, 1]$

Lemma A.3 allows us now to proof Theorem 3.1.

A.2 Proof of Theorem 3.1

In the following we extend the above result of Lemma A.3 to elliptical distributions. Recall that every elliptical distribution can be expressed as a scalar mixture of a Gaussian and, therefore, our previous calculations were based on conditioning on the scalar mixing coefficient V. Our final expressions simplify if we use the alternative parametrization $V = \mathcal{V}^{-1/2}$ and work with $\mathcal{V}$ instead. Our previous expectation can then be understood as being conditioned on $\mathcal{V}$. In particular, if $\dot{u}(t) = \mathcal{V}^{1/2}u(t)$, then by Lemma A.3

$$\begin{aligned}\mathbb{E}[\varphi_u(X)|\mathcal{V}] = \mathbb{E}[\varphi_{\dot{u}}(X/\mathcal{V}^{1/2})|\mathcal{V}] =& P(X(0) \geq u(0)|\mathcal{V}) \\ &+ \int_0^1 \frac{\tau(t)}{2\pi} \exp\left\{-\mathcal{V}\left[\frac{u(t)^2}{2} + \frac{u'(t)^2}{2\tau(t)^2}\right]\right\} \, dt \\ &- \int_0^1 \frac{u'(t)\mathcal{V}^{1/2}}{\sqrt{2\pi}} \exp\left\{-\frac{\mathcal{V}u(t)^2}{2}\right\} \Phi\left(\frac{-u'(t)\mathcal{V}^{1/2}}{\tau(t)}\right) \, dt.\end{aligned} \tag{22}$$

The expected value of the first component is clearly $P(X(0) \geq u(0))$. For the second component, we can take the expected value and use Fubini's theorem. If $F_{\mathcal{V}}$ is the cdf of $\mathcal{V}$ then this yields

$$\int_0^1 \frac{\tau(t)}{2\pi} \int_0^\infty \exp\left\{-x\left[\frac{u(t)^2}{2} + \frac{u'(t)^2}{2\tau(t)^2}\right]\right\} \, dF_{\mathcal{V}}(x) \, dx \, dt.$$

Now notice that this is simply a moment generating function (mgf) calculation. Furthermore, it is always finite since $\mathcal{V}$ is strictly positive and the argument is strictly negative. Thus, if $M_{\mathcal{V}}(x)$ is the mgf of $\mathcal{V}$ then we have that the above simplifies to

$$\int_0^1 \frac{\tau(t)}{2\pi} M_{\mathcal{V}}\left(-\left[\frac{u(t)^2}{2} + \frac{u'(t)^2}{2\tau(t)^2}\right]\right) \, dt.$$

Turning to the third component, we have

$$\begin{aligned}&- \int_0^1 \frac{u'(t)\mathcal{V}^{1/2}}{\sqrt{2\pi}} \exp\left\{-\frac{\mathcal{V}u(t)^2}{2}\right\} \Phi\left(\frac{-u'(t)\mathcal{V}^{1/2}}{\tau(t)}\right) \, dt \\ =& - \int_0^1 \frac{u'(t)\mathcal{V}^{1/2}}{\sqrt{2\pi}} \exp\left\{-\frac{\mathcal{V}u(t)^2}{2}\right\} \int_{\mathcal{V}^{1/2}u'(t)/\tau(t)}^\infty \frac{1}{\sqrt{2\pi}} e^{-x^2/2} \, dx \, dt.\end{aligned}$$

Let $y = \tau(t)x/\mathcal{V}^{1/2} - u'(t)$, then the above becomes

$$\begin{aligned}&\int_0^1 \frac{u'(t)\mathcal{V}^{1/2}}{\sqrt{2\pi}} \exp\left\{-\frac{\mathcal{V}u(t)^2}{2}\right\} \int_0^\infty \frac{\mathcal{V}^{1/2}}{\sqrt{2\pi\tau(t)^2}} e^{-\mathcal{V}(y+u'(t))^2/2\tau(t)^2} \, dy \, dt \\ =& \int_0^1 \int_0^\infty \frac{u'(t)\mathcal{V}}{2\pi\tau(t)} \exp\left\{-\mathcal{V}\left[\frac{u(t)^2}{2} + \frac{(y+u'(t))^2}{2\tau(t)^2}\right]\right\} \, dy \, dt.\end{aligned}$$

Now we can take the expected value and use Fubini's theorem to get

$$- \int_0^1 \int_0^\infty \int_0^\infty \frac{u'(t)x}{2\pi\tau(t)} \exp\left\{-x\left[\frac{u(t)^2}{2} + \frac{(y+u'(t))^2}{2\tau(t)^2}\right]\right\} \, dF_{\mathcal{V}}(x) \, dy \, dt.$$

However as before, the inner integral can be expressed using the mgf of $\mathcal{V}$, though now with the derivative, resulting in

$$-\int_0^1 \int_0^\infty \frac{u'(t)}{2\pi\tau(t)} M'_{\mathcal{V}}\left(-\left[\frac{u(t)^2}{2} + \frac{(y+u'(t))^2}{2\tau(t)^2}\right]\right)\, dy\, dt.$$

So we have the final form for elliptical distributions given as

$$\begin{aligned}\mathbb{E}[\varphi_u(X)] = P(X(0) \geq u(0)) &+ \int_0^1 \frac{\tau(t)}{2\pi} M_{\mathcal{V}}\left(-\left[\frac{u(t)^2}{2} + \frac{u'(t)^2}{2\tau(t)^2}\right]\right)\, dt \\ &- \int_0^1 \int_0^\infty \frac{u'(t)}{2\pi\tau(t)} M'_{\mathcal{V}}\left(-\left[\frac{u(t)^2}{2} + \frac{(y+u'(t))^2}{2\tau(t)^2}\right]\right)\, dy\, dt\end{aligned}$$

which equals the result in Theorem 3.1 for $t_0 = 0$. The general result for any $t_0 \in [0,1]$ follows now directly from observing that (a), when moving from t_0 down to 0, up-crossings as t decreases are equivalent to down-crossings as t increases, and (b) that the expected number down-crossings about $u(t)$ is equal to the expected number of up-crossings about $-u(t)$. $\square$

A.3 Proof of Corollary 3.3

Maybe the most useful for our purposes is the case where $X(t)$ comes from a t-process. We note that pointwise standardization does not actually produce a t-process, but can still be used to help account for the added uncertainty of estimating the covariance. In this case, the distribution of $\mathcal{V}$ is actually a chi-squared divided by its degrees of freedom. So, if we write $\mathcal{V} = \chi^2_\nu/\nu$, then we have

$$M_{\mathcal{V}}(x) = \left(1 - \frac{2x}{\nu}\right)^{-\nu/2} \qquad \text{and} \qquad M'_{\mathcal{V}}(x) = \left(1 - \frac{2x}{\nu}\right)^{-\nu/2-1}.$$

Therefore, our expression becomes

$$\begin{aligned}\mathbb{E}[\varphi_u(X)] = F_t(-u(0);\nu) &+ \int_0^1 \frac{\tau(t)}{2\pi}\left(1 + \frac{u(t)^2}{\nu} + \frac{u'(t)^2}{\nu\tau(t)^2}\right)^{-\nu/2} dt \\ &- \int_0^1 \int_0^\infty \frac{u'(t)}{2\pi\tau(t)}\left(1 + \frac{u(t)^2}{\nu} + \frac{(y+u'(t))^2}{\nu\tau(t)^2}\right)^{-\nu/2-1} dy\, dt.\end{aligned}$$

The third term can be further simplified by using the cdf of a t-distribution. In particular, let $\nu' = \nu + 1$ and $a(t)^2 = \nu\tau(t)^2(1 + u(t)^2/\nu)/\nu'$, then we have

$$\begin{aligned}&\int_0^\infty \left(1 + \frac{u(t)^2}{\nu} + \frac{(y+u'(t))^2}{\nu\tau(t)^2}\right)^{-\nu/2-1} dy \\ &= \left(1 + \frac{u(t)^2}{\nu}\right)^{-\nu/2-1} \int_0^\infty \left(1 + \frac{(y+u'(t))^2}{\nu' a(t)^2}\right)^{-\frac{\nu'+1}{2}} dy.\end{aligned}$$

Now use a change of variables $x = y/a(t) + u'(t)/a(t)$ to obtain

$$\begin{aligned}
&\left(1+\frac{u(t)^2}{\nu}\right)^{-\nu/2-1} a(t)\int_{u'(t)/a(t)}^{\infty}\left(1+\frac{x^2}{\nu'}\right)^{-\frac{\nu'+1}{2}} dx \\
&= \left(1+\frac{u(t)^2}{\nu}\right)^{-\nu/2-1} B(1/2,\nu'/2)\sqrt{\nu'}a(t)F_t(-u'(t)/a(t);\nu') \\
&= \left(1+\frac{u(t)^2}{\nu}\right)^{-\nu/2-1} B(1/2,(\nu+1)/2)\sqrt{\nu+1}a(t)F_t(-u'(t)/a(t);\nu+1) \\
&= \left(1+\frac{u(t)^2}{\nu}\right)^{-(\nu+1)/2} \frac{\Gamma((\nu+1)/2)\sqrt{(\nu+1)\pi}a(t)}{\Gamma((\nu+2)/2)} F_t(-u'(t)/a(t);\nu').
\end{aligned}$$

where B denotes the beta function, Γ the gamma function, and $F_t(\cdot;\nu')$ denotes the distribution function of a t-distribution with ν' degrees of freedom. This leads to the result in Corollary 3.3 for $t_0 = 0$. The general result for any $t_0 \in [0,1]$ follows now directly from observing that (a), when moving from t_0 down to 0, up-crossings as t decreases are equivalent to down-crossings as t increases, and (b) that the expected number down-crossings about $u(t)$ is equal to the expected number of up-crossings about $-u(t)$. □

A.4 Proof of Proposition 3.2

The proof of Proposition 3.2 follows directly from Theorems 3.1, 3.2, and 3.2, and the classic confidence interval derivations from inverting pivot statistics.[7]

A.5 Proof of Theorem 3.2

The arguments are the same for any elliptical distribution, so we assume that X is a Gaussian process. We recall two classic properties, one from analysis and the other from probability theory. First, if $f(u,\tau)$ is continuous as a mapping from $C^1 \times C \to \mathbb{R}$, and $\mathcal{U}$ is assumed to be compact, then the collection of functions $\{f_u(\tau) := f(u,\tau) : u \in \mathcal{U}\}$ are equicontinuous. Second, recall that $\tau_n \to \tau$ in probability if and only if every subsequence $\tau_{n(m)}$ has a further subsequence $\tau_{n(m_l)}$ that converges almost surely.[8] With a slight abuse of notation we will simply write $n = n(m_l)$. So, we will assume that we are working with such a subsequence $\tau_n \to \tau$ almost surely. We will then show that this implies that the corresponding properties (1.-3.) of the theorem hold almost surely. By the same logic, this implies that the main claims of the theorem hold in probability, since we will have constructed a subsequence of any subsequence where almost sure convergence holds.

1. The first property follows from the fact that the constant functions are included, and thus a constant band with the desired coverage can always be constructed. That the sets are closed follows from the continuity of $f(u,\tau)$.

[7] See, for instance, Ch. 5 in Panaretos, V. M. (2016). Statistics for Mathematicians: A Rigorous First Course (1. ed.). Compact Textbook in Mathematics. Birkhäuser/Springer. Springer.

[8] See, for instance, Theorem 2.3.2. in: Durrett, R. (2019). *Probability: Theory and Examples*. Cambridge University Press.

2. Since the f_u are equicontinuous, for any $\epsilon > 0$ there exists $\delta > 0$ such that $|f(u, \tau') - f(u, \tau)| \leq \epsilon$ whenever $\|\tau - \tau'\| \leq \delta$ and for all $u \in \mathcal{U}$. Since $\tilde{\tau}_n \to \tilde{\tau}$ almost surely, we can, with probability 1, find an N large enough such that $n \geq N$ implies $\|\tilde{\tau}_n - \tilde{\tau}\| \leq \delta$. It then follows that if $n \geq N$ then

$$|\alpha - f(u_n, \tilde{\tau})| = |f(u_n, \tilde{\tau}_n) - f(u_n, \tilde{\tau})| \leq \epsilon,$$

which proves the claim.
3. Recall that the Hausdorff distance is given by

$$d(S_n, S) = \max\left\{\sup_{u_n \in S_n} \inf_{u \in S} \|u_n - u\|, \sup_{u \in S} \inf_{u_n \in S_n} \|u_n - u\|\right\} = \max\left\{d_{1,n}, d_{2,n}\right\}.$$

In the following, we examine the terms $d_{1,n}$ and $d_{2,n}$ separately. In the first case, only compactness of $\mathcal{U}$ is needed, while in the second case, both the convexity and the inclusion of the constant functions will be crucial.

(a) We consider a proof by contradiction, so assume

$$d_{1,n} = \sup_{u_n \in S_n} \inf_{u \in S} \|u_n - u\| \not\to 0.$$

This implies that, with probability 1, there exists an $\epsilon > 0$ and infinitely many n such that $d_{1,n} \geq \epsilon$. Take a further subsequence such that $d_{1,n} \geq \epsilon$ for all n. Since the sets are compact, this implies that there exists $u_n \in S_n$ such that $\|u_n - u\| \geq \epsilon$, for all n and all $u \in S$. Now take a convergent subsequence of u_n such that $u_n \to w$. By property 2. we have

$$f(u_n, \tilde{\tau}) \to \alpha \Longrightarrow f(w, \tilde{\tau}) = \alpha,$$

which implies that $w \in S$, which is a contradiction since $\|u - w\| \geq \epsilon$ for all $u \in S$. Thus, $d_{1,n} \to 0$.

(b) We again use a proof by contradiction. Suppose that

$$d_{2,n} = \sup_{u \in S} \inf_{u_n \in S_n} \|u_n - u\| \not\to 0.$$

As the proof here is more complex, we first provide a high level overview. First, we will show that if $d_{2,n} \not\to 0$, then we can construct a band, $w \in S$ that is isolated from all but a finite number of the other S_n. We then combine the continuity of f and the convexity of $\mathcal{U}$ to construct a band in S_n with proper coverage, but which must be close to w contradicting this isolation.

Turning to the proof, with probability 1, there exists $\epsilon > 0$ such that $d_{2,n} > 2\epsilon$ for infinitely many n, take an appropriate subsequence such that it holds for all n. Again, since the sets are compact we can find $w_n \in S$, such that $\|w_n - u_n\| > 2\epsilon$ for all $u_n \in S_n$. Now take a further convergent subsequence such that $w_n \to w$. Then we can find N such that for all $n \geq N$ we have $\|w_n - w\| \leq \epsilon$, which implies that $w \notin S_n$ for $n \geq N$ and even more

$$\|u_n - w\| = \|u_n - w_n + w_n - w\| \geq \|u_n - w_n\| - \|w_n - w\| \geq \epsilon$$

for all $u_n \in S_n$. This implies that w is isolated from the S_n, that is, there is a ball of radius ϵ about w that does not intersect with any S_n.

We now have to utilize the form for f more than previously. In particular, since the constant functions are in $\mathcal{U}$ and $\mathcal{U}$ is convex, this means that $w + 1c \in \mathcal{U}$ (1 is the constant function) if $c \in \mathbb{R}$ is small (if w is on the boundary then enlarge $\mathcal{U}$ slightly) and so for any $\tilde{\tau}$, $f(w+1c, \tilde{\tau})$ is monotonically decreasing with c (since the band raises uniformly). If ϕ is the density of $X(0)$ then

$$|c|\phi(w(0) + |c|) \leq |P(X(0) \geq w(0) + c) - P(X(0) \geq w(0))| \leq |c|\phi(w(0) - |c|),$$

which means that we can raise/lower the band by c and produce a change in α at least as large in magnitude as the corresponding quantity above (note the integrals in $f(w, \tilde{\tau})$ will increase/decrease in the same direction).

Coming back to the problem at hand, we have that $f(w, \tilde{\tau}) = \alpha$, which implies that $f(w, \tilde{\tau}_n) \to \alpha$. So take N such that for all $n \geq N$ we have

$$|f(w, \tilde{\tau}_n) - \alpha| < \delta := (\epsilon/2)\phi(u(0) + \epsilon/2).$$

However, now by construction we have that there exists $u_1, u_2 \in \mathcal{U}$ with $|u_i - w| \leq \epsilon$ such that

$$f(u_1, \tau_n) < \alpha \qquad \text{and} \qquad f(u_2, \tau_n) > \alpha,$$

where $u_i = w + c_i 1$, for some $|c_i| \leq \epsilon/2$. However, $B_c(u', \epsilon) \cap \mathcal{U}$ is convex and $f(u_1 t + (1-t)u_2, \tau_n)$ is continuous in $t \in [0, 1]$ thus there must exist a $u \in B_c(w, \epsilon) \cap \mathcal{U}$ such that $f(u, \tau_n) = \alpha$ implying $u \in S_n$, which is a contradiction since no element of S_n is within ϵ of w. Thus $d_{2,n} \to 0$.

A.6 Proof of Lemma 3.2 (Fairness of $u^\star_{\alpha/2}$)

In equations (10)-(12), Algorithm 1 applies the generalized Kac-Rice formula (4) interval-wise for $\{X(t) : t \in [a_{j-1}, a_j]\}$ by substituting 0, 1, and t_0 in (4) by a_{j-1}, a_j, and a_j for odd $j = 1, 3, \ldots$ and by a_{j-1}, a_j, a_{j-1} for even $j = 2, 4, \ldots$. The interval-wise critical value functions $\{u^\star_{\alpha/2}(t) : t \in [a_{j-1}, a_j]\}$ are determined by setting the interval-wise generalized Kac-Rice formulas for $\{X(t) : t \in [a_{j-1}, a_j]\}$ equal to $(\alpha/2)(a_j - a_{j-1})$. Thus, by inequality (2) with corresponding substitutions for 0, 1, and t_0

$$P(\exists t \in [a_{j-1}, a_j] : X(t) \geq u^\star_{\alpha/2}(t)) \leq \frac{\alpha}{2}(a_j - a_{j-1}) \quad \text{for each} \quad j = 1, \ldots, p.$$

The result of Lemma 3.2 follows now by applying Boole's inequality

$$\begin{aligned} P\Big(\exists t \in \bigcup_{j \in \mathcal{J}} [a_{j-1}, a_j] : X(t) \geq u^\star_{\alpha/2}(t)\Big) &\leq \sum_{j \in \mathcal{J}} P(\exists t \in [a_{j-1}, a_j] : X(t) \geq u^\star_{\alpha/2}(t)) \\ &\leq \sum_{j \in \mathcal{J}} \frac{\alpha}{2}(a_j - a_{j-1}) \end{aligned}$$

for any $\mathcal{J} \subseteq \{1, 2, \ldots, p\}$. □

A.7 Additional Derivations for the Discussion of the Price of Fairness

To discuss the effect of the number of intervals p, let us sum up the single components produced by Algorithm 1, which yields

$$\sum_{j=1}^{p}\Bigg[\mathbb{1}_{(j \text{ is odd})}\left(P\big(X(a_j)\geq u^{\star}_{\alpha/2}(a_j)\big)\right)+\int_{a_{j-1}}^{a_j}\frac{\tau(t)}{2\pi}M_{\mathcal{V}}\left(-\frac{1}{2}\left[(u^{\star}_{\alpha/2}(t))^2+\frac{u^{\star'}_{\alpha/2}(t)^2}{\tau(t)^2}\right]\right)\,dt$$
$$+\mathbb{1}_{(j \text{ is odd})}\left(\int_{a_{j-1}}^{a_j}\int_0^{\infty}\frac{u^{\star'}_{\alpha/2}(t)}{2\pi\tau(t)}M'_{\mathcal{V}}\left(-\frac{1}{2}\left[(u^{\star}_{\alpha/2}(t))^2+\frac{(y-u^{\star'}_{\alpha/2}(t))^2}{\tau(t)^2}\right]\right)\,dy\,dt\right)$$
$$-\mathbb{1}_{(j \text{ is even})}\left(\int_{a_{j-1}}^{a_j}\int_0^{\infty}\frac{u^{\star'}_{\alpha/2}(t)}{2\pi\tau(t)}M'_{\mathcal{V}}\left(-\frac{1}{2}\left[(u^{\star}_{\alpha/2}(t))^2+\frac{(y+u^{\star'}_{\alpha/2}(t))^2}{\tau(t)^2}\right]\right)\,dy\,dt\right)\Bigg]=\frac{\alpha}{2}.$$

Over intervals $[a_{j-1},a_j]$, where j is odd/even, we compute the mean number of down-/up-crossings about u. However, since the distribution of X is symmetric, the mean of up-crossings about u equals the mean of down-crossings about $-u$. This allows us to write,

$$\sum_{j=1}^{p}\mathbb{1}_{(j \text{ is odd})}\left(P\big(X(a_j)\geq u^{\star}_{\alpha/2}(a_j)\big)\right)+\int_0^1\frac{\tau(t)}{2\pi}M_{\mathcal{V}}\left(-\frac{1}{2}\left[(u^{\star}_{\alpha/2}(t))^2+\frac{u^{\star'}_{\alpha/2}(t)^2}{\tau(t)^2}\right]\right)\,dt$$
$$+\left(\int_0^{a_1}\int_0^{\infty}\frac{u^{\star'}_{\alpha/2}(t)}{2\pi\tau(t)}M'_{\mathcal{V}}\left(-\frac{1}{2}\left[(u^{\star}_{\alpha/2}(t))^2+\frac{(y-u^{\star'}_{\alpha/2}(t))^2}{\tau(t)^2}\right]\right)\,dy\,dt\right)$$
$$-\left(\int_{a_1}^{1}\int_0^{\infty}\frac{u^{\star'}_{\alpha/2}(t)}{2\pi\tau(t)}M'_{\mathcal{V}}\left(-\frac{1}{2}\left[(u^{\star}_{\alpha/2}(t))^2+\frac{(y-u^{\star'}_{\alpha/2}(t))^2}{\tau(t)^2}\right]\right)\,dy\,dt\right)=\frac{\alpha}{2}$$
$$\Leftrightarrow\mathbb{E}[\varphi_{u^{\star}_{\alpha/2},X}(a_1)]+\sum_{\substack{3\leq j\leq p\\ j:\text{odd}}}\left(P\big(X(a_j)\geq u^{\star}_{\alpha/2}(a_j)\big)\right)=\frac{\alpha}{2}$$

B Additional Simulation Results and Figures

Table 4 shows summary statistics of the computations times for the FF bands and all comparison bands. The comparison study shown in Table 4 was done using the R package `microbenchmark` using 100 repeated computations.[9] Computations were conduced using a laptop computer with AMD-Ryzen 7 pro 4750u processor.

Table 4: Computation times (100 repetitions) for $n = 100$, Mean θ_0 and Cov3.

Band	Min.	LQ	Mean	Median	UQ	Max	% of MB_t Median
FF_z^1	0.025	0.025	0.028	0.025	0.028	0.056	2
FF_z^2	0.027	0.028	0.032	0.029	0.032	0.065	2
FF_z^4	0.032	0.034	0.037	0.035	0.037	0.083	3
FF_t^1	0.026	0.029	0.033	0.030	0.032	0.060	2
FF_t^2	0.030	0.033	0.038	0.035	0.038	0.077	3
FF_t^4	0.039	0.044	0.050	0.047	0.051	0.086	4
GKF_t	0.020	0.021	0.027	0.022	0.024	0.266	2
B_{EC}	0.030	0.033	0.037	0.034	0.038	0.076	3
B_{S}	0.137	0.148	0.163	0.160	0.169	0.388	13
IWT	0.509	0.559	0.598	0.589	0.623	0.850	46
MB_t	0.969	1.220	1.280	1.276	1.317	1.571	100

Unit: seconds (LQ: Lower Quantile; UQ: Upper Quantile)

Table 5: Average confidence band widths and rankings (in parentheses)*

	$n = 15$			$n = 100$		
Band	Cov1	Cov2	Cov3	Cov1	Cov2	Cov3
FF_t^4	0.386 (6)	0.447 (5)	0.426 (4)	0.134 (6)	0.152 (4)	0.146 (4)
FF_t^2	0.358 (5)	0.437 (4)	0.413 (2)	0.126 (4)	0.150 (3)	0.142 (2)
FF_t^1	0.336 (2)	0.432 (3)	0.415 (3)	0.120 (2)	0.148 (2)	0.144 (3)
B_{EC}	0.324 (1)	0.413 (1)	0.396 (1)	0.131 (5)	0.205 (6)	0.183 (6)
MB_t	0.353 (3)	0.431 (2)	0.426 (5)	0.120 (1)	0.140 (1)	0.139 (1)
GKF_t	0.357 (4)	0.486 (6)	0.465 (6)	0.121 (3)	0.154 (5)	0.149 (5)

*Cannot be computed for the IWT procedure. B_{S} is not shown since this band is too narrow and leads to invalid inference in small samples.

Table 5 summarizes the average widths of the bands where the widths are averaged over the domain $[0, 1]$ and over the Monte Carlo samples. The average widths of the FF_t^1 band is close to that of the MB_t band. The larger p the wider are the FF_t^p bands. The B_{EC} band is very narrow for small samples, but becomes the widest for the rough processes (Cov2-3)

[9] Mersmann, O. (2021). microbenchmark: Accurate Timing Functions. R package version 1.4.9.

and large samples. The width rankings of the GKF_t band are similar to those of the FF_t^4 band.

Table 6: Size and Power for Cov1 and $n = 15$. (Section 4.1 in the main paper.)

		4 Fair Intervals $\alpha/4 = 0.0125$				2 Fair Intervals $\alpha/2 = 0.025$		1 Interval $\alpha = 0.05$	Mean perturbations Δ					Avg.
	Band	$[0, \frac{1}{4}]$	$[\frac{1}{4}, \frac{2}{4}]$	$[\frac{2}{4}, \frac{3}{4}]$	$[\frac{3}{4}, 1]$	$[0, \frac{1}{2}]$	$[\frac{1}{2}, 1]$	$[0, 1]$	0.05	0.15	0.25	0.35	0.45	Power
Mean1	FF_t^4	0.012	0.012	0.012	0.012	0.017	0.017	0.025	0.072	0.492	0.927	0.998	1.000	0.698
Mean1	FF_t^2	0.019	0.019	0.018	0.018	0.026	0.025	0.037	0.100	0.572	0.955	0.999	1.000	0.725
Mean1	FF_t^1	0.026	0.026	0.025	0.025	0.034	0.034	0.051	0.119	0.645	0.970	1.000	1.000	0.747
Mean1	FF_z^4	0.027	0.028	0.027	0.027	0.036	0.036	0.052	0.122	0.644	0.968	1.000	1.000	0.747
Mean1	FF_z^2	0.036	0.037	0.035	0.035	0.047	0.046	0.069	0.150	0.695	0.979	1.000	1.000	0.765
Mean1	FF_z^1	0.045	0.044	0.044	0.044	0.058	0.058	0.085	0.179	0.732	0.984	1.000	1.000	0.779
Mean1	B_{EC}	0.025	0.036	0.035	0.024	0.039	0.038	0.051	0.122	0.631	0.966	1.000	1.000	0.744
Mean1	B_{S}	0.047	0.047	0.046	0.046	0.061	0.061	0.088	0.186	0.740	0.985	1.000	1.000	0.782
Mean1	MB_t	0.020	0.019	0.019	0.019	0.026	0.026	0.039	0.099	0.593	0.958	1.000	1.000	0.730
Mean1	GKF_t	0.018	0.018	0.018	0.018	0.025	0.025	0.037	0.095	0.581	0.956	1.000	1.000	0.726
Mean1	IWT							0.036	0.097	0.585	0.953	0.999	1.000	0.727
Mean2	FF_t^4	0.012	0.018	0.016	0.011	0.022	0.022	0.029	0.054	0.325	0.805	0.984	1.000	0.633
Mean2	FF_t^2	0.019	0.019	0.021	0.027	0.025	0.033	0.045	0.089	0.472	0.912	0.997	1.000	0.694
Mean2	FF_t^1	0.026	0.026	0.025	0.025	0.034	0.034	0.051	0.091	0.455	0.902	0.997	1.000	0.689
Mean2	FF_z^4	0.027	0.028	0.027	0.027	0.036	0.036	0.052	0.094	0.458	0.902	0.996	1.000	0.690
Mean2	FF_z^2	0.036	0.037	0.035	0.035	0.047	0.046	0.069	0.116	0.515	0.929	0.998	1.000	0.712
Mean2	FF_z^1	0.045	0.044	0.044	0.044	0.058	0.058	0.085	0.143	0.560	0.942	0.999	1.000	0.729
Mean2	B_{EC}	0.025	0.036	0.035	0.024	0.039	0.038	0.051	0.088	0.441	0.898	0.996	1.000	0.685
Mean2	B_{S}	0.047	0.047	0.046	0.046	0.061	0.061	0.088	0.149	0.569	0.944	0.999	1.000	0.732
Mean2	MB_t	0.020	0.019	0.019	0.019	0.026	0.026	0.039	0.072	0.406	0.875	0.995	1.000	0.670
Mean2	GKF_t	0.018	0.018	0.018	0.018	0.025	0.025	0.037	0.070	0.397	0.866	0.994	1.000	0.665
Mean2	IWT							0.036	0.049	0.218	0.605	0.923	0.997	0.558
Mean3	FF_t^4	0.012	0.018	0.016	0.011	0.022	0.022	0.029	0.049	0.319	0.817	0.989	1.000	0.635
Mean3	FF_t^2	0.019	0.019	0.021	0.027	0.025	0.033	0.045	0.074	0.395	0.873	0.995	1.000	0.667
Mean3	FF_t^1	0.026	0.026	0.025	0.025	0.034	0.034	0.051	0.088	0.455	0.909	0.997	1.000	0.690
Mean3	FF_z^4	0.027	0.028	0.027	0.027	0.036	0.036	0.052	0.092	0.460	0.911	0.997	1.000	0.692
Mean3	FF_z^2	0.036	0.037	0.035	0.035	0.047	0.046	0.069	0.118	0.518	0.939	0.999	1.000	0.715
Mean3	FF_z^1	0.045	0.044	0.044	0.044	0.058	0.058	0.085	0.142	0.572	0.955	0.999	1.000	0.734
Mean3	B_{EC}	0.025	0.036	0.035	0.024	0.039	0.038	0.051	0.077	0.432	0.906	0.998	1.000	0.683
Mean3	B_{S}	0.047	0.047	0.046	0.046	0.061	0.061	0.088	0.147	0.582	0.958	1.000	1.000	0.737
Mean3	MB_t	0.020	0.019	0.019	0.019	0.026	0.026	0.039	0.068	0.402	0.877	0.995	1.000	0.668
Mean3	GKF_t	0.018	0.018	0.018	0.018	0.025	0.025	0.037	0.065	0.392	0.871	0.995	1.000	0.664
Mean3	IWT							0.036	0.038	0.057	0.120	0.282	0.615	0.222

Table 7: Size and Power for Cov1 and $n = 100$. (Section 4.1 in the main paper.)

		4 Fair Intervals $\alpha/4 = 0.0125$				2 Fair Intervals $\alpha/2 = 0.025$		1 Interval $\alpha = 0.05$	Mean perturbations Δ					Avg.
	Band	$[0, \frac{1}{4}]$	$[\frac{1}{4}, \frac{2}{4}]$	$[\frac{2}{4}, \frac{3}{4}]$	$[\frac{3}{4}, 1]$	$[0, \frac{1}{2}]$	$[\frac{1}{2}, 1]$	$[0, 1]$	0.05	0.15	0.25	0.35	0.45	Power
Mean1	FF_t^4	0.012	0.012	0.012	0.013	0.016	0.017	0.025	0.078	0.282	0.605	0.864	0.978	0.561
Mean1	FF_t^2	0.019	0.019	0.019	0.019	0.025	0.025	0.036	0.104	0.338	0.671	0.898	0.984	0.599
Mean1	FF_t^1	0.025	0.025	0.025	0.026	0.033	0.033	0.048	0.126	0.375	0.710	0.923	0.987	0.624
Mean1	FF_z^4	0.014	0.014	0.015	0.015	0.019	0.020	0.028	0.084	0.293	0.626	0.880	0.978	0.572
Mean1	FF_z^2	0.021	0.020	0.020	0.021	0.027	0.027	0.040	0.109	0.344	0.682	0.911	0.984	0.606
Mean1	FF_z^1	0.028	0.028	0.027	0.028	0.036	0.036	0.052	0.134	0.388	0.723	0.928	0.988	0.632
Mean1	B_{EC}	0.013	0.020	0.020	0.013	0.021	0.021	0.027	0.081	0.279	0.604	0.863	0.972	0.560
Mean1	B_{S}	0.029	0.029	0.029	0.030	0.038	0.038	0.055	0.140	0.399	0.731	0.930	0.989	0.638
Mean1	MB_t	0.025	0.025	0.025	0.026	0.033	0.033	0.048	0.126	0.375	0.711	0.923	0.987	0.624
Mean1	GKF_t	0.024	0.024	0.024	0.025	0.032	0.032	0.046	0.123	0.368	0.703	0.920	0.986	0.620
Mean1	IWT							0.036	0.113	0.350	0.680	0.900	0.983	0.605
Mean2	FF_t^4	0.012	0.013	0.014	0.014	0.018	0.019	0.026	0.054	0.178	0.442	0.737	0.924	0.467
Mean2	FF_t^2	0.019	0.018	0.019	0.021	0.024	0.026	0.037	0.073	0.224	0.505	0.788	0.945	0.507
Mean2	FF_t^1	0.025	0.025	0.025	0.026	0.033	0.033	0.048	0.090	0.254	0.538	0.812	0.953	0.530
Mean2	FF_z^4	0.014	0.014	0.015	0.015	0.019	0.020	0.028	0.057	0.181	0.446	0.739	0.925	0.470
Mean2	FF_z^2	0.021	0.020	0.020	0.021	0.027	0.027	0.040	0.077	0.226	0.507	0.790	0.946	0.509
Mean2	FF_z^1	0.028	0.028	0.027	0.028	0.036	0.036	0.052	0.096	0.266	0.554	0.823	0.957	0.539
Mean2	B_{EC}	0.013	0.020	0.020	0.013	0.021	0.021	0.027	0.052	0.159	0.406	0.700	0.905	0.444
Mean2	B_{S}	0.029	0.029	0.029	0.030	0.038	0.038	0.055	0.101	0.273	0.565	0.831	0.959	0.546
Mean2	MB_t	0.025	0.025	0.025	0.026	0.033	0.033	0.048	0.090	0.255	0.538	0.813	0.953	0.530
Mean2	GKF_t	0.024	0.024	0.024	0.025	0.032	0.032	0.046	0.087	0.247	0.530	0.807	0.951	0.525
Mean2	IWT							0.036	0.053	0.112	0.224	0.429	0.672	0.298
Mean3	FF_t^4	0.012	0.013	0.014	0.014	0.018	0.019	0.026	0.052	0.178	0.432	0.734	0.925	0.464
Mean3	FF_t^2	0.019	0.018	0.019	0.021	0.024	0.026	0.037	0.072	0.224	0.502	0.794	0.950	0.508
Mean3	FF_t^1	0.025	0.025	0.025	0.026	0.033	0.033	0.048	0.092	0.265	0.556	0.830	0.967	0.542
Mean3	FF_z^4	0.014	0.014	0.015	0.015	0.019	0.020	0.028	0.057	0.191	0.455	0.752	0.933	0.477
Mean3	FF_z^2	0.021	0.020	0.020	0.021	0.027	0.027	0.040	0.077	0.237	0.521	0.805	0.956	0.519
Mean3	FF_z^1	0.028	0.028	0.027	0.028	0.036	0.036	0.052	0.098	0.278	0.573	0.842	0.971	0.553
Mean3	B_{EC}	0.013	0.020	0.020	0.013	0.021	0.021	0.027	0.048	0.161	0.401	0.711	0.915	0.447
Mean3	B_{S}	0.029	0.029	0.029	0.030	0.038	0.038	0.055	0.103	0.286	0.583	0.849	0.973	0.559
Mean3	MB_t	0.025	0.025	0.025	0.026	0.033	0.033	0.048	0.092	0.266	0.557	0.831	0.967	0.542
Mean3	GKF_t	0.024	0.024	0.024	0.025	0.032	0.032	0.046	0.087	0.259	0.546	0.825	0.963	0.536
Mean3	IWT							0.036	0.038	0.043	0.051	0.074	0.100	0.061

Table 8: Size and Power for Cov2 and $n = 15$. (Section 4.1 in the main paper.)

		4 Fair Intervals $\alpha/4 = 0.0125$				2 Fair Intervals $\alpha/2 = 0.025$		1 Interval $\alpha = 0.05$	Mean perturbations Δ					Avg.
	Band	$[0, \frac{1}{4}]$	$[\frac{1}{4}, \frac{2}{4}]$	$[\frac{2}{4}, \frac{3}{4}]$	$[\frac{3}{4}, 1]$	$[0, \frac{1}{2}]$	$[\frac{1}{2}, 1]$	$[0, 1]$	0.05	0.15	0.25	0.35	0.45	Power
Mean1	FF_t^4	0.011	0.012	0.011	0.011	0.018	0.018	0.032	0.079	0.542	0.947	0.999	1.000	0.713
Mean1	FF_t^2	0.013	0.013	0.013	0.013	0.021	0.021	0.036	0.088	0.572	0.955	1.000	1.000	0.723
Mean1	FF_t^1	0.014	0.013	0.014	0.014	0.022	0.023	0.038	0.098	0.592	0.960	1.000	1.000	0.730
Mean1	FF_z^4	0.029	0.030	0.030	0.031	0.046	0.047	0.078	0.169	0.725	0.985	1.000	1.000	0.776
Mean1	FF_z^2	0.032	0.032	0.033	0.033	0.051	0.052	0.084	0.177	0.740	0.987	1.000	1.000	0.781
Mean1	FF_z^1	0.034	0.034	0.035	0.036	0.053	0.054	0.089	0.186	0.749	0.988	1.000	1.000	0.785
Mean1	$\mathrm{B_{EC}}$	0.012	0.015	0.016	0.012	0.021	0.022	0.036	0.095	0.623	0.971	1.000	1.000	0.738
Mean1	$\mathrm{B_S}$	0.049	0.048	0.048	0.050	0.074	0.075	0.122	0.237	0.808	0.993	1.000	1.000	0.808
Mean1	MB_t	0.013	0.013	0.013	0.013	0.021	0.021	0.036	0.095	0.596	0.963	1.000	1.000	0.731
Mean1	GKF_t	0.006	0.006	0.006	0.006	0.010	0.010	0.018	0.055	0.448	0.915	0.998	1.000	0.683
Mean1	IWT							0.028	0.100	0.632	0.980	1.000	1.000	0.742
Mean2	FF_t^4	0.011	0.012	0.013	0.013	0.019	0.021	0.034	0.061	0.369	0.842	0.991	1.000	0.653
Mean2	FF_t^2	0.012	0.012	0.014	0.014	0.020	0.022	0.036	0.066	0.387	0.857	0.992	1.000	0.661
Mean2	FF_t^1	0.014	0.013	0.014	0.014	0.022	0.023	0.038	0.066	0.374	0.840	0.991	1.000	0.654
Mean2	FF_z^4	0.029	0.030	0.030	0.031	0.046	0.047	0.078	0.122	0.513	0.917	0.997	1.000	0.710
Mean2	FF_z^2	0.032	0.032	0.033	0.033	0.051	0.052	0.084	0.132	0.531	0.926	0.998	1.000	0.717
Mean2	FF_z^1	0.034	0.034	0.035	0.036	0.053	0.054	0.089	0.138	0.538	0.926	0.998	1.000	0.720
Mean2	$\mathrm{B_{EC}}$	0.012	0.015	0.016	0.012	0.021	0.022	0.036	0.066	0.396	0.871	0.995	1.000	0.666
Mean2	$\mathrm{B_S}$	0.049	0.048	0.048	0.050	0.074	0.075	0.122	0.182	0.608	0.952	0.999	1.000	0.748
Mean2	MB_t	0.013	0.013	0.013	0.013	0.021	0.021	0.036	0.064	0.373	0.845	0.992	1.000	0.655
Mean2	GKF_t	0.006	0.006	0.006	0.006	0.010	0.010	0.018	0.036	0.254	0.738	0.973	0.999	0.600
Mean2	IWT							0.028	0.045	0.225	0.695	0.961	0.998	0.585
Mean3	FF_t^4	0.011	0.012	0.013	0.013	0.019	0.021	0.034	0.049	0.275	0.771	0.983	1.000	0.616
Mean3	FF_t^2	0.012	0.012	0.014	0.014	0.020	0.022	0.036	0.054	0.297	0.795	0.986	1.000	0.627
Mean3	FF_t^1	0.014	0.013	0.014	0.014	0.022	0.023	0.038	0.058	0.310	0.804	0.987	1.000	0.632
Mean3	FF_z^4	0.029	0.030	0.030	0.031	0.046	0.047	0.078	0.115	0.454	0.903	0.998	1.000	0.694
Mean3	FF_z^2	0.032	0.032	0.033	0.033	0.051	0.052	0.084	0.124	0.474	0.913	0.998	1.000	0.702
Mean3	FF_z^1	0.034	0.034	0.035	0.036	0.053	0.054	0.089	0.131	0.486	0.915	0.998	1.000	0.706
Mean3	$\mathrm{B_{EC}}$	0.012	0.015	0.016	0.012	0.021	0.022	0.036	0.053	0.306	0.830	0.994	1.000	0.637
Mean3	$\mathrm{B_S}$	0.049	0.048	0.048	0.050	0.074	0.075	0.122	0.175	0.572	0.950	1.000	1.000	0.739
Mean3	MB_t	0.013	0.013	0.013	0.013	0.021	0.021	0.036	0.056	0.309	0.810	0.988	1.000	0.633
Mean3	GKF_t	0.006	0.006	0.006	0.006	0.010	0.010	0.018	0.029	0.199	0.679	0.964	0.999	0.574
Mean3	IWT							0.028	0.030	0.056	0.136	0.376	0.722	0.264

Table 9: Size and Power for Cov2 and $n = 100$. (Section 4.1 in the main paper.)

		4 Fair Intervals $\alpha/4 = 0.0125$				2 Fair Intervals $\alpha/2 = 0.025$		1 Interval $\alpha = 0.05$	Mean perturbations Δ					Avg.
	Band	$[0, \frac{1}{4}]$	$[\frac{1}{4}, \frac{2}{4}]$	$[\frac{2}{4}, \frac{3}{4}]$	$[\frac{3}{4}, 1]$	$[0, \frac{1}{2}]$	$[\frac{1}{2}, 1]$	$[0, 1]$	0.05	0.15	0.25	0.35	0.45	Power
Mean1	FF_t^4	0.009	0.010	0.010	0.010	0.015	0.016	0.025	0.085	0.306	0.648	0.906	0.987	0.586
Mean1	FF_t^2	0.010	0.011	0.011	0.011	0.017	0.017	0.029	0.092	0.321	0.665	0.916	0.988	0.596
Mean1	FF_t^1	0.012	0.012	0.013	0.013	0.019	0.020	0.033	0.102	0.337	0.684	0.916	0.988	0.605
Mean1	FF_z^4	0.012	0.013	0.013	0.013	0.019	0.020	0.033	0.101	0.336	0.683	0.914	0.988	0.604
Mean1	FF_z^2	0.013	0.014	0.014	0.015	0.021	0.022	0.036	0.111	0.353	0.699	0.923	0.990	0.615
Mean1	FF_z^1	0.014	0.015	0.015	0.016	0.023	0.023	0.039	0.115	0.364	0.707	0.927	0.990	0.621
Mean1	B_{EC}	0.000	0.000	0.000	0.000	0.000	0.001	0.001	0.007	0.048	0.220	0.536	0.833	0.329
Mean1	B_S	0.023	0.025	0.024	0.025	0.037	0.038	0.061	0.161	0.448	0.775	0.952	0.995	0.666
Mean1	MB_t	0.018	0.020	0.019	0.020	0.029	0.031	0.050	0.138	0.407	0.745	0.943	0.993	0.645
Mean1	GKF_t	0.008	0.009	0.009	0.010	0.014	0.014	0.024	0.081	0.293	0.638	0.893	0.983	0.578
Mean1	IWT							0.029	0.111	0.376	0.717	0.932	0.993	0.626
Mean2	FF_t^4	0.009	0.011	0.011	0.011	0.016	0.017	0.028	0.053	0.189	0.452	0.731	0.925	0.470
Mean2	FF_t^2	0.011	0.011	0.012	0.013	0.018	0.019	0.031	0.058	0.200	0.470	0.746	0.932	0.481
Mean2	FF_t^1	0.012	0.012	0.013	0.013	0.019	0.020	0.033	0.061	0.203	0.473	0.747	0.933	0.483
Mean2	FF_z^4	0.012	0.013	0.013	0.013	0.019	0.020	0.033	0.060	0.204	0.473	0.748	0.933	0.484
Mean2	FF_z^2	0.013	0.014	0.014	0.015	0.021	0.022	0.036	0.067	0.216	0.493	0.762	0.940	0.496
Mean2	FF_z^1	0.014	0.015	0.015	0.016	0.023	0.023	0.039	0.069	0.224	0.500	0.768	0.942	0.501
Mean2	B_{EC}	0.000	0.000	0.000	0.000	0.000	0.001	0.001	0.003	0.017	0.100	0.292	0.601	0.203
Mean2	B_S	0.023	0.025	0.024	0.025	0.037	0.038	0.061	0.100	0.284	0.580	0.828	0.964	0.551
Mean2	MB_t	0.018	0.020	0.019	0.020	0.029	0.031	0.050	0.084	0.257	0.545	0.803	0.955	0.529
Mean2	GKF_t	0.008	0.009	0.009	0.010	0.014	0.014	0.024	0.046	0.171	0.424	0.707	0.915	0.453
Mean2	IWT							0.029	0.052	0.122	0.268	0.493	0.762	0.339
Mean3	FF_t^4	0.009	0.011	0.011	0.011	0.016	0.017	0.028	0.044	0.142	0.380	0.676	0.902	0.429
Mean3	FF_t^2	0.011	0.011	0.012	0.013	0.018	0.019	0.031	0.050	0.155	0.401	0.696	0.911	0.443
Mean3	FF_t^1	0.012	0.012	0.013	0.013	0.019	0.020	0.033	0.054	0.162	0.412	0.706	0.915	0.450
Mean3	FF_z^4	0.012	0.013	0.013	0.013	0.019	0.020	0.033	0.052	0.159	0.409	0.703	0.914	0.448
Mean3	FF_z^2	0.013	0.014	0.014	0.015	0.021	0.022	0.036	0.059	0.171	0.426	0.723	0.924	0.461
Mean3	FF_z^1	0.014	0.015	0.015	0.016	0.023	0.023	0.039	0.063	0.180	0.437	0.731	0.928	0.468
Mean3	B_{EC}	0.000	0.000	0.000	0.000	0.000	0.001	0.001	0.002	0.011	0.068	0.236	0.534	0.170
Mean3	B_S	0.023	0.025	0.024	0.025	0.037	0.038	0.061	0.095	0.242	0.525	0.799	0.959	0.524
Mean3	MB_t	0.018	0.020	0.019	0.020	0.029	0.031	0.050	0.078	0.211	0.487	0.768	0.948	0.498
Mean3	GKF_t	0.008	0.009	0.009	0.010	0.014	0.014	0.024	0.040	0.133	0.368	0.662	0.894	0.419
Mean3	IWT							0.029	0.030	0.042	0.059	0.080	0.116	0.065

Table 10: Size and Power for Cov3 and $n = 15$. (Section 4.1 in the main paper.)

		4 Fair Intervals $\alpha/4 = 0.0125$				2 Fair Intervals $\alpha/2 = 0.025$		1 Interval $\alpha = 0.05$	Mean perturbations Δ					Avg.
	Band	$[0, \frac{1}{4}]$	$[\frac{1}{4}, \frac{2}{4}]$	$[\frac{2}{4}, \frac{3}{4}]$	$[\frac{3}{4}, 1]$	$[0, \frac{1}{2}]$	$[\frac{1}{2}, 1]$	$[0, 1]$	0.05	0.15	0.25	0.35	0.45	Power
Mean1	FF_t^4	0.013	0.012	0.011	0.012	0.017	0.019	0.031	0.084	0.561	0.956	1.000	1.000	0.720
Mean1	FF_t^2	0.016	0.019	0.017	0.010	0.025	0.023	0.038	0.094	0.587	0.961	1.000	1.000	0.728
Mean1	FF_t^1	0.008	0.010	0.015	0.030	0.013	0.037	0.044	0.116	0.641	0.976	1.000	1.000	0.747
Mean1	FF_z^4	0.027	0.027	0.029	0.040	0.037	0.055	0.077	0.171	0.738	0.988	1.000	1.000	0.779
Mean1	FF_z^2	0.030	0.037	0.037	0.034	0.047	0.058	0.083	0.180	0.746	0.989	1.000	1.000	0.783
Mean1	FF_z^1	0.019	0.024	0.034	0.067	0.031	0.082	0.097	0.205	0.780	0.993	1.000	1.000	0.796
Mean1	B_{EC}	0.015	0.022	0.017	0.008	0.025	0.021	0.035	0.097	0.601	0.970	1.000	1.000	0.734
Mean1	B_S	0.025	0.031	0.043	0.082	0.039	0.101	0.120	0.238	0.818	0.995	1.000	1.000	0.810
Mean1	MB_t	0.006	0.008	0.012	0.024	0.010	0.030	0.036	0.101	0.614	0.971	1.000	1.000	0.737
Mean1	GKF_t	0.004	0.004	0.007	0.016	0.006	0.019	0.023	0.066	0.510	0.945	0.999	1.000	0.704
Mean1	IWT							0.027	0.094	0.625	0.976	1.000	1.000	0.739
Mean2	FF_t^4	0.011	0.017	0.012	0.014	0.020	0.023	0.034	0.067	0.389	0.866	0.992	1.000	0.663
Mean2	FF_t^2	0.014	0.018	0.018	0.016	0.023	0.029	0.041	0.079	0.418	0.881	0.995	1.000	0.675
Mean2	FF_t^1	0.008	0.010	0.015	0.030	0.013	0.037	0.044	0.098	0.521	0.931	0.998	1.000	0.710
Mean2	FF_z^4	0.027	0.027	0.029	0.040	0.037	0.055	0.077	0.140	0.577	0.946	0.999	1.000	0.732
Mean2	FF_z^2	0.030	0.037	0.037	0.034	0.047	0.058	0.083	0.142	0.561	0.940	0.998	1.000	0.728
Mean2	FF_z^1	0.019	0.024	0.034	0.067	0.031	0.082	0.097	0.182	0.675	0.973	1.000	1.000	0.766
Mean2	B_{EC}	0.015	0.022	0.017	0.008	0.025	0.021	0.035	0.062	0.353	0.853	0.993	1.000	0.652
Mean2	B_S	0.025	0.031	0.043	0.082	0.039	0.101	0.120	0.217	0.721	0.980	1.000	1.000	0.784
Mean2	MB_t	0.006	0.008	0.012	0.024	0.010	0.030	0.036	0.085	0.491	0.923	0.998	1.000	0.699
Mean2	GKF_t	0.004	0.004	0.007	0.016	0.006	0.019	0.023	0.055	0.392	0.869	0.994	1.000	0.662
Mean2	IWT							0.027	0.048	0.231	0.681	0.958	0.997	0.583
Mean3	FF_t^4	0.011	0.017	0.012	0.014	0.020	0.023	0.034	0.056	0.317	0.810	0.990	1.000	0.634
Mean3	FF_t^2	0.014	0.018	0.018	0.016	0.023	0.029	0.041	0.067	0.355	0.843	0.994	1.000	0.652
Mean3	FF_t^1	0.008	0.010	0.015	0.030	0.013	0.037	0.044	0.058	0.271	0.756	0.980	1.000	0.613
Mean3	FF_z^4	0.027	0.027	0.029	0.040	0.037	0.055	0.077	0.115	0.469	0.909	0.998	1.000	0.698
Mean3	FF_z^2	0.030	0.037	0.037	0.034	0.047	0.058	0.083	0.125	0.498	0.924	0.999	1.000	0.709
Mean3	FF_z^1	0.019	0.024	0.034	0.067	0.031	0.082	0.097	0.124	0.429	0.879	0.996	1.000	0.686
Mean3	B_{EC}	0.015	0.022	0.017	0.008	0.025	0.021	0.035	0.060	0.367	0.867	0.997	1.000	0.658
Mean3	B_S	0.025	0.031	0.043	0.082	0.039	0.101	0.120	0.154	0.485	0.910	0.998	1.000	0.710
Mean3	MB_t	0.006	0.008	0.012	0.024	0.010	0.030	0.036	0.049	0.244	0.732	0.975	0.999	0.600
Mean3	GKF_t	0.004	0.004	0.007	0.016	0.006	0.019	0.023	0.030	0.177	0.636	0.947	0.998	0.558
Mean3	IWT							0.027	0.033	0.053	0.137	0.363	0.714	0.260

Table 11: Size and Power for Cov3 and $n = 100$. (Section 4.1 in the main paper.)

		4 Fair Intervals $\alpha/4 = 0.0125$				2 Fair Intervals $\alpha/2 = 0.025$		1 Interval $\alpha = 0.05$	Mean perturbations Δ					Avg.
	Band	$[0, \frac{1}{4}]$	$[\frac{1}{4}, \frac{2}{4}]$	$[\frac{2}{4}, \frac{3}{4}]$	$[\frac{3}{4}, 1]$	$[0, \frac{1}{2}]$	$[\frac{1}{2}, 1]$	$[0, 1]$	0.05	0.15	0.25	0.35	0.45	Power
Mean1	FF_t^4	0.013	0.012	0.011	0.011	0.017	0.018	0.029	0.092	0.330	0.660	0.918	0.990	0.598
Mean1	FF_t^2	0.015	0.019	0.016	0.009	0.024	0.021	0.034	0.102	0.346	0.674	0.921	0.991	0.607
Mean1	FF_t^1	0.007	0.009	0.013	0.025	0.012	0.031	0.038	0.118	0.379	0.730	0.933	0.993	0.631
Mean1	FF_z^4	0.014	0.014	0.012	0.013	0.019	0.021	0.033	0.104	0.356	0.706	0.927	0.992	0.617
Mean1	FF_z^2	0.018	0.020	0.018	0.010	0.027	0.024	0.038	0.112	0.370	0.717	0.927	0.993	0.624
Mean1	FF_z^1	0.009	0.011	0.015	0.029	0.014	0.036	0.044	0.132	0.404	0.754	0.943	0.994	0.645
Mean1	B_{EC}	0.004	0.004	0.001	0.000	0.005	0.001	0.006	0.024	0.134	0.388	0.706	0.922	0.435
Mean1	B_{S}	0.013	0.015	0.021	0.039	0.020	0.049	0.059	0.161	0.462	0.796	0.957	0.996	0.674
Mean1	MB_t	0.010	0.012	0.017	0.032	0.016	0.040	0.048	0.141	0.422	0.768	0.947	0.995	0.655
Mean1	GKF_t	0.005	0.007	0.010	0.019	0.009	0.024	0.029	0.096	0.338	0.690	0.917	0.991	0.606
Mean1	IWT							0.028	0.110	0.379	0.722	0.929	0.994	0.627
Mean2	FF_t^4	0.012	0.013	0.011	0.011	0.017	0.018	0.029	0.059	0.209	0.482	0.783	0.947	0.496
Mean2	FF_t^2	0.015	0.018	0.016	0.009	0.024	0.021	0.034	0.062	0.198	0.460	0.763	0.937	0.484
Mean2	FF_t^1	0.007	0.009	0.013	0.025	0.012	0.031	0.038	0.091	0.296	0.603	0.866	0.975	0.566
Mean2	FF_z^4	0.014	0.014	0.012	0.013	0.019	0.021	0.033	0.067	0.225	0.505	0.799	0.954	0.510
Mean2	FF_z^2	0.018	0.020	0.018	0.010	0.027	0.024	0.038	0.070	0.214	0.481	0.779	0.944	0.497
Mean2	FF_z^1	0.009	0.011	0.015	0.029	0.014	0.036	0.044	0.104	0.317	0.626	0.877	0.978	0.580
Mean2	B_{EC}	0.004	0.004	0.001	0.000	0.005	0.001	0.006	0.007	0.022	0.089	0.258	0.537	0.183
Mean2	B_{S}	0.013	0.015	0.021	0.039	0.020	0.049	0.059	0.127	0.365	0.672	0.899	0.984	0.610
Mean2	MB_t	0.010	0.012	0.017	0.032	0.016	0.040	0.048	0.110	0.330	0.639	0.885	0.980	0.589
Mean2	GKF_t	0.005	0.007	0.010	0.019	0.009	0.024	0.029	0.074	0.260	0.559	0.840	0.968	0.540
Mean2	IWT							0.028	0.052	0.113	0.242	0.494	0.748	0.330
Mean3	FF_t^4	0.012	0.013	0.011	0.011	0.017	0.018	0.029	0.054	0.176	0.425	0.731	0.928	0.463
Mean3	FF_t^2	0.015	0.018	0.016	0.009	0.024	0.021	0.034	0.061	0.196	0.457	0.758	0.938	0.482
Mean3	FF_t^1	0.007	0.009	0.013	0.025	0.012	0.031	0.038	0.054	0.149	0.367	0.673	0.895	0.428
Mean3	FF_z^4	0.014	0.014	0.012	0.013	0.019	0.021	0.033	0.060	0.190	0.448	0.750	0.935	0.476
Mean3	FF_z^2	0.018	0.020	0.018	0.010	0.027	0.024	0.038	0.067	0.212	0.477	0.774	0.945	0.495
Mean3	FF_z^1	0.009	0.011	0.015	0.029	0.014	0.036	0.044	0.063	0.164	0.390	0.696	0.909	0.444
Mean3	B_{EC}	0.004	0.004	0.001	0.000	0.005	0.001	0.006	0.017	0.086	0.275	0.580	0.847	0.361
Mean3	B_{S}	0.013	0.015	0.021	0.039	0.020	0.049	0.059	0.081	0.200	0.444	0.742	0.933	0.480
Mean3	MB_t	0.010	0.012	0.017	0.032	0.016	0.040	0.048	0.067	0.175	0.406	0.712	0.917	0.455
Mean3	GKF_t	0.005	0.007	0.010	0.019	0.009	0.024	0.029	0.042	0.123	0.327	0.627	0.872	0.398
Mean3	IWT							0.028	0.038	0.037	0.058	0.075	0.121	0.066

Table 12: The type-I error rates and power values of the fragment bands $\mathrm{FF}^p_{\mathrm{frag},t}$ and $\mathrm{FF}^p_{\mathrm{frag},z}$, $p \in \{1, 2\}$, in the stationary covariance scenario Cov1. (Section 4.2 in the main paper.)

		H_0	H_1					Avg.
DGP	Band	$\Delta = 0$	$\Delta = 0.02$	$\Delta = 0.04$	$\Delta = 0.06$	$\Delta = 0.08$	$\Delta = 0.1$	Power
Mean1 Cov1	$\mathrm{FF}^2_{\mathrm{frag},t}$	0.042	0.241	0.774	0.991	1.000	1.000	0.80
Mean1 Cov1	$\mathrm{FF}^1_{\mathrm{frag},t}$	0.044	0.247	0.781	0.991	1.000	1.000	0.80
Mean1 Cov1	$\mathrm{FF}^2_{\mathrm{frag},z}$	0.055	0.282	0.811	0.994	1.000	1.000	0.82
Mean1 Cov1	$\mathrm{FF}^1_{\mathrm{frag},z}$	0.058	0.290	0.820	0.994	1.000	1.000	0.82
Mean2 Cov1	$\mathrm{FF}^2_{\mathrm{frag},t}$	0.042	0.117	0.410	0.800	0.975	0.999	0.66
Mean2 Cov1	$\mathrm{FF}^1_{\mathrm{frag},t}$	0.044	0.118	0.412	0.802	0.975	1.000	0.66
Mean2 Cov1	$\mathrm{FF}^2_{\mathrm{frag},z}$	0.055	0.140	0.454	0.828	0.981	1.000	0.68
Mean2 Cov1	$\mathrm{FF}^1_{\mathrm{frag},z}$	0.058	0.147	0.460	0.832	0.983	1.000	0.68
Mean3 Cov1	$\mathrm{FF}^2_{\mathrm{frag},t}$	0.042	0.080	0.288	0.640	0.928	0.993	0.59
Mean3 Cov1	$\mathrm{FF}^1_{\mathrm{frag},t}$	0.044	0.085	0.297	0.651	0.931	0.994	0.59
Mean3 Cov1	$\mathrm{FF}^2_{\mathrm{frag},z}$	0.055	0.100	0.330	0.683	0.944	0.996	0.61
Mean3 Cov1	$\mathrm{FF}^1_{\mathrm{frag},z}$	0.058	0.104	0.338	0.692	0.947	0.996	0.62

Table 13: The type-I error rates and power values of the fragment bands $\mathrm{FF}^p_{\mathrm{frag},t}$ and $\mathrm{FF}^p_{\mathrm{frag},z}$, $p \in \{1, 2\}$, in the stationary covariance scenario Cov2. (Section 4.2 in the main paper.)

		H_0	H_1					Avg.
DGP	Band	$\Delta = 0$	$\Delta = 0.02$	$\Delta = 0.04$	$\Delta = 0.06$	$\Delta = 0.08$	$\Delta = 0.1$	Power
Mean1 Cov2	$\mathrm{FF}^2_{\mathrm{frag},t}$	0.042	0.249	0.806	0.994	1.000	1.000	0.81
Mean1 Cov2	$\mathrm{FF}^1_{\mathrm{frag},t}$	0.044	0.254	0.812	0.994	1.000	1.000	0.81
Mean1 Cov2	$\mathrm{FF}^2_{\mathrm{frag},z}$	0.056	0.292	0.847	0.996	1.000	1.000	0.83
Mean1 Cov2	$\mathrm{FF}^1_{\mathrm{frag},z}$	0.058	0.299	0.852	0.997	1.000	1.000	0.83
Mean2 Cov2	$\mathrm{FF}^2_{\mathrm{frag},t}$	0.042	0.118	0.458	0.832	0.983	0.999	0.68
Mean2 Cov2	$\mathrm{FF}^1_{\mathrm{frag},t}$	0.044	0.120	0.459	0.832	0.983	0.999	0.68
Mean2 Cov2	$\mathrm{FF}^2_{\mathrm{frag},z}$	0.056	0.147	0.503	0.862	0.986	0.999	0.70
Mean2 Cov2	$\mathrm{FF}^1_{\mathrm{frag},z}$	0.058	0.151	0.510	0.864	0.987	0.999	0.70
Mean3 Cov2	$\mathrm{FF}^2_{\mathrm{frag},t}$	0.042	0.077	0.275	0.650	0.920	0.994	0.58
Mean3 Cov2	$\mathrm{FF}^1_{\mathrm{frag},t}$	0.044	0.081	0.283	0.656	0.923	0.994	0.59
Mean3 Cov2	$\mathrm{FF}^2_{\mathrm{frag},z}$	0.056	0.103	0.320	0.695	0.937	0.996	0.61
Mean3 Cov2	$\mathrm{FF}^1_{\mathrm{frag},z}$	0.058	0.107	0.326	0.701	0.940	0.996	0.61

Table 14: The type-I error rates and power values of the fragment bands $\mathrm{FF}^{p}_{\mathrm{frag},t}$ and $\mathrm{FF}^{p}_{\mathrm{frag},z}$, $p \in \{1, 2\}$, in the non-stationary covariance scenario Cov3. (Section 4.2 in the main paper.)

		H_0	H_1					Avg.
DGP	Band	$\Delta = 0$	$\Delta = 0.02$	$\Delta = 0.04$	$\Delta = 0.06$	$\Delta = 0.08$	$\Delta = 0.1$	Power
Mean1 Cov3	$\mathrm{FF}^{2}_{\mathrm{frag},t}$	0.042	0.244	0.803	0.992	1.000	1.000	0.81
Mean1 Cov3	$\mathrm{FF}^{1}_{\mathrm{frag},t}$	0.042	0.243	0.798	0.992	1.000	1.000	0.81
Mean1 Cov3	$\mathrm{FF}^{2}_{\mathrm{frag},z}$	0.055	0.286	0.835	0.994	1.000	1.000	0.82
Mean1 Cov3	$\mathrm{FF}^{1}_{\mathrm{frag},z}$	0.056	0.286	0.836	0.994	1.000	1.000	0.82
Mean2 Cov3	$\mathrm{FF}^{2}_{\mathrm{frag},t}$	0.042	0.119	0.455	0.835	0.984	0.999	0.68
Mean2 Cov3	$\mathrm{FF}^{1}_{\mathrm{frag},t}$	0.042	0.130	0.486	0.855	0.987	0.999	0.69
Mean2 Cov3	$\mathrm{FF}^{2}_{\mathrm{frag},z}$	0.055	0.149	0.504	0.865	0.988	0.999	0.70
Mean2 Cov3	$\mathrm{FF}^{1}_{\mathrm{frag},z}$	0.056	0.160	0.538	0.884	0.990	0.999	0.71
Mean3 Cov3	$\mathrm{FF}^{2}_{\mathrm{frag},t}$	0.042	0.078	0.273	0.645	0.919	0.994	0.58
Mean3 Cov3	$\mathrm{FF}^{1}_{\mathrm{frag},t}$	0.042	0.074	0.254	0.620	0.908	0.992	0.57
Mean3 Cov3	$\mathrm{FF}^{2}_{\mathrm{frag},z}$	0.055	0.102	0.318	0.688	0.936	0.997	0.61
Mean3 Cov3	$\mathrm{FF}^{1}_{\mathrm{frag},z}$	0.056	0.096	0.298	0.666	0.927	0.995	0.60

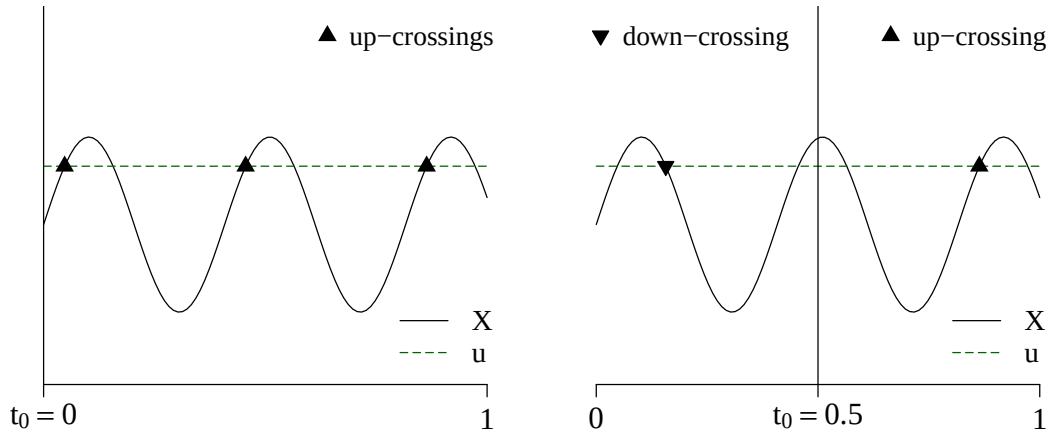

Figure 8: Left Plot: Three exceedance events counted as three up-crossing events to the right of $t_0 = 0$. Right Plot: The same three exceedance events, but counted as one down-crossing event to the left of $t_0 = 0.5$, one exceedance event at $t_0 = 0.5$, and one up-crossing event to the right of $t_0 = 0.5$.

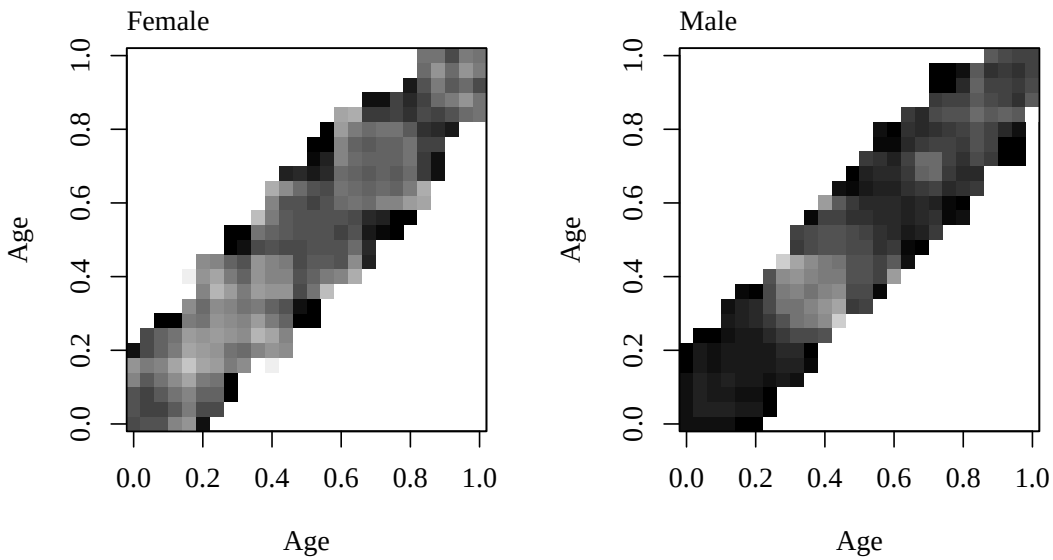

Figure 9: The estimable parts of the sample covariances, $\hat{C}^{\mathrm{f}}_{\mathrm{frag}}$ and $\hat{C}^{\mathrm{m}}_{\mathrm{frag}}$, of the bone mineral acquisition data application in Section 5.2.